ADVANCED SINTERING TECHNIQUES OF ALUMINUM: SPARK PLASMA SINTERING

by

Gregory Alexander Wilson Sweet

Submitted in partial fulfilment of the requirements
for the degree of Master of Applied Science

at

Dalhousie University
Halifax, Nova Scotia
August 2014

Table of Contents

List of Tables

List of Figures

Abstract

Spark plasma sintering (SPS) of air atomized aluminum powders was conducted in a fundamental investigation of processing and chemical effects on physical and mechanical properties. Five air atomized aluminum powders, one of commercial purity, one magnesium-doped (0.4 wt%), one iron-doped (1.0 wt%), one nickel-doped (1.0 wt%) and one iron (1.0 wt%) and nickel-doped (1.0 wt%) were processed by SPS means. Where applicable, powders were also processed by conventional powder metallurgy (PM). An investigation of SPS processing parameters and their effect on sinter quality were of primary concern. Applied pressure and ultimate processing temperature bore the greatest influence on processing, while heating rate and hold time showed a minor effect. Full density specimens were achieved for both powders under select processing conditions. To compliment this, large (80 mm) and small (20 mm) diameter samples were made to observe possible up-scaling effects, as well as tensile properties. Large samples were successfully processed, albeit with somewhat inferior densities to the smaller counterparts presumably due to the temperature inhomogeneity during processing. An investigation into tensile properties for SPS samples exhibited extensive ductility (~30%) at high sintering temperatures, while lower temperature SPS samples as well as all conventional PM processed samples exhibited a brittle nature. The measurement of residual oxygen and hydrogen contents showed a significant elimination of both species in SPS samples under certain processing parameters when compared to conventional PM equivalents. None of the transition metal additions had an overtly negative impact on SPS response. As such, all powders were successfully processed to the full density condition provided that an appropriate minimum SPS temperature was employed. Hardness improved as the net concentration of transition metals increased and was found to be greatest in the Al-Fe-Ni ternary powder (78 HRH). Microstructural coarsening was apparent in all alloys as a result of SPS processing. However, the consolidated products maintained desirable microstructures comprised of homogenous distributions of sub-micron intermetallics such as Al_9FeNi, $Al_{13}Fe_4$ and $AlNi_3$.

List of Abbreviations Used

AC	Alternating Current
APM	Aluminum Powder Metallurgy
ARB	Accumulative Roll Bonding
ASTM	American Society for Testing and Materials
CAPAD	Current Activated, Pressure-Assisted Densification
DC	Direct Current
DSC	Differential Scanning Calorimetry
EDC	Electrical Discharge Compaction
FAST	Field Assisted Sintering Technique
HIP	Hot Isostatic Press
HRB	Rockwell Hardness: Scale B
HRH	Rockwell Hardness: Scale H
(HR)TEM	(High Resolution) Transmission Electron Microscope
ICP-OES	Inductively Coupled Plasma – Optical Emission Spectroscopy
LPS	Liquid Phase Sintering
MN	MegaNewton
MPa	MegaPascal
MPIF	Metal Powder Industries Federation
PM	Powder Metallurgy
PDS	Pulse Discharge Sintering
PECS	Pulsed Electric Current Sintering
PID	Proportional Integral Derivative
ppm	Parts per million
RS	Resistance Sintering
SPS	Spark Plasma Sintering
T1	Temper Designation: Cooled from fabrication temperature and naturally aged
T6	Temper Designation: Solution treated and artificially aged
TD	Theoretical Density
TGA	Thermogravimetric Analysis
UTS	Ultimate Tensile Strength
WEE	Wire Electrical Explosion
wt%	Weight Percent
XRD	X-Ray Diffraction

Acknowledgements

The authors would like to acknowledge the Auto21 Networks of Centres of Excellence and the Natural Sciences and Engineering Research Council of Canada, (NSERC) for financial support via grant C502-CPM. Dr. Bernhard Mais (Ecka Granules) is acknowledged for the provision of the powders employed, as are Mr. Rene Kirchner (FCT Systeme GmbH), Dr. Jason Milligan (McGill University) and Mr. David Walker (McGill University) for their assistance with SPS trials.

CHAPTER 1. INTRODUCTION

1.1 Conventional aluminum powder metallurgy

Traditionally, aluminum-based components have been fabricated in several ways. In one, wrought aluminum stock is machined and/or mechanically deformed (rolled, forged, etc.) into the required geometry [1]. The second option is cast aluminum. In this, an aluminum-based melt is poured into a mold that embodies the shape of the final part sought. A third, less common, method of manufacturing aluminum parts is known as aluminum powder metallurgy (APM). Here, aluminum powder is consolidated into the desired shape and then sintered to improve mechanical and physical properties. A detailed description of the processing stages involved in APM is given in the following section.

1.1.1 Processing of conventional aluminum powder metallurgy parts

Before forming a part, an appropriate powder system must be constructed. This typically begins with the atomization of metallic constituents into fine powders. Figure 1 is a schematic of the predominant atomization mechanism used in APM. In this, a molten aluminum 'melt stream' is forced through a nozzle where it is impacted by a pressurized flow of air. The rapid depressurization of this gas forms a local expansion zone adjacent to the molten metal thereby disintegrating the stream into fine droplets [2]. These droplets then solidify into discrete powder particles that are then collected for subsequent use within APM processing technologies.

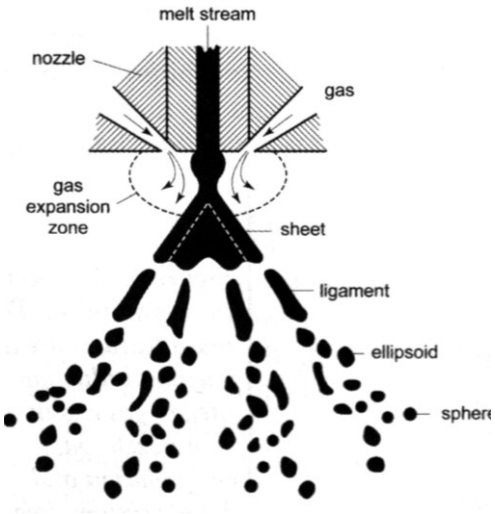

Figure 1 – Schematic illustrating the formation of a metal powder by gas atomization [2].

Since APM involves aluminum alloys, not just pure aluminum, the required alloying constituents must also be introduced by some means. One option is to blend individual elemental powders in appropriate proportions; a technique known as blended elemental. The second approach is one whereby the additions are introduced in the form of powdered master alloys, which are later admixed with pure aluminum powder. Finally, a third technique, is to fully alloy a melt prior to atomization, thus ensuring all individual powder particles have identical, homogenous chemistries. This concept is called prealloying. Each technique possesses its own advantages and disadvantages, some of which are described below.

With the powder system chosen, the second major operation in APM is to consolidate this powder into a part close to the geometry of the required product. This is frequently accomplished by pressing the aluminum powder within a rigid tool set in a uniaxial manner. The applied force rearranges the particles and then plastically deforms them into a denser, mechanically-bonded "green" part. This sequence of events is shown in Figure 2. Due to the inherent malleability of pure aluminum, it is not uncommon to attain a part that possesses a green density that is some 90-95% of full theoretical even when pressed at

relatively low pressures such as 200 MPa [2]. However, as particle hardness increases, the response to compaction is lowered [2]. This means that harder, pre-alloyed aluminum is generally more difficult to compact. To aid particle rearrangement and compact density, a dry lubricant is generally added. This feature reduces interparticle friction, as well as die-wall friction so as to extend the longevity of tooling members.

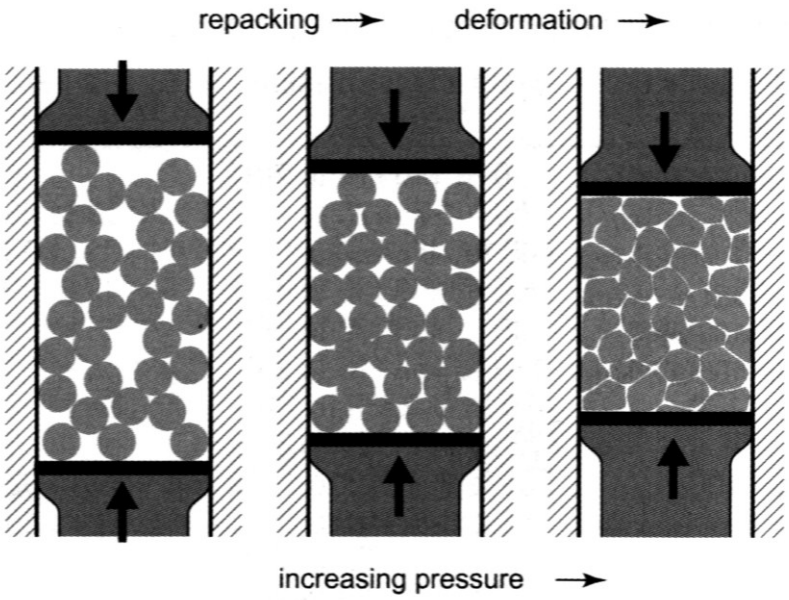

Figure 2 – Schematic of powder compaction mechanisms, showing particle rearrangement and plastic deformation [2].

The final step in APM is to sinter the part so as to invoke an overall increase in mechanical and physical properties. Here, a part is given sufficient thermal energy to promote inter-particle diffusion, and possibly even the formation of a liquid phase. This stage allows a compact to release much of the energy associated with the powder largely derived from its inherently high surface area to volume ratio. This step is primarily a function of temperature and time. For aluminum, sintering temperatures are generally around 600°C [2, 3, 4], and sintered densities routinely exceed 98% of theoretical. Energy is also released by the annihilation of grain boundaries. This mechanism, which accelerates as the sinter progresses [2], results in an increasing grain size.

1.1.2 Conventional sintering mechanisms

Sintering is generally categorized under two principal types: Solid-state and liquid phase sintering (LPS). In the former, individual powder particles bond through an array of solid-state diffusion mechanisms. In the latter, a secondary, liquid phase is produced that typically intensifies densification through the combined action of capillary forces and enhanced kinetics of diffusion.

1.1.2.1 Solid state sintering

This type of sintering inherently involves only solid state diffusion mechanisms and is therefore relatively slow when compared to LPS. The means by which interparticle bonding and densification occurs includes four mass transport mechanisms: evaporation-condensation, surface diffusion, volume diffusion and grain boundary diffusion. These concepts can be illustrated using the classical "two-sphere model" wherein two particles are in contact with a joining neck "X" formed between them (Figure 3).

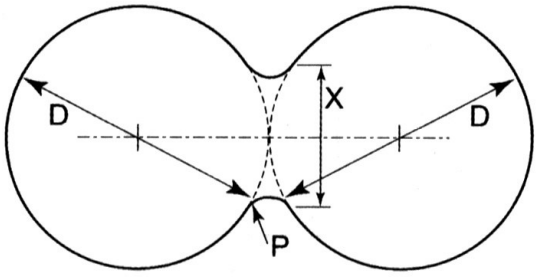

Figure 3 – Two-sphere model illustrating the terminology used to describe the solid state sintering of two spherical particles [2].

The neck between the two particles manifests itself as a concave surface, while the particle itself is convex. This curvature difference develops a minute vapor pressure difference between these two surfaces (high at convex and low at concave) and a localized departure from equilibrium. The corresponding pressure gradient causes vapour (and in turn, atoms) to migrate from the convex surface to the concave region of particle contact where it then

condenses and deposits new atoms so as to increase the size of the neck [2]. This evaporation-condensation step only forms the neck between the particles and causes little densification. Surface diffusion is similar to evaporation-condensation, in that the curvature of the particles is again the driving force. Here, a locally high vacancy concentration exists at the concave neck surface whereas a much lower concentration prevails within the convex region. The compact attempts to eliminate this gradient through the diffusion of vacancies away from the neck. This is invariably accompanied by a counter-current flux of mass into the neck between the particles causing it to grow. Both mechanisms are functions of the powder/neck curvatures and become sluggish as the neck grows and concavity is diminished.

Upon heating to higher temperatures, bulk transport mechanisms denoted as volume diffusion and grain boundary diffusion become operative. These are responsible for the majority of shrinkage and densification that occurs during solid state sintering. Volume diffusion is similar to surface diffusion, but rather than surface atoms exchanging with vacancies in the neck, the migrating atoms diffuse within the bulk of the material instead. Vacancies are transported to, and ultimately annihilated, at the grain boundary between the particles. Similarly, grain boundary diffusion involves the movement of atoms along the particle grain boundary. Vacancies travel inward from the concave neck surface, while a concurrent flow of atoms occurs towards the neck surface. The four solid-state sintering mechanisms are conceptually shown in Figure 4. The arrows represent the flow of materials during the appropriate mechanisms.

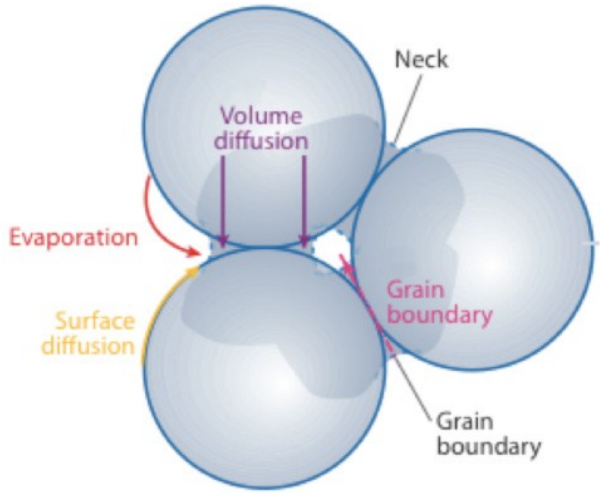

Figure 4 – Schematic of the solid state sintering mechanisms [5].

As sintering progresses, there are three fundamental steps that characterize the state of the final product. These are the initial, intermediate, and final stages of sintering. During the initial stage, inter-particle necking is the primary transition. Very little property change (mechanical or physical) occurs and the compact largely appears as it did prior to sintering. This occurs primarily at low temperatures and short hold times; in this stage the compact remains under sintered. By increasing the sintering temperature and hold time, the compact then enters the intermediate stage. At this point, bulk properties are improved as a stronger, denser product is achieved. However, properties remain far from optimized. In the final stage, the compact is held at the desired sintering temperature for a prolonged period. Internal porosity is reduced appreciably while simultaneously increasing properties. This stage becomes kinetically slow as time progresses.

1.1.2.2 Liquid phase sintering

Due to the presence of a liquid phase, this sintering approach possesses significantly higher diffusion rates and thus expedient sintering. Figure 5 shows the progression that conceptually occurs during classical LPS wherein a base powder is combined with an additive powder of relatively low melting point. Upon heating, the secondary addition forms a liquid, while the primary base material remains solid. This liquid phase

spontaneously spreads through the compact when appropriate wetting conditions prevail. Liquid is drawn into the pores through the action of capillary force. This pulls the particles together and improves density. With continued time at temperature, the liquid allows the solution-reprecipitation stage to become active. Here, small solid particles of the base material are preferentially dissolved into the liquid phase. This causes a localized increase in the base concentration within the liquid phase that is subsequently relieved through reprecipitation upon the larger particles. Growth of solid grains occurs by way of this mechanism as sintering proceeds. This occurs in a manner that invokes grain shape accommodation whereby adjacent particles form parallel flat facets to allow for improved particle packing and increased densification. Eventually, much of the residual porosity is eliminated through these mechanisms and the solid grains come in direct contact. At this point the liquid phase becomes ineffective and the system behaves as a solid, rigid material with no further densification possible from a practical perspective. In general, an LPS compact will sinter faster and to a higher density than a solid-state counterpart of the same material.

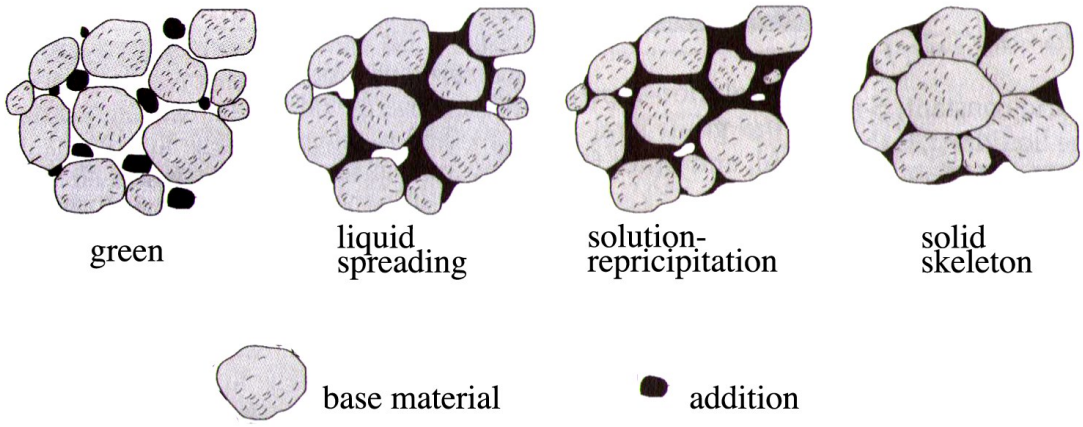

Figure 5 – Schematic illustrating the principal stages of LPS [2].

Consider a base aluminum alloy that is to be sintered by LPS. In order to promote a liquid phase, a secondary metallic addition must be added. Obviously, this addition has the requirement of melting at a temperature below that of aluminum (or a capacity to react with

aluminum so as to form a low melting point eutectic), but there are also several other key requirements. First, the solubility of the addition must be very low in the base material [6], so as to reduce the tendency for the liquid phase to dissolve into the base prior to sintering. Furthermore, aluminum should be soluble in the liquefied base metal. This allows a more coherent bond of the base with the liquid phase and the engagement of the solution-reprecipitation mechanism. Lastly, aluminum should have substantial diffusivity in the liquid to promote rapid mass transfer, and thus fast sintering rates [6].

Specific to aluminum, one system that exhibits such idealized traits is the Al-Sn binary. However, since aluminum powder particles are covered in a stable oxide layer, the liquefied tin phase is insulated from metallic aluminum. Furthermore, the wetting angle of Sn and Al_2O_3 is such that Sn is actually rejected from a compact [6]. To oppose this, it has been shown that additions of Mg with Sn have the ability to reduce the wetting angle of the liquid phase, as well as reduce the oxide layer on aluminum. This reaction is shown in Equation 1 [6].

$$3Mg + 4Al_2O_3 \leftrightarrow 3MgAl_2O_4 + 2Al \qquad \text{Equation 1}$$

With the oxide layer disrupted in this manner, the liquid Sn-rich phase then facilitates successful LPS. While not the sole system for LPS, Mg-Sn additions in aluminum are universally applied to many systems as a means to intensify the sintering response, among other amiable effects [7, 8, 9, 10].

1.1.3 Advantages and disadvantages to powder metallurgy

The process by which APM parts are made is drastically different than both wrought and cast aluminum. Thus, APM possesses certain advantages and disadvantages when compared to the traditional metal forming processes. In this sense, APM is considered a near-net shape process, meaning that a part will require little post-process machining to conform to the required geometric tolerances [2, 11]. Since parts are created in a rigid die,

and can be easily ejected, this approach to processing is suitable for the high-volume production rates required in automotive scenarios [11]. Furthermore, high-performance alloys with non-metallic phases can be synthesized with a homogenous microstructure [12].

However beneficial conventional APM may be, it is not without drawbacks. Depending on sinter conditions, a compact may exhibit shrinkage or growth when compared to original die measurements [4]. Furthermore, this change may be manifested as dimensional instability, meaning that changes are not isotropic [3, 13]. Moreover, it is common for APM parts to attain some 95-99% of their theoretical density in the final, sintered state [3, 6]. This can be problematic in certain end-use applications. In this sense, pores (and the associated volume fraction of void space) decrease key mechanical properties such as ductility and fatigue resistance.

1.1.4 Mechanical properties of select APM alloys

Table 1 shows the nominal chemistries and mechanical properties of select commercial APM alloys. Of particular note are the density and elongation to failure values. Density, represented as the percent of the maximum theoretical density (TD) indicates that there is generally at least 1% residual porosity in these particular materials. Furthermore, the elongation at fracture, ε, for all alloys in their T6 condition tends to be very small. This limited ductility is a common attribute of APM components that exhibit residual porosity.

Table 1 - Properties of select APM alloys [12, 14, 15, 16].

Name	**Chemistry**	**Yield (MPa)**	**Elongation (%)**	**Density (% TD)**	**Hardness (HRB)**
Alumix 431D	1.5Cu-2.5Mg-5.5Zn	480[1]	0.9[1]	99	159[1]
Alumix 231	14Si-2.5Cu-0.5Mg	230[2]-350[1]	1[2]-0.5[1]	97-90	100[2]-145[1]
Alumix 123	4.5Cu-0.5Mg-0.7Si	190[2]-320[1]	5[2]-1[1]	92-97	60[2]-100[1]

[1] Alloy solutionized and artificially aged to the T6 condition
[2] Alloy tested in T1 condition

1.2 Spark Plasma sintering

Similar to conventional PM, Spark Plasma Sintering (SPS), is the consolidation of a powdered material into a near-net shape compact. However, due to the vastly different processing conditions, the mechanisms described for densification in the previous sections are not applicable when compared to those that arise in SPS. These mechanisms will be discussed in later sections. Fundamentally, this process involves heating a powder by passing a current through it, while simultaneously applying uniaxial pressure.

Despite the naming convention, it has been widely disputed as to whether the presence of sparks and plasmas truly exist during the process, and even if they do, whether their occurrence has any beneficial effect on the end product. Other beneficial traits have been proposed, such as spark impact pressure, plasma cleaning of particles, which have been proposed to modify the surface conditions to eliminate surface contaminants and improve particle bonding [17]. Furthermore, field assisted diffusion and electron wind force have been theorized to explain the enhanced densification of SPS processing in comparison to other consolidation techniques [18]. However, Hubert et al conducted SPS experiments using a variety of detection techniques and concluded that "no plasma generation, sparking or arcing [was] present during the SPS process" [18]. Furthermore, Garay et al noted that there was very little convincing evidence of such field effects during SPS processing [5]. Despite the widespread use of SPS technology worldwide, a complete understanding of the mechanism of SPS has not been developed [17]. More appropriate names have been associated with this technology, such as Pulsed Electric Current Sintering (PECS); Pulse Discharge Sintering (PDS); Current Activated, Pressure-Assisted Densification (CAPAD) and Field Activated Sintering Technique (FAST) [5, 17]. However, the dominant convention in publications is still to refer to this process as SPS, and will be such for the remainder of this document.

A distinction must be first made before describing this process in depth. Two fundamentally different methods of current application are considered under the umbrella of SPS. First, electrical discharge compaction, EDC, involves rapidly discharging a series of capacitors and directing the current through a powdered material. In this, process times are very short

and achievable densities are less than ideal [17]. Alternatively, resistive sintering involves a semi-continuous flow of current through a powdered part by way of an AC or pulsed-DC power source. Process times are longer, but are still on the order of seconds. Resistance sintering is the only form of SPS considered in this report.

1.2.1 Apparatus

Conceptually, the apparatus used in SPS is analogous to a uniaxial press, where pressure is applied to a die assembly. Here, the loose powder is compacted within a tool set comprising a die and two punches. In addition to this pressure effect, a power source applies a low-voltage potential across the rams. This allows for a high-current flow of electricity to pass through the conductive die and powder. A schematic of this process is shown in Figure 6. The arrows indicate the direction of the applied pressure.

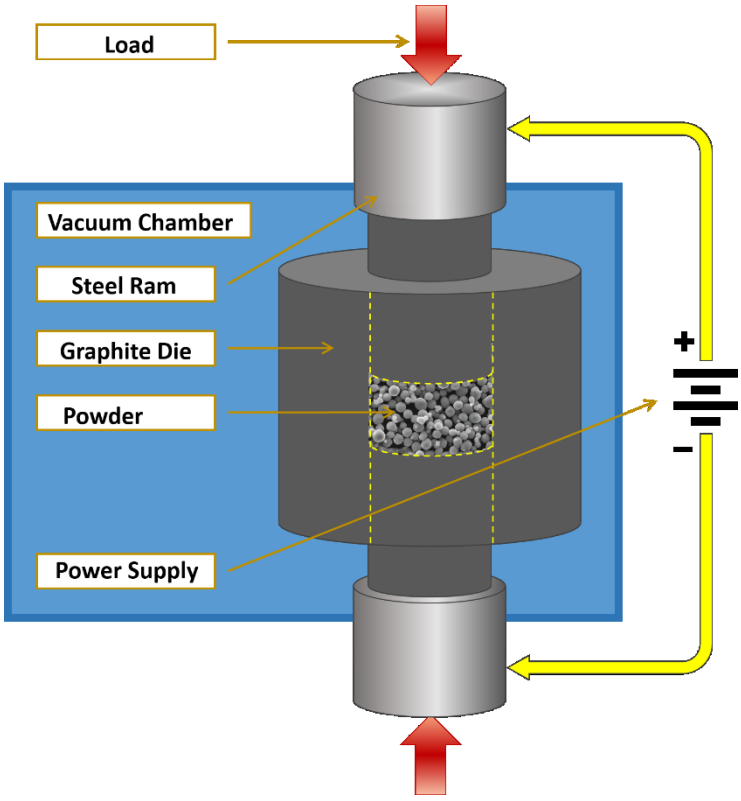

Figure 6 - Schematic of a SPS system.

The die assembly used in SPS processing is most commonly a high-purity, high strength graphite. These graphite components possess excellent high temperature strength, as well as excellent thermal and electrical conductivity [5]. However, when compared to conventional uniaxial die materials that can easily exceed pressures of 600 MPa, this high purity graphite is limited to roughly 100 MPa [17]. For more affordable, lower purity graphite, this value is further reduced to roughly 60 MPa. Another benefit of graphite, when considering an aluminum sample, is the non-reactive nature of the two. Carbon has effectively zero solubility in solid aluminum, and allows for an aluminum sample to be essentially isolated from the die during processing. A further aspect of the SPS process is the presence of a rough vacuum as the entire die-sample configuration is held within a vacuum chamber to minimize the extent of oxidation during sintering.

A typical SPS apparatus will be computer controlled and monitored continuously throughout a sinter. Firstly, the current and pressure are entirely independent and variable, with user selectable ramp rates and hold times. Rather than selecting a current value, a user defines a temperature profile, and a proportional integral derivative (PID) controller will continuously vary current in order to maintain this value. Furthermore, the actual applied current is variable in terms of the profile used. Since the direct current is pulsed, a user may define the intensity and length of each current impulse, as well as the on-off times of current. For example, a user may program the current to be applied for 5 milliseconds, followed by a 50 millisecond period without current flow. The importance of this is defined in the latter sections of this report.

1.2.2 Aluminum and SPS

Thus far, SPS work has been completed on a number of aluminum alloy systems (ie X7091 [17], 7075 [17], 6061 [19], 2124 [19], etc). Xie et al. have published many papers on the effects of SPS on air atomized pure aluminum and magnesium-doped aluminum powders [20, 21, 22, 23, 24, 25, 26, 27]. These papers emphasize tensile and electrical properties of the resultant materials, as well as the resultant bond interface from SPS processing.

Studies have demonstrated that commercially pure aluminum powder can be successfully processed by SPS to near full theoretical density [28]. These coarse air atomized powders were studied using a conservative sintering temperature of 525°C and an applied pressure of 50 MPa using a graphite die assembly. Furthermore, a subset of samples were processed with thin alumina discs in contact with punch faces. These electrically insulting discs discouraged the flow of current through the metal powder, eliminating any electrical effects other than heating that may contribute to the densification mechanism. Since heating is known to occur through Joule heating of the powder bed as well as the graphite die, these select samples were only heated via the latter. Those processed without the alumina discs showed tensile strengths essentially identical to counterpart specimens fabricated with electrical isolation. However, ductility was found to be significantly better for samples produced with current flowing through the powder bed. It was theorized that the pulsed current promoted a more uniform heating of the powder bed and thereby allowed for the development of an increased concentration of metallic bonds throughout the compact.

The effects of sintering temperature on the grain growth within air atomized aluminum powder has been studied with interesting conclusions. Kwon et al processed samples at 50 MPa between 280 and 540°C, with isothermal holds of 20 minutes [29]. Sinter quality was quantified in terms of density and grain size. For the temperature range considered, the authors noted no measureable grain growth. It was hypothesized that a pinning effect from the pre-existing aluminum oxide surface shell inhibited any grain boundary movement.

Due to the inherently short processing times present in SPS, there has been a large focus on the development of bulk nano-crystalline aluminum compacts [17]. However, to establish nano-crystallinity, an aluminum powder is typically mechanically milled by either cryo-milling [30, 31] or some other mechanical means [32]. This lengthy step is effective at reducing the grain size of a feed powder, albeit significantly increasing the cost over an air atomized counterpart. Through this technique, it has been observed that powders with a grain size on the order of ~25nm prior to SPS were able to maintain a final grain size of some 50nm [32]. Using this milling and sintering technique, the tensile strength of Al5083

has been shown to exceed 700MPa; significantly higher than that achievable through any conventional means [12, 14].

1.2.3 Characteristics of SPS

There are three defining characteristics of SPS which contribute to its widespread success and adaptability to many materials systems. These include the ability to achieve high heating rates, the effects of applied current, and the simultaneous effects of an applied pressure. Since all three characteristics are concurrent, and only benefit a process when applied at the same time [33], it is difficult to determine which parameter bears the greatest influence. Hence, the individual contributions will be outlined below to the level of modern understanding.

1.2.4 Effects of heating rate

One of the principal characteristics of the SPS technique is the ability to achieve very high heating rates. When compared to more conventional sintering approaches, where the heating rate may be on the order of 5-20 Kelvin per minute, SPS can heat material almost instantaneously. With equipment capable of heating up to 1000 K m^{-1} [17] [5], and most cycles commonly run between 50 and 600 K m^{-1}, [34] [35], SPS is able to lessen the detrimental effects of microstructure coarsening that occur upon heating. Olevsky et al derived models which predicted that sufficiently high heating rates would essentially skip the low-temperature surface diffusion mechanism that is readily apparent in conventional sintering [34]. Surface diffusion primarily allows the development of a neck between particles, and is classified as a non-densifying mechanism of sintering [33]. Avoiding this neck development maintains the small radius of curvature of pore-tips at higher temperatures. When processing temperatures reach that sufficient for grain boundary diffusion, this smaller pore-tip radius drives higher diffusion rates, and ultimately more rapid densification kinetics.

To complement the improved densification that results from high heating rates, several other associated effects have been studied. One is the inhibition of grain growth due to the

reduced level of thermal exposure [34]. Here, Munir et al [33]concluded that the heating rate was inversely proportional to the resultant grain growth of a compact. Another effect of high heating rates is the ability to use coarser particle size powders. In conventional powder metallurgy, it is known that the driving force for sintering increases with decreasing particle size. Conversely, when heating rates are large, the driving force is sufficiently pronounced so as to allow larger particles to attain the same extent of densification [34].

1.2.5 Effects of electrical current

In SPS processing, electrical current is typically supplied as a pulsating DC current. Essentially, the current is applied for a set time frame, on the order of milliseconds, and then turned off for a similar time so as to give a rectangular pulse shape. It has been postulated that the application of current in this manner allows for the relatively small contact area between adjacent particles to possess very large current densities, and thus, high heating rates. The 'off' time of the electric current corresponds to a period of zero heating, that allows the bulk of the particle to remain cool [17]. This approach manifests the fundamental heating mechanism for conductive (metallic) powders known as Joule heating [5, 17, 18, 34, 36].

Recent investigations have shown that SPS densification mechanisms seem to be independent of the flow of current through a sample [37]. In this sense, the Joule heating generated by the intense current flow seems to dominate all other current effects, and that any effects related to the pulsed nature of DC seem to be secondary. As demonstrated by Olevski et al [38], the thermal effects can be divided into four categories, as follows: high heating rates; high local temperature gradients; highly nonuniform local temperature distributions, and highly nonuniform macroscopic temperature distributions. As previously discussed, high heating rates allow for increased sinterability. The other effects can be summarized as temperature differentials within a compact. Together, they promote thermal diffusion [34], while simultaneously producing internal stress fields that cause dislocation creep. In instances of very small contact area between adjacent particles, localized melting has been shown, which instantaneously welds particles [39]. Figure 7 shows a simulated

result of the temperature distribution between two spherical particles, assuming no physical or phase changes occur [39]. It can be seen that extreme temperatures are expected at the immediate contact point between particles. This can then manifest itself as localized melting. For instance, Figure 8 shows evidence of localized melting in a SPS compact from the same study that remains heavily under sintered.

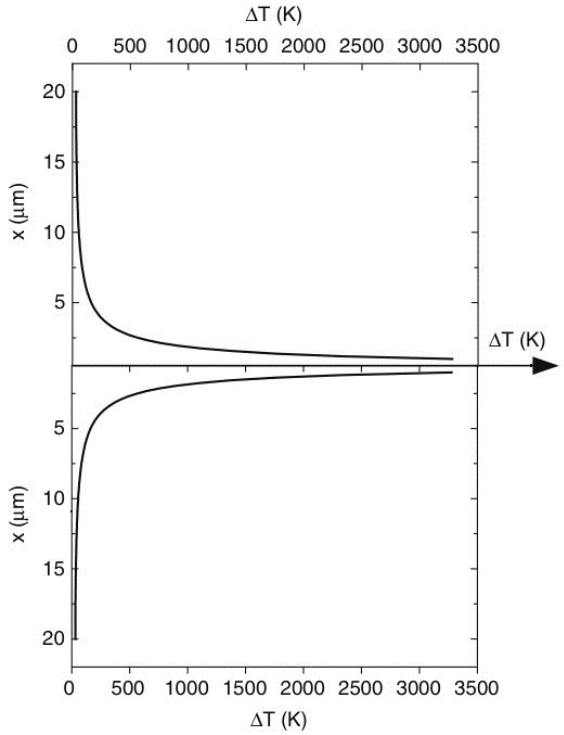

Figure 7 – Results from a mathematical model that illustrate the expected temperature distribution between two adjacent powder particles [39].

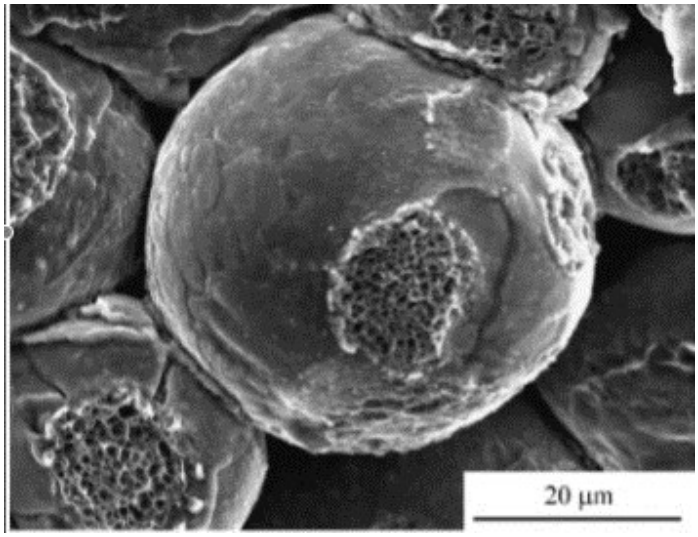

Figure 8 - Fracture surface of a semi-sintered compact showing evidence of localized melting [39].

In addition to thermal effects, it is worthwhile to mention that athermal effects of current can also be present during SPS. Commonly noted factors include electromigration, ponderomotive forces, electroplasticity, and the dielectric breakdown of oxide layers [38]. The latter of which is specifically interesting for aluminum, as the oxide layer typically inhibits sintering. However, these effects are all related to the densification of a compact, and as discussed earlier, are most likely secondary effects of influence. Aside from densification effects, electrical current has also been shown to cause an increased driving force for secondary phase nucleation and growth [33, 35, 40]. Specifically, Munir et al showed that flowing a current through a heated sample allowed the growth of a secondary phase that would otherwise not form in the absence of current [33]. Furthermore, they also showed that increasing the current density increased the rate at which these phases grew. They attributed this heightened intermetallic phase growth rate to result from enhanced atomic mobility or concentration of defects [40]. Munir further concluded that the growth of the phase is independent of current direction and of the pulse pattern utilized [35]. For example, Figure 9 shows the formation of columnar $MoSi_2$ and Mo_5Si_3 intermetallics between stacked layers of elemental Mo and Si foils that were processed via SPS. By

increasing the dwell time at peak temperature, these intermetallic layers became thicker whereas increases in the processing temperature increased the intermetallic growth rate.

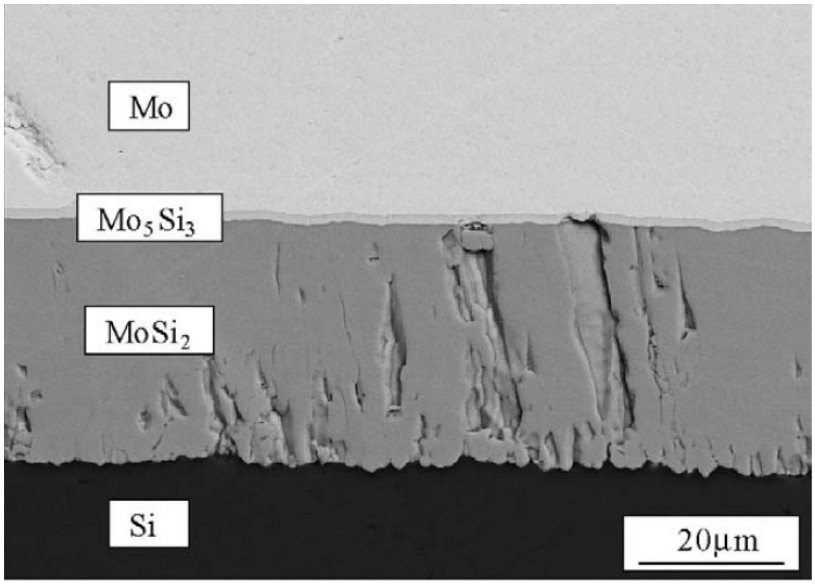

Figure 9 – Intermetallic $MoSi_2$ and Mo_5Si_3 layers formed between Mo and Si foils as a result of an applied current.

1.2.6 Effects of applied pressure

In addition to current, the effects of an applied pressure significantly contribute to the high extent of densification observed in SPS. Similar to the compaction stage in conventional PM, applied pressure plays a crucial role in increasing density as well as allowing for greater particle interaction. For instance, particle rearrangement and particle sliding occur early in the SPS process, as they would normally do so during the cold compaction of powders. However, densification through these early stage mechanisms is limited, as the pressures permissible/applied using a graphite die are typically an order of magnitude smaller than that those routinely attained with conventional tool steel dies and well below the yield strength of the material being consolidated. However, with increasing process temperature, the yield strength of most metallic powders drops significantly. In this

weakened state, the applied SPS pressure is then sufficient to invoke significant plastic deformation, and in turn, densification [5].

Given the beneficial effects of pressure, the required time and temperatures for SPS are generally much lower than those employed in conventional sintering practices. The associated reduction in thermal exposure can be optimized to maintain essentially fully dense compacts yet with abnormally low levels of microstructural coarsening. For instance, Equation 2 represents the significant effect that this has on minimizing grain growth [41].

$$D = D_0(te^{-\frac{Q}{RT}})^n \qquad \text{Equation 2}$$

In Equation 2, D and D_0 represent the final and initial grain sizes respectively. The variable t is time at a specific temperature, while n is a material attribute determined through experimental work. For pure aluminum, n was found to vary in a linear manner between 350°C and 500°C with values of 0.06 and 0.16, respectively [41]. Q represents the activation energy for surface or grain boundary diffusion and creep (250 kJ/mol [41]). R and T represent the ideal gas constant and temperature, respectively. From this expression, it can be readily concluded that reductions in temperature and time will lessen the amount of grain growth. Figure 10 shows the grain growth trends for pure aluminum modeled via Equation 2 at four different temperatures. This plot is however for pure aluminum, and is not expected to accurately represent alloyed variants thereof.

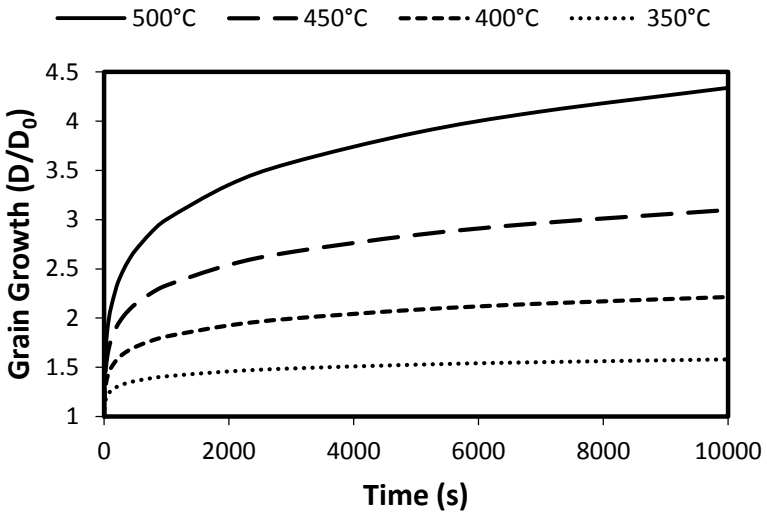

Figure 10 – Modelled grain growth trends in aluminum as functions of temperature and time.

1.2.7 Densification mechanism

As previously discussed, the processing parameters for SPS are dramatically different than conventional PM. It is therefore evident that a different family of densification mechanisms based on electrical current, temperature and stress are to be expected. Early research by Olevsky et al presented evidence that both current-induced heat and pressure may stimulate a creep mechanism, known as dislocation climb-controlled creep [34]. Further research by Olevsky using multi-step pressure dilatometry confirmed this creep mechanism for pure copper powders [37]. In addition, their experiments were conducted on samples that were both current-assisted (current flowing through the copper powder) and current-isolated (powder mass was insulated by an alumina bushing). Their results concluded that the densification for the two differing setups was essentially the same, and that dislocation climb-controlled creep was the primary mechanism at hand. As such, the current passing through the material appeared to have a minimal influence on the densification mechanism.

Dislocation climb-controlled creep, also known as power law creep, is a scenario wherein dislocations pass through a material and overcome obstacles by way of climbing. The

ability for a material to exhibit this style of creep is dependent on the tendency for vacancies to be rapidly formed and annihilated adjacent to the dislocation line. The activation energy for self-diffusion in aluminum is such that these vacancy-based phenomena can readily occur. Furthermore, the size of the stacking faults within the alloy is also a factor of influence. For aluminum, these stacking faults are on the order of 2 atoms in thickness and are relatively easy to overcome, whereas noble metals can present more troublesome stacking faults on the order of 20 atoms. It can therefore be assumed that aluminum, with the same crystal structure as copper, is expected to densify by a dislocation climb-controlled creep mechanism.

1.3 Oxide layer formation on aluminum

The reactive nature of pure aluminum in an oxidizing environment is a well-known phenomenon. The oxidation reaction is spontaneous even under the highest achievable vacuum levels. Hence, when producing aluminum powder, the surface of individual particles are inevitably covered with an 'oxide skin' roughly 2-4 nm thick [42, 43, 44, 45]. As trace concentrations of moisture are also unavoidable within this scenario, particle surfaces also contain hydroxyl ions, thereby forming a hydrated oxide (i.e $Al_xO_y(OH)_z$ [44, 46]) within the exterior surface layer as well. Furthermore, due to the rapid cooling in air atomization, the resultant oxide layer is not necessarily in a state of complete equilibrium. For instance, up to a critical thickness of ~5 nm, it is favorable for the oxide to develop in an amorphous nature [43]. Regardless of the nature of the surface film, the oxidation reaction is self-limiting as increasing thickness quickly stifles inward oxygen diffusion thereby stopping oxidation. Therefore, without further thermal processing, air atomized aluminum powders are generally said to be covered with a 5 nm, amorphous and hydrated oxide skin [43].

A microstructural investigation into pure aluminum powders confirms the thermodynamic work of Trunov *et al*. [43]. HRTEM imaging of a cross section of an individual powder particle surface (Figure 11) shows a crystalline aluminum substructure and an amorphous shell roughly 3 nm in thickness [44]. This was attributed to the hydrating and oxidizing environment in which the powder was prepared and stored. It should be noted that this layer

is consistent for coarse air atomized powders [44] as well as fine Wire Electrical Explosion (WEE) aluminum nanoparticles [45].

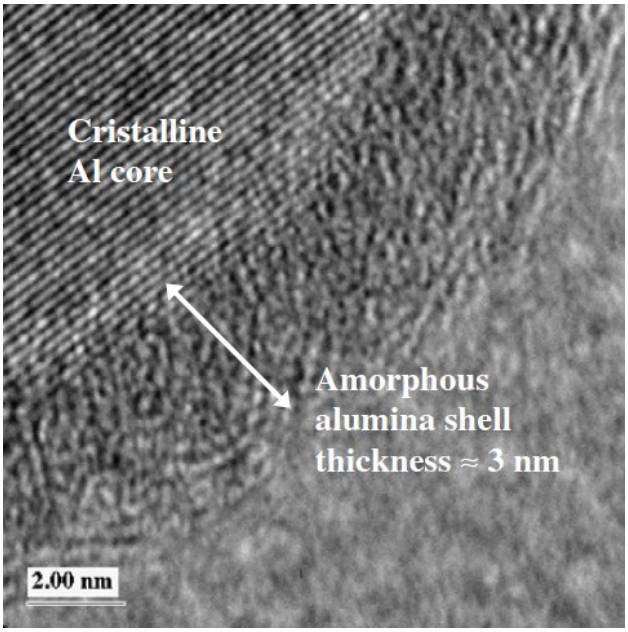

Figure 11 - HRTEM micrograph of aluminum powder skin cross-section [44].

Thermal exposure after powder production is known to alter the physical properties of the oxide skin. In this sense, heating the amorphous hydrated oxide allows a crystalline form of aluminum oxide to develop [43]. Figure 12 shows a HRTEM micrograph of a crystalline oxide phase that was produced after two DSC scans (2 K min^{-1} up to 700°C) [45]. In this instance, a portion has crystallized to transient γ-Al_2O_3. Further heating up to 950°C is expected to allow α-Al_2O_3 formation [43], the ultimate form of aluminum oxide.

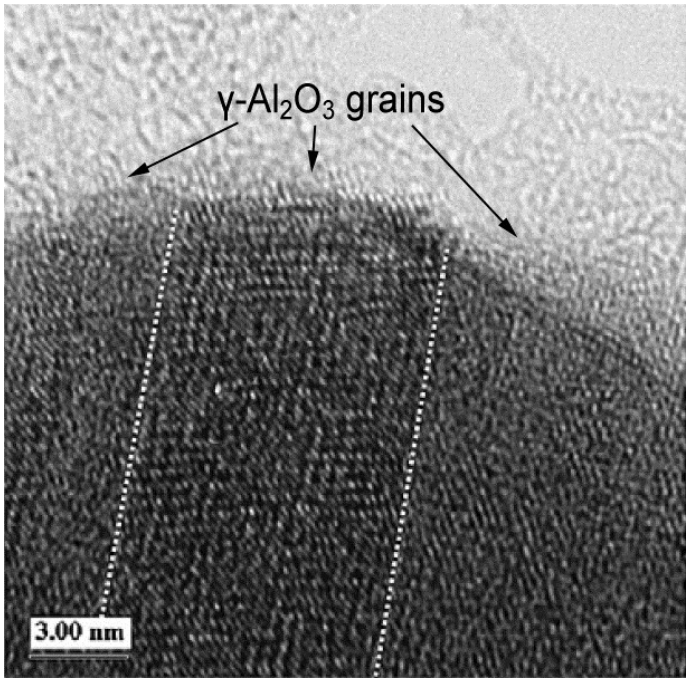

Figure 12 – HRTEM micrograph of the oxide shell region of an aluminum powder particle, showing the transient crystalline phase γ-Al_2O_3 [45].

To further understand the nature of the surface film changes, Dirras et al performed a DSC study on aluminum powders HIP processed at 450°C and 550°C [42]. These samples (with amorphous oxide skins on the starting raw powders) were heated to 700°C from ambient at a heating rate of 10 K min^{-1} and corrected to only show the heating event that occurred at ~500°C. Figure 13 shows the scan of aluminum HIP processed at 450°C. Here, an endothermic event at 527°C was noted; one that did not reverse upon cooling. For the sample processed at 550°C, this peak did not appear at all in heating or cooling traces. XRD spectra acquired from the HIP processed samples prior to DSC scanning are shown in Figure 14 [42]. At a HIP temperature of 450°C, metallic aluminum was the only observable phase; when sintered at 550°C a second set of peaks correlating to crystalline aluminum oxide was present. Thus, it was deduced that the DSC peak at 527°C resulted from the crystallization of the amorphous oxide film.

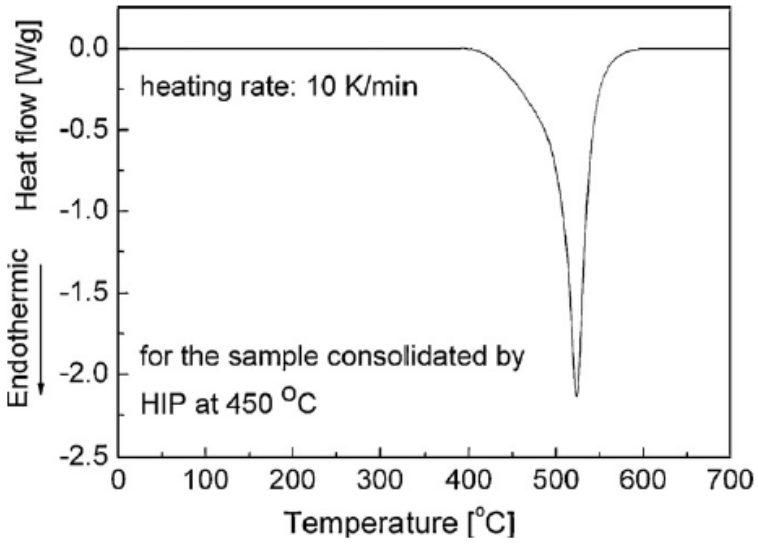

Figure 13 - DSC scan for a sample of pure aluminum powder HIP processed at 450°C [42].

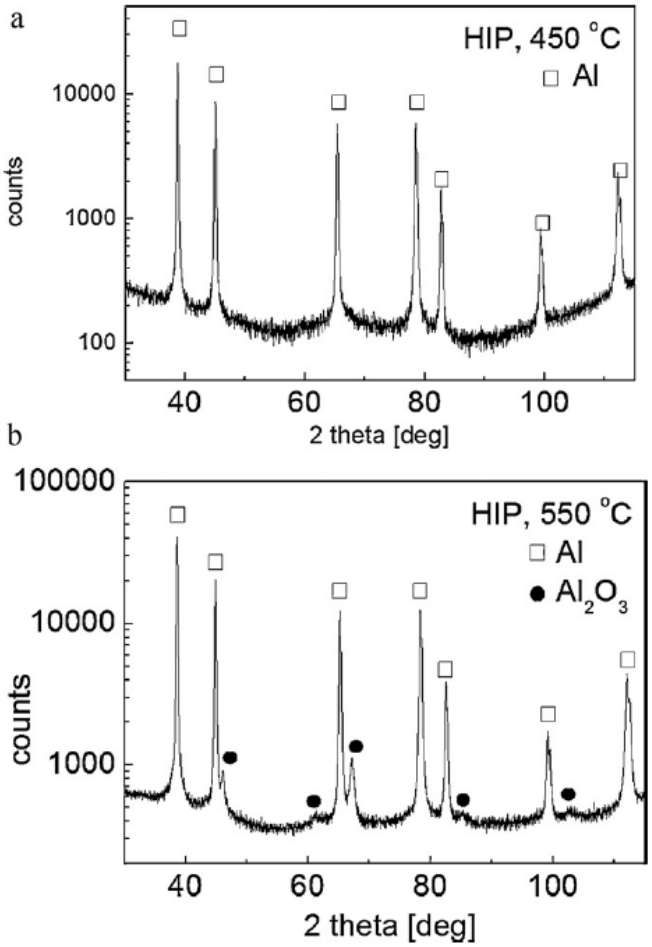

Figure 14 - XRD scan of aluminum powder HIP processed at (a) 450°C and (b) 550°C [42].

Equation 3 shows the possible progression of crystallization (phases in square brackets may not develop) that occurs due to thermal exposure of amorphous oxide [43].

$$Amorphous \rightarrow \gamma \rightarrow [\delta] \rightarrow [\theta] \rightarrow \alpha - Al_2O_3 \qquad \text{Equation 3}$$

Solid state powder consolidation/sintering techniques such as conventional pressing and sintering, cold isostatic pressing, hot isostatic pressing and hot pressing are generally not ideal processes for creating highly densified aluminum parts from powder feedstock. In these scenarios, the oxide phase on the surface is stable and remains on particle surfaces throughout processing. This inhibits the formation of strong metallic bonds [29] and leads to a semi-continuous network of residual oxides within the final product prompting brittle fracture in materials that should otherwise be ductile [44]. It is now known that this situation can be partially avoided through the use of SPS. Here, widespread metallic bonding has been found to exist throughout compacts of aluminum powders consolidated by SPS. This bonding is a product of the elevated temperature and the applied pressure involved in the process. When heated, the metallic component of an aluminum powder particle softens appreciably. The refractory aluminum oxide skin however does not undergo a similar degradation of mechanical strength. Ultimately, the very weak metallic aluminum is surrounded by a hard, brittle shell that fractures under the forces of the applied load. This fracture liberates the underlying metallic phase, allowing for adjacent particles to develop metallic bonds.

Ultimately, the nature of inter-particle bonds in SPS and APM products is quite different. For instance, Figure 15 and Figure 16 are HRTEM images contrasting the bonding that can occur when sintering pure aluminum by these techniques. Figure 15 represents the ideal condition, where two distinguishable grain orientations are identified, and there are no obstructions at the intersection of these grains. Figure 16 shows a more poorly sintered condition, where the precursory surface oxide film remains as a readily discernible feature at the intersection of two adjacent grains. In certain instances, this inter-particle region

manifests itself as a semi-continuous 3D oxide network, drastically reducing mechanical properties [47].

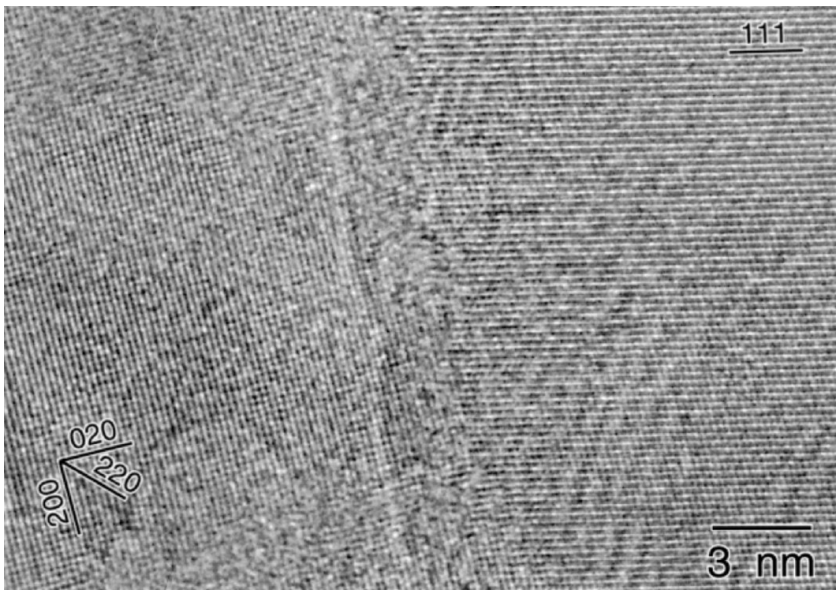

Figure 15 - HRTEM micrograph of typical metal/metal bonding in a compact of pure aluminum powder consolidated through SPS [25].

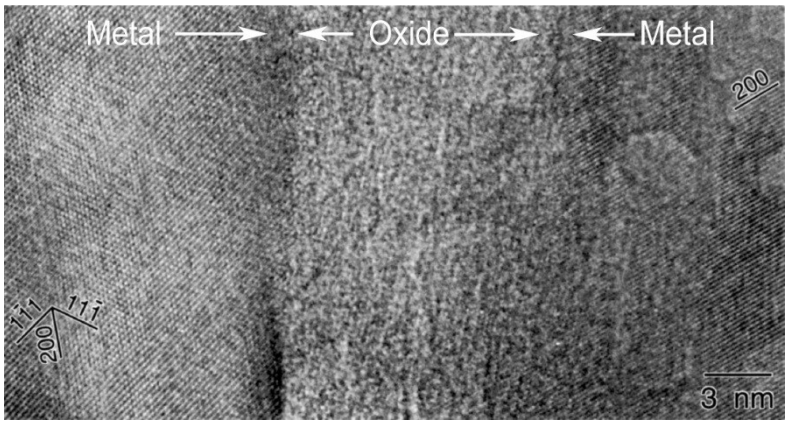

Figure 16 - HRTEM micrograph of typical metal/oxide/metal bonding in a compact of pure aluminum powder consolidated through APM [25].

1.3.1 Reducing the oxide layer

Given that magnesium plays such a crucial role in conventional APM, the effect of this addition in SPS was a logical progression from pure aluminum powders [9, 48]. For instance, Xie et al published several papers on this topic [26, 27]. Similar to pure aluminum, SPS invoked areas of metal/metal bonding in powders with prealloyed magnesium. However, in the magnesium doped samples, the amorphous oxide layer was replaced with magnesium-based precipitates. For samples with low magnesium content (<2.5wt%) or high sintering temperatures, a thermitic reaction was believed to have transpired thereby producing spinel ($MgAl_2O_4$) in accordance with Equation 1 [25]. Conversely, for lower temperatures and higher magnesium contents, magnesia (MgO) was the primary reaction product per Equation 4 [25]. In both cases, there was no definitive evidence of any Al_2O_3 remaining within the sintered product [20, 26, 27].

$$3Mg + Al_2O_3 \rightarrow 2Al + 3MgO \qquad \text{Equation 4}$$

Microstructurally, these reactions ultimately led to an inter-particle bonding zone that was comprised of a distribution of secondary phases within a metal matrix as shown schematically in Figure 17. The distinct change from an intermediate Al_2O_3 layer to discrete oxide particles is evident. With increasing magnesium content, the total volume fraction of these oxides increased accordingly, with MgO replacing $MgAl_2O_4$ for larger magnesium additions [25, 26, 27]. Overall, magnesium additions were found to bear decisive benefits to critical attributes such as tensile properties. The ideal magnesium content for SPS was determined to be in the range of 0.3-2.5wt%.

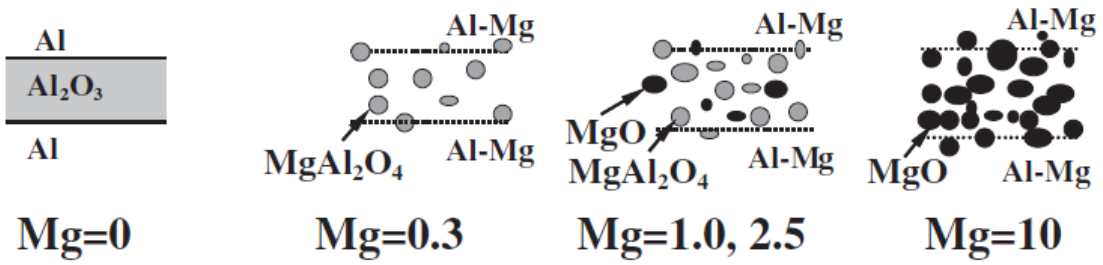

Figure 17 – Schematics that illustrate the effects of prealloyed magnesium additions (wt%) on the microstructure of the inter-particle bond formed between aluminum powders after SPS processing [21]. crystallisation

Several authors have also noted a possibility to reduce aluminum oxide by carbon in circumstances where temperatures are very high [29, 49]. From a thermodynamic standpoint, carbothermic reduction of alumina becomes spontaneous at temperatures above 2047°C [49]. During the initial stages of SPS processing, it has been theorized that interface temperatures may exceed several thousand degrees [39]. Furthermore, as the most common die material in SPS processing of aluminum is graphite, the possibility of a carbon-bearing atmosphere exists.

1.3.2 Volatilizing the oxide layer

Although a good understanding of SPS mechanisms has not been fully developed, it has been suggested that a surface cleansing effect may arise from the presence of a plasma [18]. In this, the adsorbed gas and impurities on the surface of powder particles would be eliminated by a spark impact pressure [50]. While little proof of sparking or the presence of a plasma during SPS processing exists, there is evidence of an ability to eliminate surface gasses.

Work by Bloch on the dispersion strengthening of aluminum from its residual oxide layer included an analysis of gas evolution from APM compacts [46] (Figure 18). For sintering

carried out between 300°C and 500°C, both the oxide and gas contents appeared to change very little. Residual gasses attributed with the powder were neither consumed nor removed by other means. However, sintering between 500°C and 550°C saw a drastic loss in gas content with a concurrent increase in the level of residual oxide in the compact. Hence, it was concluded that a decomposition reaction of the hydrated oxide layer at higher temperatures produced a water phase, prompting a subsequent reaction with aluminum to ultimately produce a heightened oxide content within the sintered product.

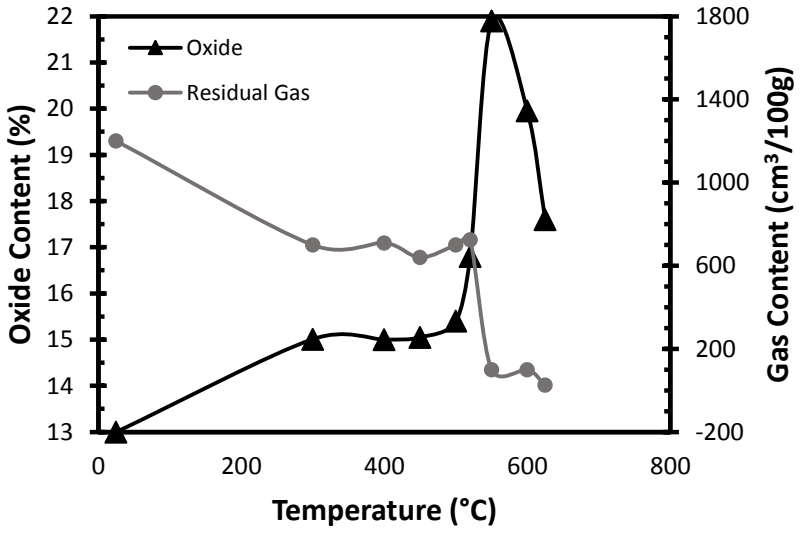

Figure 18 – Effect of sintering temperature on the variation of residual oxide and gas contents in compacts of sintered aluminum powder [46].

A more recent investigation of this phenomenon in SPS has revealed strikingly different results, as shown in Figure 19 [29]. Here, a pure aluminum powder was found to contain an oxide content of 0.403 wt% prior to SPS processing. Up to a temperature of 480°C the oxide content was similar to that of the starting powder. However, when processed at temperatures upwards of 540°C, a significant drop in oxide content was observed. While the temperature regime of this occurrence agrees with the work of Bloch, the result is opposing; rather than a gain in oxide upon exposure to elevated temperatures, there was actually a decrease. Since the oxide content was lowered, it is conceivable that a cleansing

effect by sparking, microplasma formation, and/or some other means unique to SPS processing may have actually occurred.

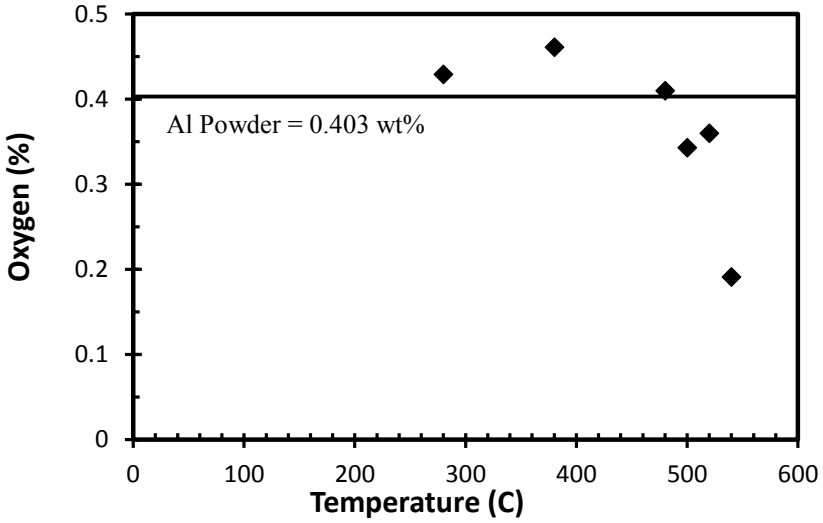

Figure 19 – Effect of SPS temperature on the residual oxide contents of sintered aluminum powder [29].

1.3.3 Fracturing the oxide layer

Beyond the aforementioned effects, studies have also shown that SPS processing can invoke physical fracturing of the oxide skin. This effect has been ascribed to the presence of high temperatures and an applied pressure, and emerges as another means to foster the formation of metallic bonds between adjacent powder particles [24]. As previously mentioned, the amorphous oxide skin inevitably crystallizes upon heating. Accompanying this crystallization is a significant densification of the oxide from roughly 2.4 g cm^{-3} (amorphous) to 3.97-3.98 g cm^{-3} (α-Al_2O_3). Hence, this densification is accompanied by a contraction in the oxide shell, whereby the corresponding state of stress at the surface is sufficient to fracture the oxide [51]. Thermogravimetric analysis (TGA) of aluminum powders heated to 1500°C in air is one approach that has been employed to demonstrate the fracturing effect (Figure 20). Here, from ambient to 600°C, referred to as 'Stage I', there is essentially no mass change. At ~600°C, 'Stage II' commences, as highlighted by a

small mass increase. At this point amorphous alumina crystallizes and fractures. This exposes metallic aluminum that oxidizes, thereby triggering the noted mass increase. This trend is then repeated two more times as γ-Al_2O_3 transforms progressively to θ-Al_2O_3 (Stage III) and ultimately α-Al_2O_3 (Stage IV), further fracturing the oxide layer and allowing progressively greater amounts of the underlying aluminum to oxidize. Given that this full range of temperatures (and well beyond) is expected to transpire at inter-particle contacts during SPS (Figure 7), it is conceivable that this entire sequence of phase transformations occurs. This should manifest appreciable fracturing of the oxide skin to the benefit of sintering and the attenuation of an increased fraction of metallic bonds.

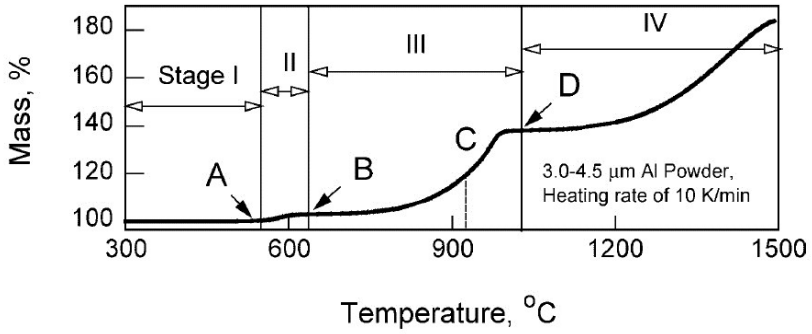

Figure 20 - Stages of oxidation of aluminum powders measured by TGA [43].

Figure 21 reveals the effect of particle size on oxide layer fracture [43]. Since the stresses developed on the surface of particles during a phase change are influenced by particle geometry, particle size is expected to have a significant affect. The rate of heating of a powder is plotted for three different particle sizes versus temperature, and simultaneously against the furnace heating rate. For relatively coarse powders self-heating exceeds furnace heating (termed 'ignition') only when relatively high temperatures are reached. Decreasing powder particle size sees this ignition phenomena occur at progressively lower temperatures. The fracture of oxide skin thus appears to be dependent on the size of powder particles considered. Smaller powders exhibit an ability to efficiently fracture their oxide layer at lower temperatures, while simultaneously providing a self-heating effect from the exothermic oxidation of aluminum.

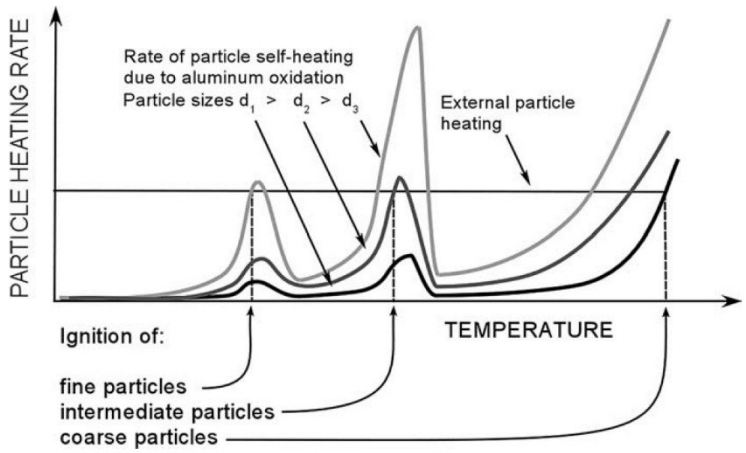

Figure 21 - Plot of the self-heating rate and 'ignition' for aluminum powders of differing average particle sizes [43].

CHAPTER 2. RESEARCH OBJECTIVES

The central objective of this research was to perform a fundamental assessment of the SPS response of air atomized aluminum powders and in doing so, determine the process parameters that have the greatest effect on the finished product. Key variables included the chemistry of the starting powder and the parameters (time, temperature, pressure) employed in SPS processing. In this, commercially pure air atomized aluminum was the baseline powder studied. A parallel study on a magnesium-doped powder was performed to determine the efficacy of this element as a sinter aid in SPS processing. Furthermore, iron and nickel-doped powders were investigated to assess their role and the ensuing strengthening mechanisms via secondary phase additions.

CHAPTER 3. MICROSTRUCTURE AND MECHANICAL PROPERTIES OF AIR ATOMIZED ALUMINUM POWDER CONSOLIDATED VIA SPARK PLASMA SINTERING

G.A. Sweet[1], M. Brochu[3], R.L. Hexemer Jr[4], I.W. Donaldson[5], and D.P. Bishop[2]

1 – Graduate Student, Dalhousie University, Halifax, Nova Scotia, Canada
2 – Professor, Materials Engineering, Dalhousie University, Halifax, Nova Scotia, Canada
3 – Professor, Materials Engineering, McGill University, Montreal, Quebec, Canada
4 – Research Engineer, GKN Sinter Metals LLC, Conover, North Carolina, USA
5 – Director of R&D North America, GKN Sinter Metals LLC, Auburn Hills, Michigan, USA

Status: Published. Materials Science and Engineering A. (2014) Volume 608. Pages 273-282

The following experimental procedures, results and discussions were completed by G.A. Sweet, with reviewer and editorial roles played by the subsequent authors.

Abstract

Two air atomized aluminum powders, one of commercial purity and the other magnesium-doped (0.4 wt%), were processed by SPS and APM means. An investigation of SPS processing parameters and their effect on sinter quality were investigated. A comparison with APM counterparts was also conducted. Applied pressure and ultimate processing temperature bore the greatest influence on processing, while heating rate and hold time showed a minor effect. Full density specimens were achieved for both powders under select processing conditions. To compliment this, large (80 mm) and small (20 mm) diameter samples were made to observe possible up-scaling effects, as well as tensile properties. Large samples were successfully processed, albeit with somewhat inferior densities to the smaller counterparts presumably due to the temperature inhomogeneity during processing. An investigation into tensile properties for SPS samples exhibited extensive ductility (~30%) at high sintering temperatures, while lower temperature SPS samples as well as all APM samples exhibited a brittle nature. The measurement of residual oxygen and hydrogen contents showed a significant elimination of both species in SPS samples under certain processing parameters when compared to APM equivalents

Keywords: Spark plasma sintering, Air atomization, aluminum, Mechanical properties, Microstructure, Residual Impurities.

3.1 Introduction

Spark plasma sintering (SPS) is a material processing technology in which powdered materials are consolidated into parts using the simultaneous application of pressure and electrical current. Unlike conventional press and sinter powder metallurgy (PM), where compaction and sintering are separate operations [52], SPS processing provides concurrent application of these stages. Specifically, a uniaxial pressure applied in conjunction with a pulsed direct-current flow through the powder and/or die is the fundamental concept of the process. While the exact underlying mechanisms of consolidation remain in dispute, several of those more commonly accepted are outlined by Hulbert *et al*. [53]. In systems where the current is able to pass through an electrically conductive powder, such as in aluminum, the heating is known to occur through Joule heating [54]. From this, relatively high heating rates are achievable, allowing very high thermal gradients to develop from the core to the surface of individual particles [55]. It has been hypothesized that during the initial stages of SPS, the interfaces of adjacent spherical particles have minimal contact area, and will consequently have high current densities. The joule heating effect is therefore concentrated at these contact points, resulting in a temperature far exceeding that of the set point [55], while the core remains relatively cool. In essence, the surfaces of particles are sintered, while the core is exposed to minimal thermal effects.

Regarding the relationship between aluminum and SPS, there has been extensive work completed on increasing the strength of aluminum [17]. Specifically, SPS processing of nano-grained materials has been shown to produce aluminum alloys with relatively high strengths [30, 56] as expected from a Hall-Petch standpoint. However, the tensile behavior of these nano-materials is more complex than this relationship leads it to be. For instance, research on wrought aluminum processed by accumulative roll bonding (ARB) has shown that as grain size is progressively reduced towards nano-sized territory, the susceptibility to a yield drop phenomena increases [57]. Essentially, when the grain size is reduced to or below 1 μm, the material rapidly becomes plastically unstable and can no longer maintain uniform ductility. While the microstructure of ARB and SPS processed aluminum differ with regards to the existence of prior particle boundaries, this phenomenon has been shown to be evident in SPS processed pure aluminum [51].

While the majority of aluminum SPS research pertains to the processing of nano-structured powders, there is a growing list of studies that are concerned with SPS response of aluminum powders in the as-atomized condition. Here, the effect of the oxide-based film that invariably exists on the surface of aluminum particles has been a key focal point [22, 23, 24, 25, 29]. In general, lower SPS temperatures result in metal/oxide/metal bonding, where adjacent powder particles can remain separated by the original refractory film [29] [25]. With higher temperatures, however, an increased ability to eliminate and/or disrupt the oxide-based layer has been observed, resulting in a high frequency of direct metal/metal bonding between powder particles. This ameliorated bonding appears to be a product of the physical breakdown of the hard oxide layer from the mechanical pressure applied [24]. However, in addition to this mechanism, Kwon et al. have noted a trend of decreasing residual oxygen content with increasing sintering temperature, far below that of the original powder [29]. This trend is unlike traditional PM, where the net concentrations of oxygen are more apt to increase during sintering as the compact reacts with the trace levels of oxygen invariably present in the gaseous sintering atmosphere.

Similar to conventional PM, it is now known that magnesium additions are beneficial to the sintering behaviour in SPS [21, 26, 27, 58]. In small amounts, magnesium reportedly reacts with the aluminum oxide skin to produce a magnesium-based oxide by-product of spinel ($MgAl_2O_4$) and/or periclase (MgO). This chemical action presents yet another means of disrupting the oxide film. As such, the relative density and tensile properties are substantially improved when the base powder is doped with magnesium [21]. In this study, a direct comparison of the conventional and SPS sintering behaviours of nominally pure aluminum powder and another doped with 0.4 wt% magnesium was undertaken. The investigation emphasized their response to select process parameters including applied pressure, heating rate, hold time, hold temperature and specimen size. These results have been quantified by physical and mechanical property tests supported by microstructural observations.

3.2 Materials

Two powders were considered in this work. One was commercial purity aluminum powder while the second was aluminum prealloyed with 0.4 weight % magnesium. These will be referred to in this work as 'Al' and 'Al-0.4Mg' respectively. Both powders were produced at Ecka Granules GmbH (Feurth, Germany) through gas atomization. The nominal starting chemistries are shown in Table 2. The average particle sizes of the powders were 133 μm for Al and 97 μm for Al-0.4Mg. To accurately calculate the extent of densification that occurred during sintering experiments, a concise theoretical density was calculated for each powder. This was done using a rule of mixtures approach based off the nominal composition and the measured oxide contents of the starting raw powders in accordance with the methods employed by the Aluminum Association [59]. Hence, full theoretical density values of 2.707 g cm^{-3} and 2.699 g cm^{-3} were calculated for Al and Al-0.4Mg respectively. In SPS experiments, all powders were processed in the as-received state. However, when a press-and-sinter APM approach was employed, each powder was admixed with a powdered lubricant (1.5 wt% Licowax C; Clarient Corporation) to facilitate die compaction.

Table 2 – Concentrations of the elements detected in raw powders (weight %).

	Composition (wt%)					
	Si	Fe	Cu	Mg	O	H
Al	0.072	0.105	0.001	0.002	0.3000	0.0069
Al-0.4Mg	0.029	0.110	0.001	0.398	0.1730	0.0045

3.3 Experimental

Samples processed by SPS were consolidated using a Model 10-3 unit manufactured by Thermal Technologies Inc. This was completed under a mechanical vacuum with graphite tooling, so as to yield a sintered disc with nominal dimensions of 20 mm diameter x 3 mm thick. The graphite die was ISO-Carb85 with a thermocouple hole drilled into the lower punch to within 2 mm of the sample surface. Sinter profiles involved heating rates of 50 K min^{-1}, 100 K min^{-1} or 500 K min^{-1} to an isothermal hold temperature (400 to 600°C) where

samples were held for 30 s, 120 s, or 300 s. Current was pulsed-DC, with a 36 ms on, 8 ms off pulse profile. Sintered samples were then furnace cooled to ambient under the vacuum atmosphere. A uni-axial pressure of 50 MPa was applied to each sample throughout the entire heating/cooling cycle. Larger (80 mm diameter x 15 mm) pucks were also consolidated via SPS, at FCT Systeme GmbH (Frankenblick, Germany). In an effort to maximize the relevance to lab-processed specimens, the majority of SPS processing parameters remained fixed for the larger specimens. These included a heating rate of 50 °C/min, sintering hold time of 120 s, and a uni-axial pressure of 50 MPa that was applied through the full sintering cycle. Isothermal sintering temperature was the key variable assessed with pucks produced at set points of 400, 450, 500, and 550°C.

For APM processing, an Instron 5594-200HVL load frame with a capacity of 1 MN was utilized for die compaction. All specimens were compacted at a fixed pressure of 200 MPa using rigid tooling that incorporated a floating-die concept. The geometries considered were flat dog bone specimens for tensile properties and discs (30 mm diameter x 4.5 mm height) for general sintering studies. Standard pressureless sintering was carried out using a three-zone horizontal tube furnace with a vacuum-tight stainless steel chamber. This chamber was evacuated and backfilled with high purity nitrogen (99.999%) twice, prior to the start of the heating cycle. A constant flow of nitrogen (34 m^3 hr^{-1}) was then maintained during the entire sintering cycle. This thermal profile began with a 20 minute isothermal hold at 400°C for delubrication purposes. This was followed by a secondary hold for sintering (20 minutes at 630°C) and cooling to ambient in a water jacketed section of the tubular retort. The heating rate was nominally 10°C/min.

Preliminary characterization included density measurements (MPIF standard 42) and apparent hardness using the Rockwell H scale. Samples were ground planar with 240 grit SiC abrasive paper prior to hardness measurements, but after density observations. Sections were then cold-mounted in epoxy and polished using a standard series of abrasive papers and diamond compounds. Final polishing was obtained using non-agglomerating colloidal silica on a Vibromet vibrating polisher for up to 24 hours. Optical imaging was completed

using an Olympus model BX51 light microscope. All samples were etched with Keller's reagent prior to imaging. To assess tensile properties, round tensile bars were machined from the 80 mm SPS samples while conventionally sintered tensile samples were of a flat dog bone geometry. All machined specimens were prepared with a geometry that was compliant with ASTM E8-M [60]. Dog bone tensile samples were tested on the same load frame used for pressing, with a 50 kN load cell and a 25mm gauge length extensometer. For machined round bars, a servo-hydraulic Instron load frame equipped with a 100 kN load cell was used. In both cases, an Epsilon Technology axial extensometer (model 3542) collected strain data, up to and including fracture. Bulk chemical assays were completed using ICP-OES whereas the analyses of oxygen and hydrogen contents were accomplished using inert gas fusion techniques.

3.4 Results and discussion

Preliminary work concentrated on the effect of applied pressure and heating rate solely on the Al powder. Specifically, this was done to identify a reasonable pressure that could be implemented during subsequent testing that explored the effects of sintering temperature, hold time at peak temperature, and sample size. For comparisons sake, data on conventionally sintered (press and sinter) specimens are also included. These will be referred to as "PM" samples, while the "SPS" designation represents those that were spark plasma sintered.

3.4.1 Effects of applied pressure

Al was SPS processed under a variety of applied pressures, from 20 MPa to 50 MPa. For these tests, a heating rate of 100 °C/min, a sintering temperature of 500°C and a hold time of 300 s were maintained in all instances. Data on the effect of this parameter on specimen density and hardness are shown in Figure 22. The findings showed a clear advantage of processing under higher applied pressures. In this sense, the density rapidly increased from 96.73% at 20 MPa up to 99.77% at 50MPa. This was accompanied by a concurrent increase in hardness from 46 to ~53HRH. This behaviour was typical of sintered parts, where a decrease in residual porosity generally increases mechanical properties such as hardness.

The applied pressure during SPS processing allows powder particles to slide and rearrange in a way that increases the packing factor [52]. Furthermore, the heated particles are much weaker than they would be at room temperature. This softening allows for significant plastic deformation and further densification. Increasing pressure both aids in the rearrangement of particles in the early stages of sintering, as well as increasing the ability to plastically deform and densify. This trend has been shown before in aluminum powders [22], where dramatic increases in relative density were observed with pressure increases comparable to those assessed in this work. Given that the benefit of using the highest pressure was obvious, all subsequent SPS tests employed a singular pressure of 50 MPa.

3.4.2 Effects of heating rate

When assessing the impact of heating rate, values of 50, 100 and 500 K min^{-1} were considered. Data on sintered density and hardness as functions of this attribute are shown in Figure 23. Unlike applied pressure, heating rate effects were minimal. Relative density increased from 99.24% to 99.75% when the heating rate was increased 10-fold from 50 to 500 K min^{-1}, respectively. A temperature difference between thermocouple output and powder bed has been shown to exist, and is prominent during early stages of heating [61], leading to an erroneously low process temperature value. With increased heating rates these temperature gradients would increase, meaning the powder is subject to greater temperatures earlier in the run. It is therefore difficult to isolate the effects of the increased heating rate and the temperature overshoot. While this resulted in as an ability to densify, the overall benefit was manifested as a marginal increase [61]. From a density perspective, it was determined these gains were not substantial enough to warrant the highest heating rate for future tests. Hardness also remained essentially unchanged hovering at a value of ~52 HRH for all heating rates. Although it is expected that a shorter consolidation time from the expedited heating would better preserve a fine grain structure [34] this did not yield any tangible hardness improvement in the current work. With relatively small changes in density, it appears any mechanical gains are overshadowed by measurement error. Hence, a heating rate of 100 K min^{-1} was employed in all subsequent SPS trials unless otherwise noted.

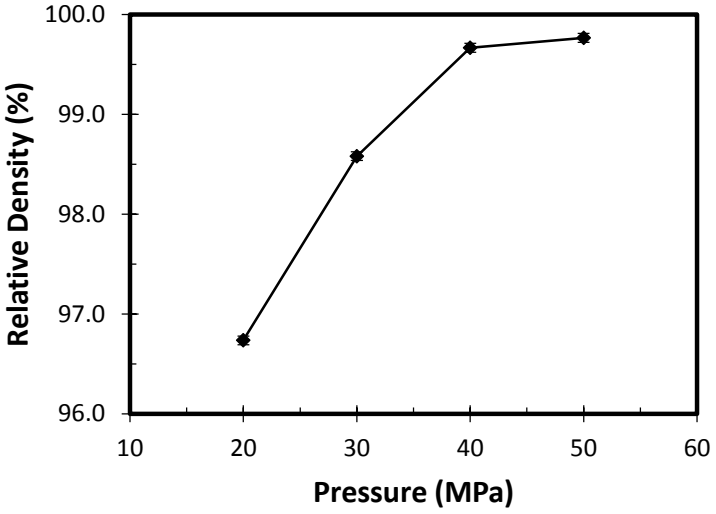

(a)

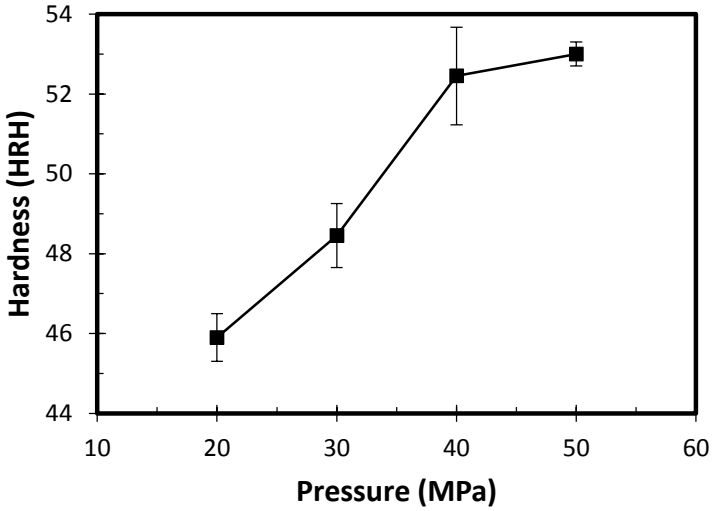

(b)

Figure 22 - Effect of applied pressure on the (a) relative density and (b) hardness of SPS-processed compacts of Al powder. All samples heated at 100 K min-1 to 500°C and isothermally held for 300 seconds prior to cooling.

3.4.3 Effects of hold time

The effect of hold time was investigated by performing experiments wherein specimens were heated to a sintering temperature of 500°C. Hold time ranged from 30 to 300 s and parallel experiments were completed on Al and Al-0.4Mg powders. Data on the effect of this parameter on density and hardness are shown in Figure 24. Regarding the former, several interesting points were noted. For instance, it was clear that even with an abbreviated sintering time of 30 s that both powders were processed to a relatively high density in excess of 99% of theoretical. Extensions in the sintering time prompted minor density gains in both materials yet the effect was more pronounced in the Al powder. It was also observed that Al-0.4Mg was processed to a higher density in all instances. Indeed, at a hold time of 300s, it appears the magnesium doped sample was essentially void of any residual porosity.

Enhanced densification in the magnesium bearing powder was consistent with the works of other authors wherein magnesium additions were found to invoke positive gains in densification during SPS studies [21] and in APM processing [62]. In these works metallic magnesium possessed a higher affinity for oxygen than aluminum, and thus was able to reduce the inevitable Al_2O_3-based skin on the surface of aluminum powder particles. The magnesium oxide by-products precipitated many discrete crystalline particles, rather than a coherent layer. Adjacent powder particles were then able to achieve metallic bonds and promote densification. Hence, it was postulated that a similar phenomenon transpired in this instance thereby allowing samples of Al-0.4Mg to attain a higher sintered density under all conditions assessed.

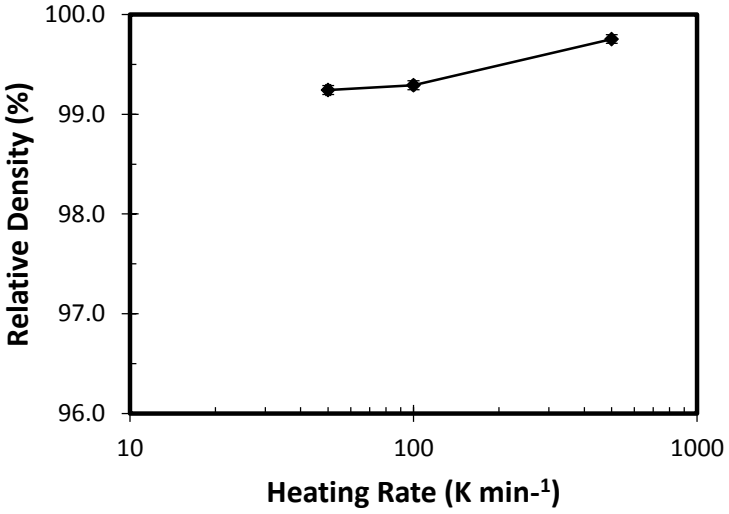

(a)

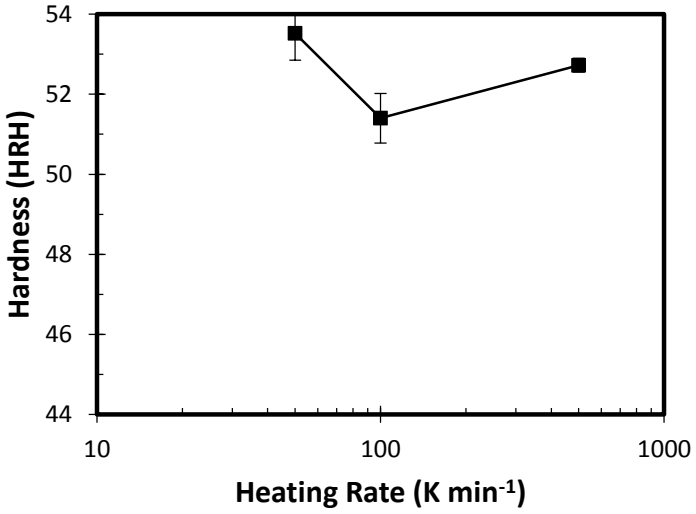

(b)

Figure 23 - Effects of heating rate on the (a) relative density and (b) hardness of SPS-processed samples of Al powder. All samples were subjected to an applied pressure of 50MPa, heated to 500°C and isothermally held for 300 seconds prior to cooling.

Under all hold times an appreciably higher hardness was recorded in the samples alloyed with magnesium (Figure 24(b)). This element is an effective strengthening agent for aluminum in light of its ability to form a solid solution and dispersoid phases such as

Al_3Mg_2. Given the comparable density in materials with and without magnesium, the increased hardness in Al-0.4Mg was ascribed to the aforementioned strengthening features. As all samples were sintered to a density that impinged upon 100% of full theoretical, dramatic increases in hardness with hold time were not anticipated. This was consistent with the trends noted in Figure 24(b) in that no measureable change occurred in the Al powder samples and, if anything, a modest decrease in hardness transpired in specimens of Al-0.4Mg for hold times in excess of 120s. The downward trend for this was believed to be the result of a coarsening grain size and the elimination of subgrain microstructure as discussed in subsequent sections. To avoid this transition yet maintain a relatively high sintered density, a sintering time of 120s was deemed to be a reasonable target. This was employed in all of the tests pertaining to the effects of sintering temperature and specimen size described in the following sections.

3.4.4 Effects of hold temperature

To explore the effects of hold temperature, samples of each powder were sintered at 400 to 600°C and characterized. The resultant data on density and hardness are shown in Figure 25. The effect of sintering temperature appeared to be the most dramatic of all processing parameters. For Al powder samples a steep linear increase in density was observed from 98.42% at 400°C to 99.92% at 600°C, wherein essentially full density was attained. This coincided with the densification mechanisms in SPS (power-law creep [34, 37], plastic yielding and grain boundary diffusion [61]), whereby increased temperatures facilitate plastic deformation. A similar trend was observed for Al-0.4Mg where increasing sintering temperatures improved density up to 99.97% at 600°C. For sintering temperatures below 600°C, a difference of >0.5% of theoretical was observed between Al and Al-0.4Mg samples. This was attributed to the ability of small additions of magnesium to disrupt the oxide layer on particle surfaces as discussed in the previous section. It appeared that when densification occurred through mechanical fracture, as is the case for the Al system, full densification was only achieved at a temperature of 600°C. By coupling these mechanisms with the aid of a chemical reduction reaction (i.e. Al-0.4Mg) fully densified samples were achieved at temperatures ~100°C lower. This trend was consistent with observations of other authors [21].

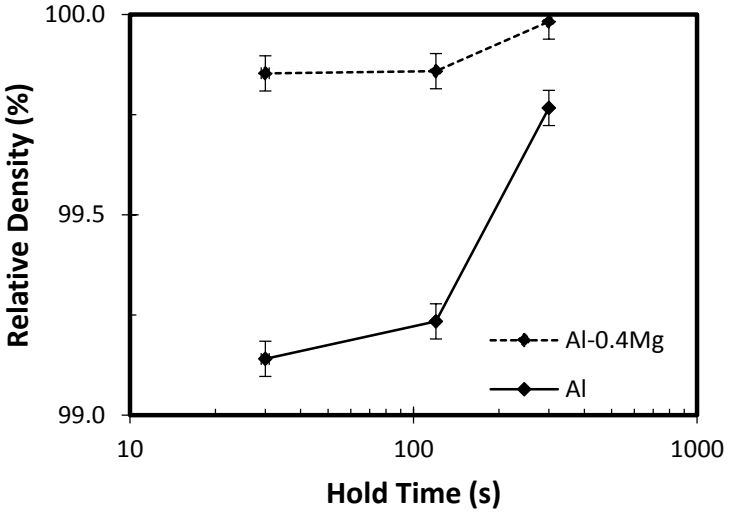

(a)

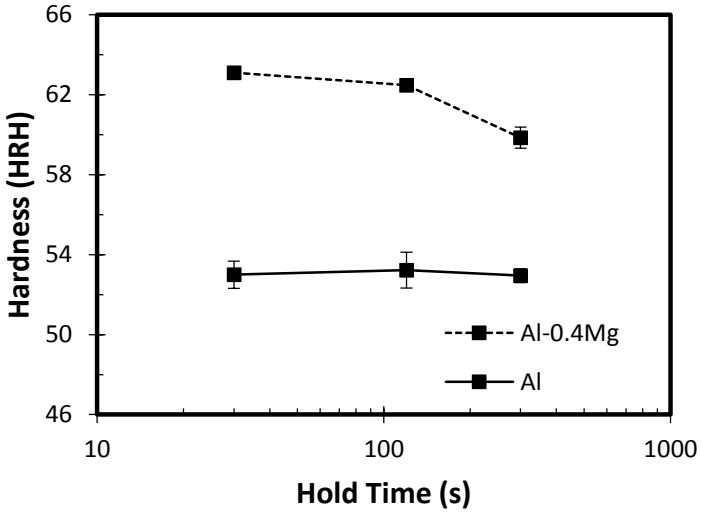

(b)

Figure 24 - The effect of hold time at sintering temperature on (a) relative density and (b) hardness of samples prepared from Al and Al-0.4Mg powder. All samples were subjected to an applied pressure of 50MPa, heated to 500°C at a rate of 100K min^{-1} and isothermally held for the times indicated.

A decrease in hardness with increased thermal exposure temperature was observed for both powders. This phenomenon was best explained with reference to Figure 26, which includes optical micrographs of raw Al powder, as well as samples sintered at 400°C and 600°C. The microstructure of the starting Al powder (Figure 26 (a)) was equiaxed with a nominal cell size on the order of 5μm. When sintered at 400°C (Figure 26 (b)) the initial cellular microstructure was still clearly evident in many regions while in others it had begun to coarsen. Prior-particle boundaries were also apparent as dark, continuous lines that represented oxide rich regions stemming from the original surfaces of the raw particles [22]. When the extent of thermal exposure was increased through sintering at 600°C (Figure 26 (c)), widespread microstructural coarsening occurred, given that the starting cellular structure was now eliminated. However, the oxide-rich particle boundaries were still present and appeared to be largely consistent in morphology and size to those of the 400°C sample. Hence, the softening effect noted in Figure 24(b), was principally attributed to the gradual elimination of the starting cellular structure.

SEM examination of the dark feathered regions persistent in etched mounts of both the raw powder and sintered products revealed localized pitting and small concentrations of iron. Hence, it is likely that they were simply the result of preferential etching of an iron aluminide phase present within the microstructure. This was consistent with the detection of iron in the starting powder (Table 2) and the absence of such features in unetched specimens. Considering the SPS processing parameters assessed, it can be summarized that the most influential variables were applied pressure and sintering temperature. While hold time and heating rate showed positive gains in properties, the effects were relatively minor.

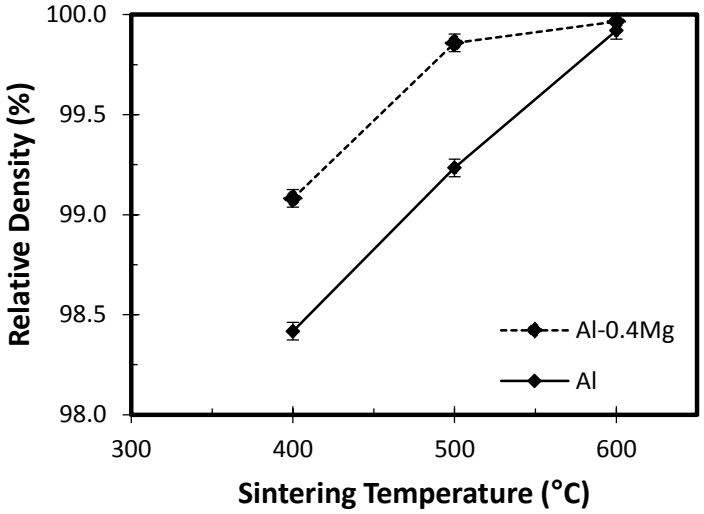

(a)

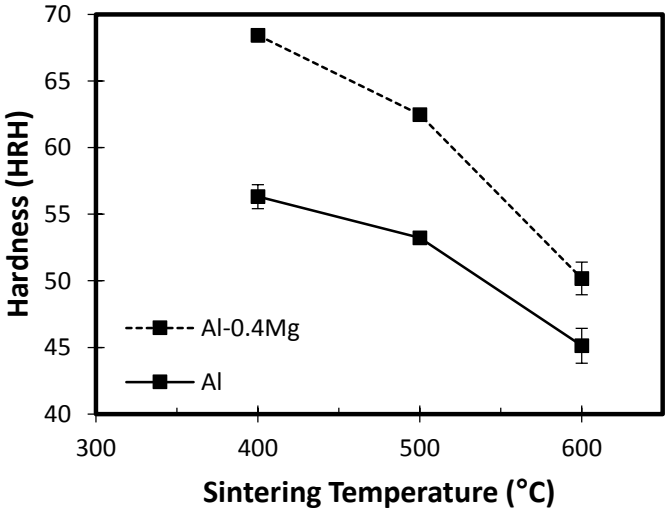

(b)

Figure 25 - Effect of sintering temperature on the (a) relative density and (b) hardness of samples prepared from Al and Al-0.4Mg powders. All samples were subjected to an applied pressure of 50MPa, heated to the temperatures indicated at a rate of 100 K min^{-1}.

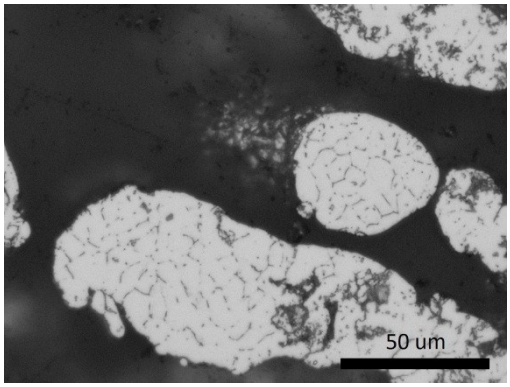

(a)

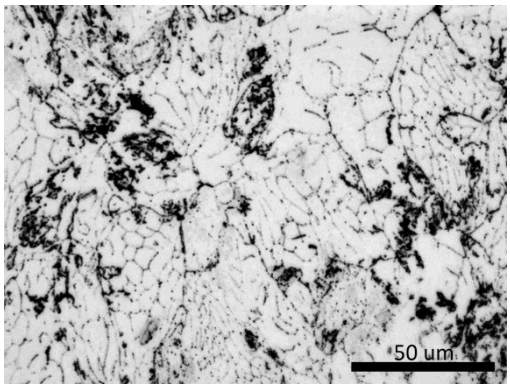

(b)

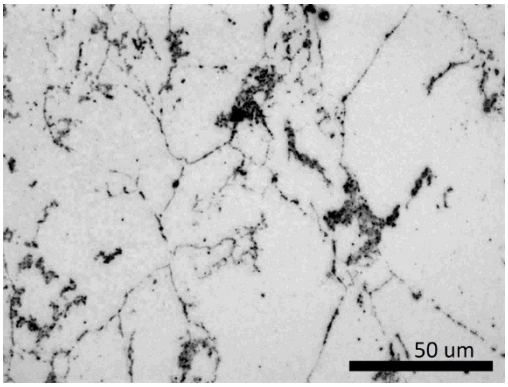

(c)

Figure 26 - Optical micrographs of Al powder specimens highlighting the progressive change in microstructure with increasing SPS temperature. (a) Raw Al powder, (b) sintered at 400°C and (c) sintered at 600°C.

Prior studies have suggested that SPS may offer an ability to remove impurities from the surfaces of sintering particles [29]. As this was viewed as a potentially unique and strategic advantage, the residual concentrations of oxygen and hydrogen were assessed for numerous SPS products (Figure 27). When sintered at 400°C the concentrations of both impurities were reduced to levels below those measured in the starting raw powders, although the effect was relatively minor. Impurity reduction then improved as sintering temperature increased. The impact was greatest for hydrogen as the majority of this gas was eliminated through SPS processing at the highest temperature considered (600°C). Here, the final values were in the range of 5-10ppm; concentrations that were largely comparable to wrought aluminum alloys. The general extent of hydrogen removal was similar for both powders implying that prealloyed magnesium did not play a decisive role. Oxygen contents were also appreciably reduced in samples processed by SPS at 600°C. However, unlike hydrogen, tangible amounts remained in the final compact and it appeared that prealloyed magnesium was a factor of influence.

It was postulated that the observed trends in oxygen and hydrogen removal were partially related to the hydrated surface oxide film known to exist on atomized aluminum powders. The nature of this phase is a direct result of fabrication and handling of powders in moisture laden environments [63]. In these settings, water enters the system in a physisorbed (H_2O) and/or chemisorbed ($Al_2O_3 \cdot 3H_2O$ [63, 64, 65, 66] or $Al(OH)_3$ [65, 67]) manner, dependant on the nature of the environment and the length of exposure [64, 68]. It is also known that powder chemistry influences the extent of hydration [64]. For instance, the work of Yamasaki and Kawamira has shown that prealloyed magnesium additions reduce the effect [66]. In addition to the Al_2O_3 component itself, water molecules (and the respective contents of hydrogen and oxygen) play a significant role in the end composition of a sintered aluminum product, regardless of the processing approach employed. Hence, extensive research has been conducted on the vacuum degassing response of aluminum powders [63, 64, 65, 66, 67, 68]. In these processes, the low pressures coupled with moderate temperatures reduce the free energy of decomposition of these hydrate phases to a value sufficient for the reactions to become spontaneous. The off-gassing of the ensuing reaction products then occurs through interconnected porosity (for loosely compacted

samples or raw powders) and is removed via the vacuum pump. Degassing time is generally on the order of hours to maximize the elimination of gaseous products [64, 66, 68].

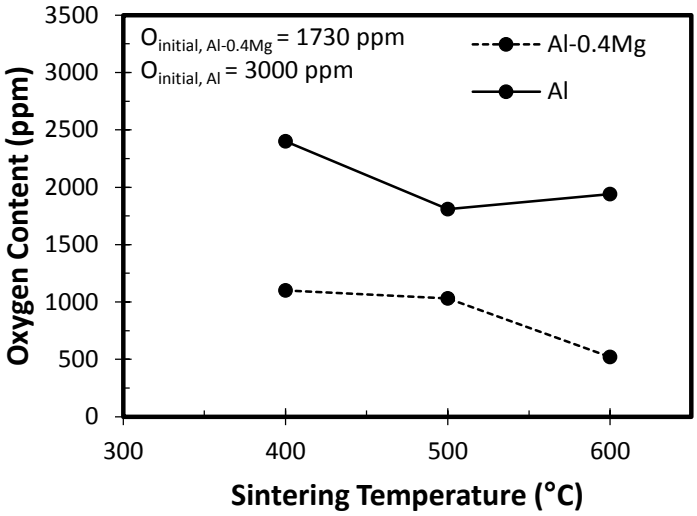

(a)

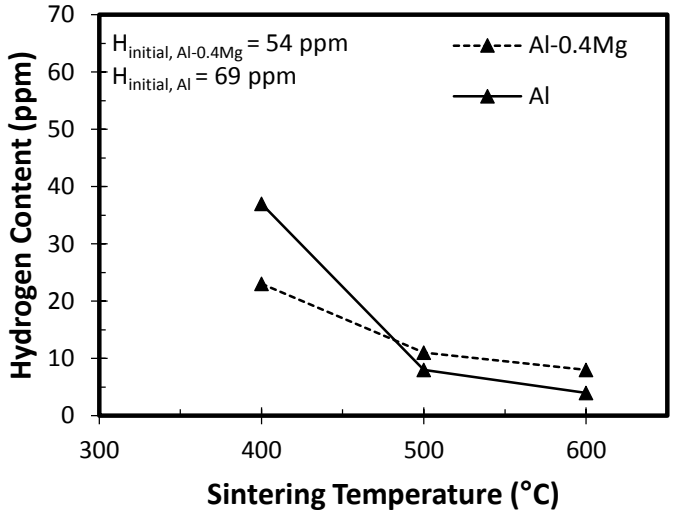

(b)

Figure 27 - Effect of sintering temperature on the residual contents of (a) oxygen and (b) hydrogen measured in SPS samples processed in a laboratory environment.

As the degassing temperature increases, several phenomenon are known to occur. First, the release of loosely-bound physisorbed water transpires at low temperatures, generally below 175°C [63, 66, 68]. This is then followed by the release of chemisorbed water. Due to the varying nature of this phase and its response to thermal exposure, decomposition occurs over a wider temperature range known to span from 150°C to 550°C [63, 64, 65, 66, 68]. While the specific decomposition reactions in the open literature are numerous, Equation 5 [64, 65, 66] and Equation 6 [42, 51, 65] represent the net transformation that occurs for the two most commonly cited phases. Another phenomenon is the liberation of hydrogen gas, which occurs above 200°C [64] and then peaks at ~450°C [65]. This is typically accepted as a product of metallic aluminum (and/or magnesium if present) reacting with water vapor liberated through Equation 5 and Equation 6 to form a fresh oxide phase as well as gaseous hydrogen [51, 63, 64, 65, 66] per Equation 7 and Equation 8.

$$Al_2O_3 \cdot 3H_2O \rightarrow Al_2O_3 + 3H_2O \qquad \text{Equation 5}$$

$$2Al(OH)_3 \rightarrow Al_2O_3 + 3\,H_2O \qquad \text{Equation 6}$$

$$2\,Al + 3\,H_2O \rightarrow Al_2O_3 + 3\,H_2 \qquad \text{Equation 7}$$

$$Mg + H_2O \rightarrow MgO + H_2 \qquad \text{Equation 8}$$

Evaluation of the net change in hydrogen and oxygen contents between the initial powders and the final sintered products can provide a measure of insight on the degassing condition(s) that had likely occurred during SPS processing. In this sense, if the ratio of the net mass loss of O:H was on the order of 8:1, it would be expected that the principal product off gassed through SPS was water and that Equation 5 and Equation 6 would be dominant. If this ratio was less than the nominal 8:1 value then it could be inferred that a stoichiometric excess of hydrogen was released and that the full sequence of Equation 5-Equation 8 had likely transpired. Quantification of the O:H ratios revealed values that ranged from 16:1 to 20:1 for Al powder specimens and from 16:1 to 27:1 for those prepared from Al-0.4Mg powder. Hence, in all instances a stoichiometric excess of oxygen was released in contrast to the anticipated result that the O:H ratio would be ≤ 8:1. Plausible

sources of the excess oxygen include the removal of adsorbed gaseous oxygen [63] and the release of CO and/or CO_2 gases [64, 68]. Overall, it is worthy to note that the residual O/H concentrations in SPS samples were appreciably lower than those typically measured in conventionally degassed/sintered APM products [69, 70].

3.4.5 Effects of specimen size

Laboratory-scale processing indicated that sintering temperature was a critical processing variable and that the presence of prealloyed magnesium had a positive impact on the extent of sintering as well as impurity removal. In an effort to determine if these same findings would persevere in specimens of a more commercially relevant size, slugs with a 16-fold increase in surface area were produced from Al-0.4Mg powder and characterized. Increased sample size had a significant impact on sintered density (Figure 28). For example, the 20 mm samples exhibited a relative density in excess of 99% over the full range of temperatures studied. Conversely, sintering temperature was clearly a factor of greater influence for the density of the larger slugs, as values only impinged on the full theoretical limit at the highest temperature considered. Although data in the open literature that address the effects of SPS sample size are limited, it has been demonstrated that temperature uniformity with an SPS compact is influenced by tooling geometry [71]. Hence, it is postulated that the actual internal temperatures were farther removed from the set point in the case of the larger specimens. This would have reduced the extent of plastic deformation achieved during the SPS cycle and in turn, lowered the final sintered density attained.

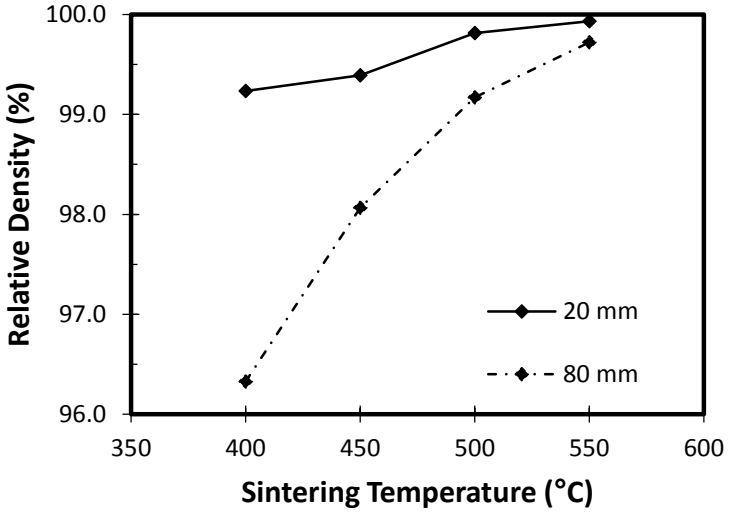

Figure 28 - Effect of sintering temperature on the density of 20mm and 80mm diameter slugs consolidated by SPS.

Data on the measured concentrations of residual oxygen and hydrogen are shown in Figure 29. At 400°C, the residual gas contents were higher than those measured in the starting powder. At 450°C a mixed response was then noted as the hydrogen content was greater than the initial powder while the oxygen was lower. At even higher temperatures ($T \geq 500°C$), the concentrations of both residuals were significantly lower than the levels measured in the raw powder and similar to data acquired from the smaller 20mm samples processed in a laboratory setting (Figure 27). The steep transitions noted in the larger pucks were theorized to be a result of varying concentrations of residual porosity coupled with surface activation. In this sense, specimens sintered at the lower temperatures had a relatively low density and in turn, relatively high surface area/unit volume in the post-sintered condition. Furthermore, the effects of SPS processing are largely concentrated on the surfaces of powder particles. This clearly had an impact on the aluminum hydroxide surface film in the powders of this study as evident by the data of Figure 27 wherein reductions in oxygen and hydrogen content were confirmed. While the exact state of the residual surface area remains unclear, it would have invariably been disturbed from the equilibrium condition (aluminum hydroxide) and thereby displaced into an active condition

as a result of SPS processing. It is postulated that the active surface area of sintered specimens would have then re-hydrated upon removal from the protective vacuum environment of the SPS unit to an extent that exceeded that measured in the starting raw powder. The extent of this phenomenon would have scaled directly with the amount of surface area in a sintered compact (and inversely with density) prompting the observed trends in oxygen and hydrogen concentrations. Regardless of the exact mechanism at hand, processing the larger slugs at higher temperatures was ultimately able to produce samples with a modest concentration of residual oxygen and wrought-like levels of hydrogen.

Given the size of the larger slugs, a series of full-sized tensile bars were readily machined from each specimen. Tensile properties were then quantified as functions of SPS temperature (Figure 30). For all temperatures considered, the 0.2% offset yield strength was relatively consistent whereas the ultimate tensile strength (UTS) and elongation to fracture trended upward with rising temperature. The most acute transition occurred for ductility. This attribute increased from 0.9% at 400°C to 2.5% at 450°C indicating a gradual improvement in the quality of inter-particle bonds. However, a continued increase in sintering temperature to values ≥500°C facilitated an order of magnitude spike in ductility to ~28%. The progressive improvement in ductility led to an increase in UTS as well given the enhanced capacity for work hardening within the material.

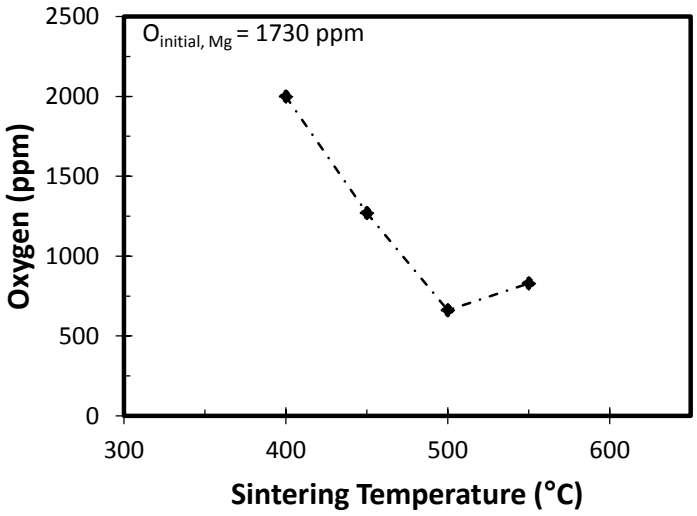

(a)

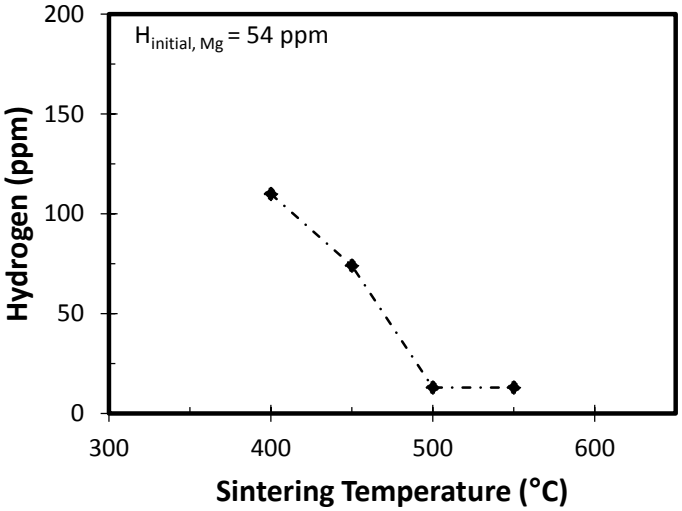

(b)

Figure 29 - Effects of sintering temperature on the residual contents of (a) oxygen and (b) hydrogen measured in 80mm diameter SPS samples processed in an industrial setting.

Prior studies have noted that the volume fraction of metal-metal particle bonding (i.e. inter-particle interfaces wherein the oxide film was disrupted or completely eliminated) was largely responsible for the development of enhanced tensile properties [27]. In this regard, higher temperatures softened powder particles sufficiently to allow the applied

current/pressure to fracture the thin oxide shell and expose the underlying aluminum. Metallic bonding was then realized between adjacent particles prompting a rise in tensile ductility. It is assumed that a similar mechanism had transpired in this instance. However, it is also worthy to note that the amounts of residual hydrogen and oxygen in the larger slugs tracked well with tensile ductility (Figure 30). In this sense, the concentration of each element trended downward with rising ductility and then flattened at higher temperatures as ductility gains likewise became less acute. These data indicated that the surface impurities (and reducing the concentrations thereof) also played a key role in the attenuation of SPS products with enhanced tensile properties.

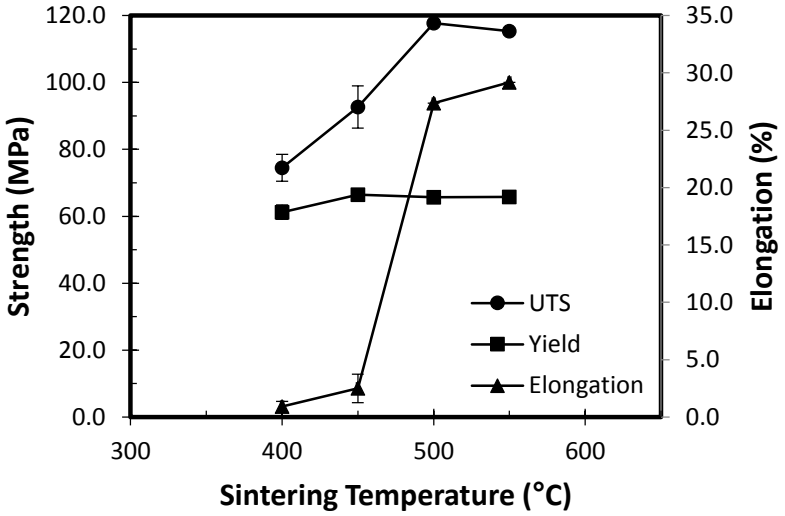

Figure 30 -Effects of SPS temperature on the tensile properties of Al-0.4Mg.

3.4.6 Comparison to conventional PM

The conventional processing of aluminum-based powders is most commonly accomplished through a press-and-sinter approach. Referred to here as APM processing, this route yields sintered compacts through a combination of uni-axial die compaction coupled with pressureless sintering in an atmosphere of flowing, high purity nitrogen. This procedure is utilized on a commercial scale for numerous materials largely premised on the Al-Cu-Mg [72, 73, 74], Al-Si-Mg [75] and Al-Zn-Mg [76, 77] systems. Given the commercial

importance of this technology, a direct comparison between SPS samples and those fabricated through an APM approach was undertaken. Data on sintered density for the two processes are displayed in Figure 31. It can be seen that for SPS samples alone, full density was achieved for both powders. Densification was appreciably lower in the APM products with a maximum value of 95% realized. APM samples lacked the pressure assisted densification of SPS [5]. Furthermore, the powders in question were exceptionally challenging materials to sinter in a conventional manner given the absence of a liquid phase and the thermodynamic stability of the oxide surface layer encasing the powder particles. Hence, a similar final density was not attained in the APM specimens.

The residual oxygen/hydrogen contents of SPS and APM samples are compared in Table 3. In each instance the SPS products were clearly advantageous offering lower concentrations of both impurities relative to the starting raw powders and the sintered APM counterparts. APM processing was somewhat effective at lowering hydrogen concentration, yet it also imparted an increase in the bulk oxygen content; observations consistent with the work of others studying the conventional sintering response of aluminum powders [78]. This effect was ascribed to the thermal de-hydration/oxidation of the surface film, consistent with the work of Le et al [51]. Here, the initial heating of aluminum powder caused the hydroxide surface layer to decompose. However, continued heating caused the liberated water vapour to react with metallic aluminum per equation 3. This oxidized the aluminum and left hydrogen as the only gaseous species effectively removed from the sintered compact.

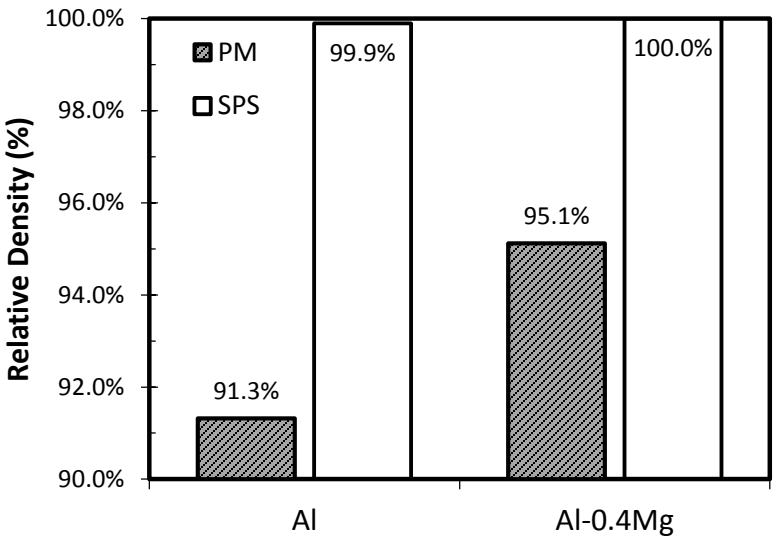

Figure 31 - Comparison of the sintered densities measured for materials prepared through SPS processing and conventional PM.

Figure 32 compares the tensile response of SPS samples as well as their APM counterparts for both Al and Al-0.4Mg powders. For Al powder, SPS processing provided a dramatic benefit over conventional PM. Not surprisingly, sintered APM compacts offered no capacity for plastic deformation. This was consistent with microstructural observations (Figure 33(a)) that confirmed a lack of microstructural development and the effective absence of inter-particle bonding. Here, residual porosity was evident throughout the image as was an abundance of prior particle boundaries. In contrast, the properties of SPS Al products were very well aligned with 1xxx series wrought aluminum materials in an annealed condition [79]. The metallurgical quality of the SPS material was also evident in the microstructure (Figure 33(c)) as none of the deleterious attributes rampant within the APM material were observed.

Table 3 – Comparison of the oxygen and hydrogen contents (ppm) measured in the raw powders and sintered products consolidated via APM and SPS processing.

	Al (ppm)		Al-0.4Mg (ppm)	
	Oxygen	Hydrogen	Oxygen	Hydrogen
Powder	3000	69	1730	54
APM	3200	26	2400	30
SPS	**1940**	**4**	**520**	**8**

With the addition of magnesium, the tensile behaviour of APM samples improved. This was as expected given the beneficial role that this element is known to play in the sintering of aluminum powders [62, 78, 80]. Evidence in support of the improved properties was apparent in the sintered microstructure (Figure 33(b)). This included a reduced amount of residual porosity and the presence of a secondary phase along the majority of particle interfaces. This constituent was most likely AlN, based on prior studies of similar APM materials [62]. Its presence confirms that the oxide-based shell on powder particles was disrupted by the magnesium addition to a point where exposed metallic aluminum was able to react with the nitrogen atmosphere. Despite the gains accrued through magnesium addition, properties of the APM product were still significantly inferior to those of the SPS counterpart. Once again, the difference was most acute for ductility as the SPS samples maintained a 10-fold advantage.

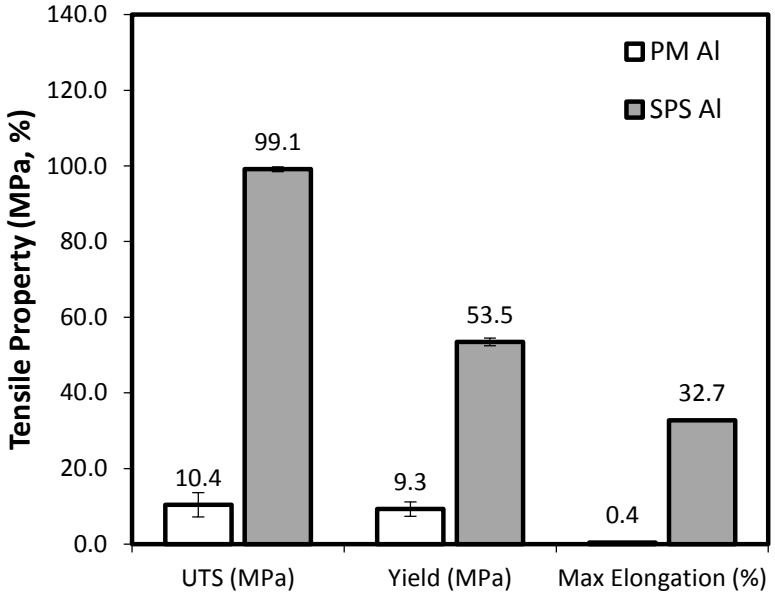

(a)

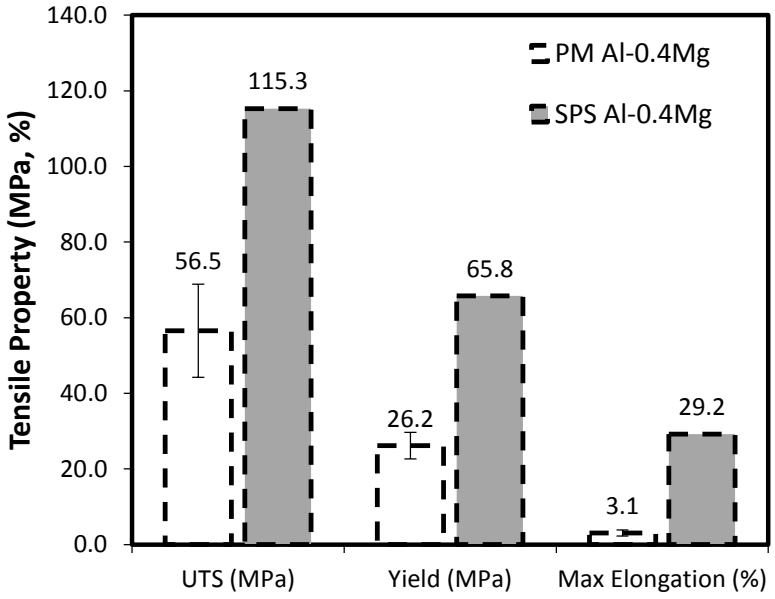

(b)

Figure 32 - Comparison of the tensile properties measured for materials prepared through conventional APM and SPS processing. (a) Al and (b) Al-0.4Mg powders.

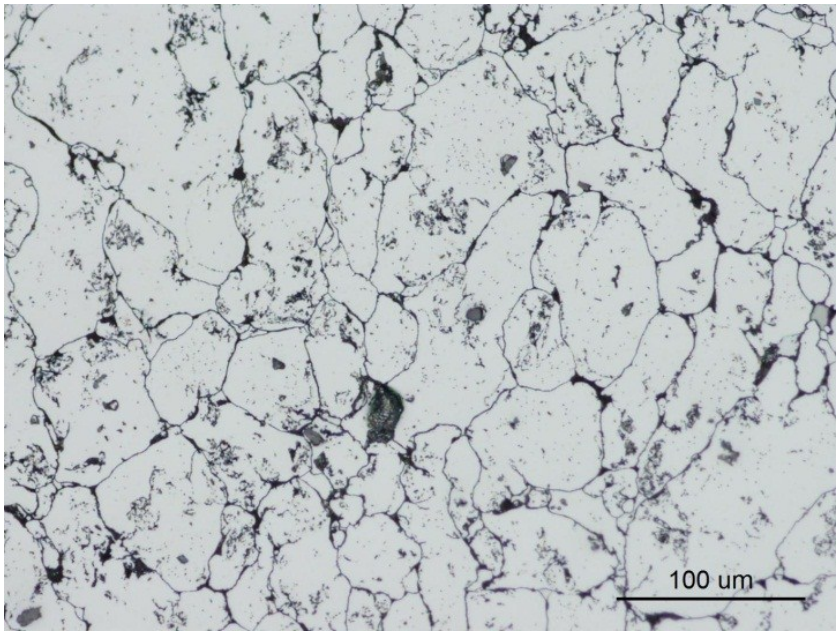

(a)

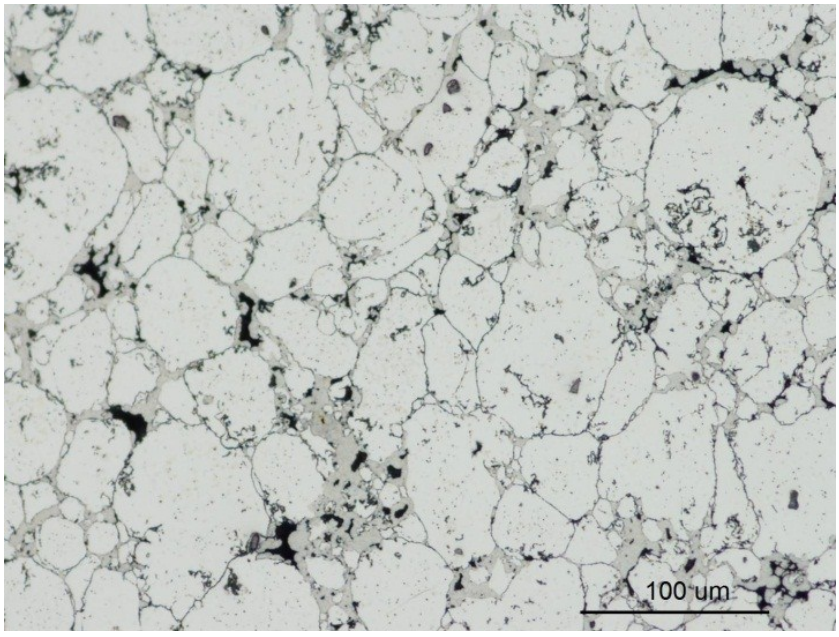

(b)

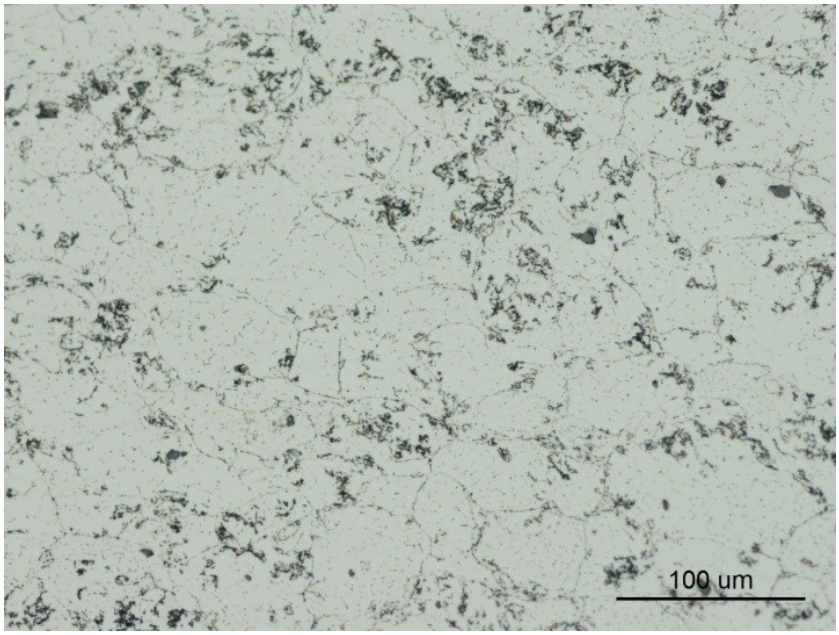

(c)

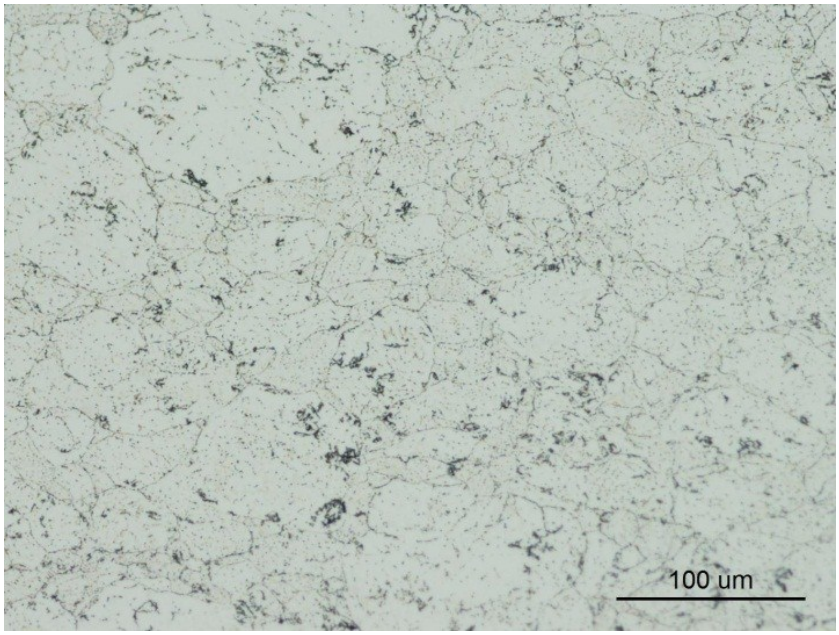

(d)

Figure 33 - Optical images of the microstructures in (a) APM Al, (b) APM Al-0.4Mg, (c) SPS Al and (d) SPS Al-0.4Mg.

3.5 Conclusions

Pure aluminum and a 0.4 wt% magnesium prealloyed aluminum powder were sintered by SPS using a variety of sintering schedules as well as conventional PM. Characterization of the sintered products enabled the following conclusions to be reached:

1. Increasing the pressure applied during SPS processing caused significant increases in density hardness. A pressure of 50MPa facilitated complete densification.
2. Variations in the SPS heating rate and sintering time had minimal influence on the density and hardness of Al compacts.
3. Sintering temperature was found to be the most influential variable in SPS processing. Under the highest temperature assessed (600°C) full theoretical density was realized in both powders studied.
4. SPS processing was found to be an effective means of reducing the concentrations of residual oxygen and hydrogen in the sintered products. This was observed for samples of appreciably different size and was in contrast to APM products wherein higher concentrations persisted. The lowest concentrations were observed when using the powder prealloyed with magnesium.
5. Increased sample size had a direct impact on sintered density. Relatively small (20 mm) samples exhibited densities >99% over the full range of temperatures studied whereas larger (80 mm) samples were only able to achieve comparable densification at the highest temperature considered (550°C).
6. The UTS and elongation to fracture of SPSed materials increased sharply as the sintering temperature surpassed 450°C. Wrought-like ductility (~30%) was attained using both Al and Al-0.4Mg powders.

3.6 Acknowledgements

The authors would like to acknowledge the Auto21 Networks of Centres of Excellence and the Natural Sciences and Engineering Research Council of Canada, (NSERC) for financial support via grant C502-CPM. Dr. Bernhard Mais (Ecka Granules) is acknowledged for the provision of the powders employed, as are Mr. Rene Kirchner (FCT Systeme GmbH), Dr. Jason Milligan (McGill University) and Mr. David Walker (McGill University) for their assistance with SPS trials.

CHAPTER 4. PAPER 2 EFFECTS OF TRANSITION METAL ADDITIONS ON THE SPARK PLASMA SINTERING RESPONSE OF ALUMINUM POWDERS

G.A. Sweet[1], M. Brochu[3], R.L. Hexemer Jr[4], I.W. Donaldson[5], and D.P. Bishop[2]

1 – Graduate Student, Dalhousie University, Halifax, Nova Scotia, Canada
2 – Professor, Materials Engineering, Dalhousie University, Halifax, Nova Scotia, Canada
3 – Professor, Materials Engineering, McGill University, Montreal, Quebec, Canada
4 – Research Engineer, GKN Sinter Metals LLC, Conover, North Carolina, USA
5 – Director of R&D North America, GKN Sinter Metals LLC, Auburn Hills, Michigan, USA

Status: Conference Proceedings, Presented at World Congress PM2014 in Orlando USA, on May 22, 2014

The following experimental procedures, results and discussions were completed by G.A. Sweet, with reviewer and editorial roles played by the subsequent authors.

Abstract

The objective of this study was to determine if prealloyed transition metals had a measureable effect on the spark plasma sintering (SPS) response of aluminum powder. In doing so, a variety of atomized powders were considered. These included commercial purity aluminum as a baseline and a suite of other powders that contained systematically different concentrations of prealloyed iron and/or nickel. Each powder was processed under a range of SPS temperatures. The sintered density, hardness, and microstructures were then assessed for all sintered products. None of the transition metal additions had an overtly negative impact on SPS response. As such, all powders were successfully processed to the full density condition provided that an appropriate minimum SPS temperature was employed. Hardness improved as the net concentration of transition metals increased and was found to be greatest in the Al-Fe-Ni ternary powder (78 HRH). Microstructural coarsening was apparent in all alloys as a result of SPS processing. However, the consolidated products maintained desirable microstructures comprised of homogenous distributions of sub-micron intermetallics such as Al_9FeNi, $Al_{13}Fe_4$ and $AlNi_3$.

4.1 Introduction

Spark plasma sintering (SPS) is a material processing technology, in which powdered materials are consolidated into parts using the simultaneous application of pressure and electrical current. Unlike conventional press and sinter powder metallurgy (PM), where compaction and sintering are separate operations [52], SPS processing provides concurrent application of these stages. Specifically, a uniaxial pressure applied in conjunction with a pulsed direct-current flow through the powder and/or die is the fundamental concept of the process. While the exact underlying mechanisms of consolidation remain in dispute, several of those more commonly accepted are outlined by Hulbert et al [53]. In systems where the current is able to pass through an electrically conductive powder, such as in aluminum, the heating is known to occur through Joule heating [54]. From this, relatively high heating rates are achievable, allowing very high thermal gradients to develop from the core to the surface of individual particles [55]. The end result is a process that exhibits turnover rates greater than other powder forming operations, while simultaneously being able to consolidate a wide variety of powdered materials without the need for sintering aids [33] and/or post sintering secondary operations such as forging.

Regarding the relationship between aluminum and SPS, there has been extensive work completed on increasing the strength of aluminum [17]. Specifically, SPS processing of nano-grained materials has been shown to produce aluminum alloys with high strengths [30, 56],as expected from a Hall-Petch standpoint. In addition to this, there have been studies on the effects of transition metal additions (Fe [56, 81, 82], Ni [82]) in a nanocrystalline compact. In these studies, several beneficial effects had been noted. These include high thermal stability due to impurity pinning and solute drag, very high room temperature strength (>1000 MPa) and elevated temperature strength (500 MPa at 350°C) [56], and plastic strain values in excess of 15%. Strengthening was established to be a function of the refined grain size and the introduction of dispersoid strengtheners (O, N) as well as the evolution of phases bearing the transition metal additions. These include, but are not limited to Al_6Fe, $Al_{13}Fe_4$ (sometimes referred to as Al_3Fe), and Al_9NiFe [82].

While the majority of aluminum SPS research pertains to the processing of nano-structured powders, there is a growing list of studies that are concerned with SPS response of aluminum powders in the as-atomized condition. Here, the effect of the oxide-based film that invariably exists on the surface of aluminum particles has been a key focal point [29, 22, 23, 24, 25]. In general, lower SPS temperatures result in metal/oxide/metal bonding, where adjacent powder particles can remain separated by the original refractory film [25, 29]. With higher temperatures, however, an increased ability to eliminate and/or disrupt the oxide-based layer has been observed, resulting in a high frequency of direct metal/metal bonding between powder particles. This ameliorated bonding appears to be a product of the physical breakdown of the hard oxide layer from the mechanical pressure applied [24]. APM generally requires magnesium additions to reduce the aluminum oxide skin and develop metallic bonding, while SPS has proven to be able to establish sufficient metallic bonding without this addition [83]. In this study, the ability to sinter prealloyed aluminum powders containing various transitions metals was studied. The investigation emphasized their response to select process parameters including hold temperature and composition. These results have been quantified by physical and mechanical property tests supported by microstructural observations.

4.2 Materials

Four powders were considered in this work. One was commercial purity aluminum powder, while the remaining were prealloyed powders with dilute additions of iron and/or nickel. In some instances, powders contained singular prealloyed additions while in others, multiple elements were incorporated simultaneously. These powders are represented in Table 4 and will be referred to in this work as ‘Al’, ‘Al-Fe’, ‘Al-Ni’ and ‘Al-Fe-Ni’, respectively. All powders were produced at Ecka Granules GmbH (Furth, Germany) through conventional air atomization.

Table 4 - Nominal compositions, particle size and apparent density of the raw powders studied.

Powder	Composition (wt%)			Particle Size (µm)			Apparent Density (g cm^{-3})
	Al	Fe	Ni	D_{10}	D_{50}	D_{90}	
Al	>99.8	0	0	71.6	133.4	270.0	1.038
Al-Fe	Bal.	1.0	0	52.7	93.3	165.5	1.101
Al-Ni	Bal.	0	1.0	50.1	96.7	177.4	1.155
Al-Fe-Ni	Bal.	1.0	1.0	56.4	102.4	188.6	1.148

4.3 Experimental techniques

Samples were processed using a SPS Model 10-3 unit manufactured by Thermal Technologies Inc., using pulsed DC current and a vacuum atmosphere. All tooling members were fabricated from graphite machined so as to yield a sintered disc with nominal dimensions of 20 mm diameter x 3 mm thick. A thermocouple hole was drilled into the lower punch to within 2mm of the sample surface for temperature monitoring purposes. Sinter profiles involved a heating rate of 100 K min^{-1} to a temperature from 400°C to 550°C where they were isothermally held for 300 s. Sintered samples were then furnace cooled to ambient under the vacuum atmosphere. A uni-axial pressure of 50 MPa was applied to each sample throughout the entire heating/cooling cycle.

Preliminary characterization included density measurements (MPIF standard 42) and apparent hardness using the Rockwell H scale. Samples were ground planar with 240 grit SiC abrasive paper prior to hardness measurements, but after density observations. Sections were then cold-mounted in epoxy and polished using a standard series of abrasive papers and diamond compounds. Imaging was completed using a Hitachi S-4700 Field Emission Scanning Electron Microscope (SEM) operated with an accelerating voltage of 20kV and an emission current of 15 µA. X-ray diffraction (XRD) work was completed using a Bruker D8 Advance equipped with a copper source. Cu Kα radiation was generated using a tube

voltage and current of 40kV and 40mA, respectively. The diffracted beam was filtered through a nickel foil prior to detection.

4.4 Results and discussion

The following sections discuss the effects of individual transition metal additions to aluminum, as well as multiple simultaneous additions. These were quantified in terms of their density, hardness and microstructure.

4.4.1 Singular transition metal additions

Data on the sintered density and hardness as functions of peak SPS temperature are shown in Figure 34 for Al, Al-Fe and Al-Ni powders. In each instance it was noted that densification increased with SPS temperature. This agreed well with the densification mechanisms of SPS (power-law creep [34, 37], plastic yielding and grain boundary diffusion [61]) whereby higher temperatures facilitate increased levels of plastic deformation. The Al powder achieved 98.10% of its theoretical maximum density at 400°C and increased to 99.92% at the highest sintering temperature investigated (550°C). However, the majority of densification was achieved by 500°C with only minor gains realized at the higher temperature. Data for Al-Fe and Al-Ni largely mirrored this trend. For these powders, effectively full densification was also realized for SPS temperatures ≥500°C. The one notable difference was in the level of densification attained with the lowest temperature assessed. Here, data for the Al-Ni did not show the sharp decline observed in the trends for Al and Al-Fe.

The hardness of each binary system exceeded that of Al for all temperatures considered (Figure 34(b)). Samples prepared from prealloyed Al-Fe were the hardest and maintained an improvement of 18 HRH relative to the baseline Al material. Similarly, the addition of Ni also invoked hardness benefits, although the effects were less pronounced at 11 HRH. Solid solubilities of Fe and Ni in aluminum are essentially nil [84], and each element possesses a high thermodynamic tendency to form aluminide phases. As such, noted increase in hardness of Al-Fe and Al-Ni systems should have been principally driven by

the presence of intermetallic aluminides. To investigate this in greater detail, microstructural analyses were completed on select specimens of each alloy through SEM imaging and XRD.

Figure 35 shows SEM images for the three powders sintered at the temperature extremes of this study. These highlight the progressive microstructural transitions as a function of SPS temperature. The effective elimination of porosity was clearly accomplished for all samples sintered at 550°C, consistent with density data presented in Figure 34(a). Regarding secondary phases, Al was largely free of any contrasting areas, indicating that it was principally a single phase composition. This was as expected given the lack of any deliberate alloying additions. SEM images of Al-Ni and Al-Fe samples showed an abundance of bright secondary phases in all instances as a result of atomic contrast. EDS analyses confirmed that these features were enriched in aluminum and the respective transition metal added, but an explicit assay was not possible given their sub-micron size. As no other differences were observed, these features were invariably responsible for the measured hardness differences.

Beyond the absolute differences in hardness, it was also noted that each material experienced a gradual hardness decline with progressively higher SPS temperatures despite the fact that densification improved steadily over the same domain. Considering the base Al material, hardness fell 5 HRH, yet density improved from ~98% to ~100% of full theoretical. Although Al-Fe densified in a comparable fashion, the net loss was more pronounced at 7 HRH. The hardness decline in Al-Ni was closer to 8 HRH. These transitions indicated that thermally-induced metallurgical transitions had also occurred and that the deleterious effects of these phenomenon outweighed any hardening accrued through densification.

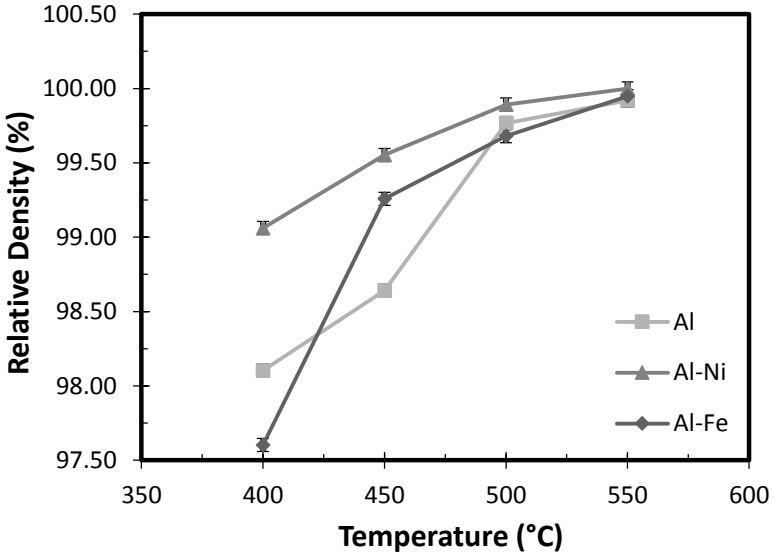

(a)

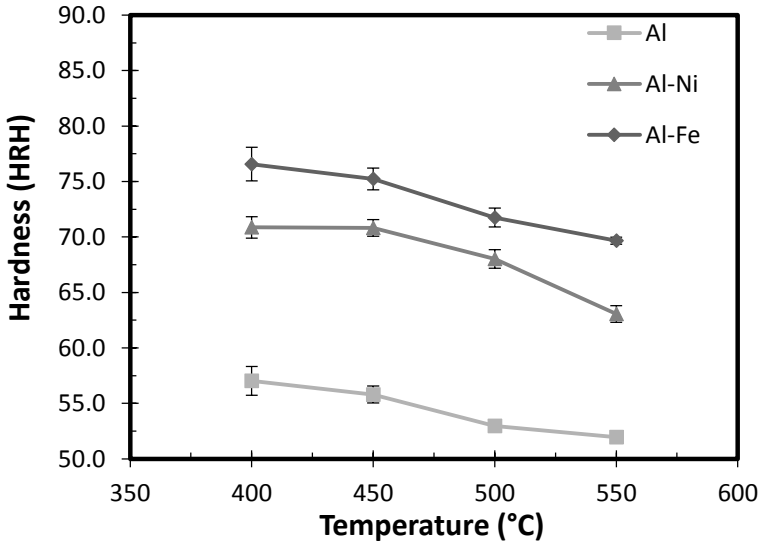

(b)

Figure 34 - Data describing the transitions in (a) sintered density and (b) hardness as a function of peak SPS temperature measured for Al and binary alloys Al-Fe and Al-Ni.

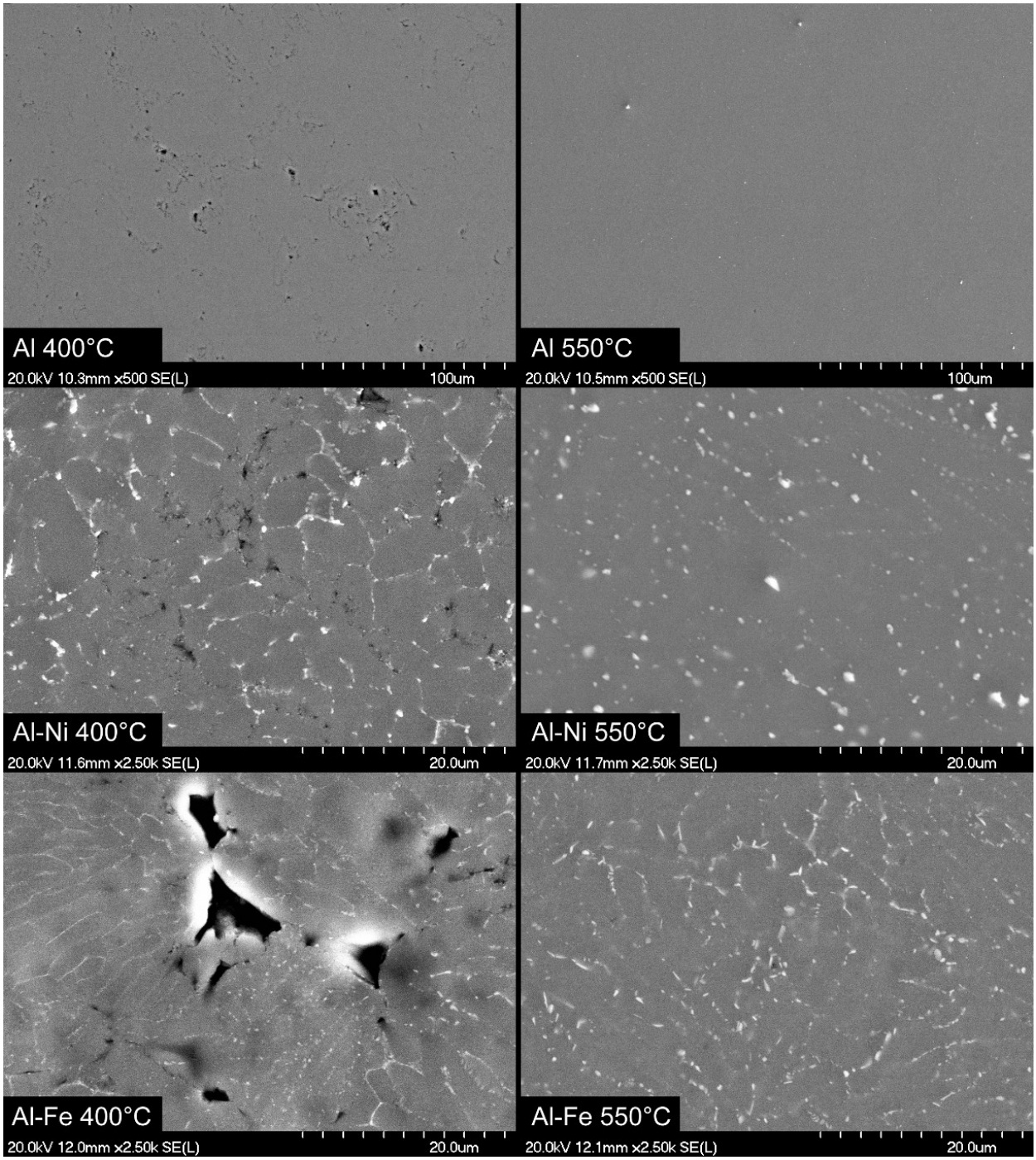

Figure 35 - SEM micrographs of Al, Al-Fe and Al-Ni powders processed via SPS at 400°C and 550°C.

For the case of Al, SEM images (Figure 35) implied that this was a single phase material. This was consistent with XRD traces (Figure 36) acquired from the Al powder before and after SPS processing. These spectra confirmed that the only phases detected were aluminum in conjunction with a minor presence of Al_2O_3 attributable to the air atomization method of production. Hence, the noted hardness decline for this material would have most likely been driven by grain growth and/or the relief of residual strain [85] within the powder particles initially instilled during atomization.

In Al-Fe and Al-Ni the aforementioned mechanisms had likely transpired as well, and thereby contributed to the overall softening behaviour of these materials. However, since the net changes were greater than those noted for Al, transitions in the secondary phases would have also been a factor of influence. One transition readily apparent in SEM images was that of coarsening (Figure 35). In this sense, at 400°C the microstructures of Al-Fe and Al-Ni were very similar to those present within the starting raw powders - a cellular microstructure wherein the secondary phase was concentrated as a thin, continuous film within the inter-cellular regions. However, upon sintering at 550°C, the increased thermal energy had evolved the secondary phases into coarser, discrete particles. This would have reduced their relative strengthening effect and in doing so, contributed to the net decline in hardness observed. For Al-Ni the final morphology of the secondary phase was one of blocky/globular character consistent with Al_3Ni [86]. However, the continuous, inter-dendritic structure in Al-Fe evolved into discrete needle-shaped particles; a morphology typical of the phase $Al_{13}Fe_4$ [86].

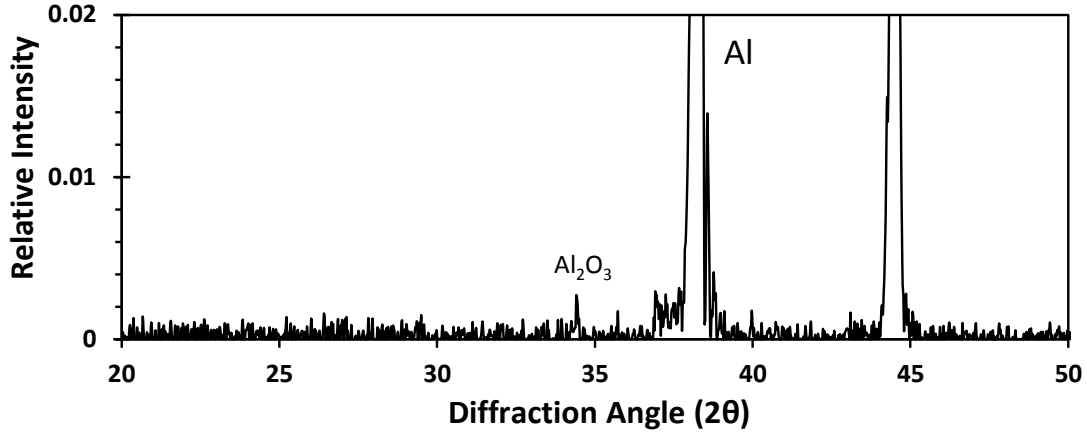

(a)

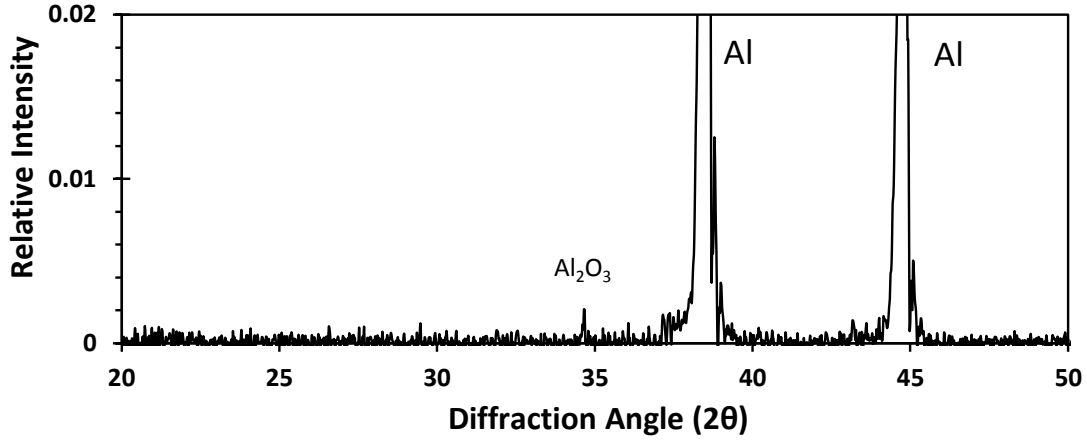

(b)

Figure 36 - XRD traces acquired from Al powder (a) before and (b) after SPS processing at 550°C.

To determine if these phases were in fact present, XRD spectra were gathered from Al-Fe and Al-Ni as raw powders and as full density discs produced through SPS at 550°C. Considering Al-Fe (Figure 37), the presence of α-aluminum and Al_2O_3 was again confirmed in the raw powder, as expected. Small peaks consistent with the two principal diffraction angles for $Al_{13}Fe_4$ were also present implying that this phase existed in a form amenable to detection via XRD but in a low volume fraction. After SPS processing the principal peaks associated with $Al_{13}Fe_4$ had grown significantly and a series of secondary peaks for the phase emerged at lower diffraction angles. This indicated that the volume

fraction of the intermetallic detectable by XRD had increased. Although the raw powder and SPS product thereof both possessed an equivalent bulk concentration of iron, the detectable volume fraction of $Al_{13}Fe_4$ with an equilibrium crystalline structure was evidently not the same in each instance. This implied that the non-equilibrium conditions of rapid solidification (atomization) had enabled iron to reside within the starting powder in alternate forms such as a supersaturated solid solution or as coherent metastable phases [87]. Thermal input during SPS then shifted the microstructure of the powder to one that would be expected in equilibrium. Consistent with other studies on rapidly quenched aluminum alloys, this would have caused the observed increase in the concentration of $Al_{13}Fe_4$ detected. Detailed XRD studies that are beyond the scope of this conference article are currently underway in an effort to refine the SPS-induced transitions in greater detail.

XRD spectra for Al-Ni materials are shown in Figure 38. Data from the raw powder revealed the presence of three small, broad peaks in addition to the features common to all prior traces (α-aluminum and Al_2O_3). The minor peaks did not correlate to any phase contained within the diffraction pattern database of the XRD system. Hence, it was postulated that they were associated with a metastable phase such as Al_9Ni_2, known to exist within rapidly solidified Al-Ni alloys [88]. These peaks persisted after SPS at 550°C (Figure 38(b)), confirming that the associated phase still persisted within the microstructure. However, such processing clearly had some microstructural impact as the complete pattern for the equilibrium phase Al_3Ni had become readily apparent. These findings confirmed that the intermetallics present in both Al-Fe and Al-Ni systems changed as a result of SPS processing. Ultimately, the sintered microstructures largely resembled those anticipated in equilibrium although the lingering presence of metastable phases (especially in Al-Ni) could not be ruled out at this time.

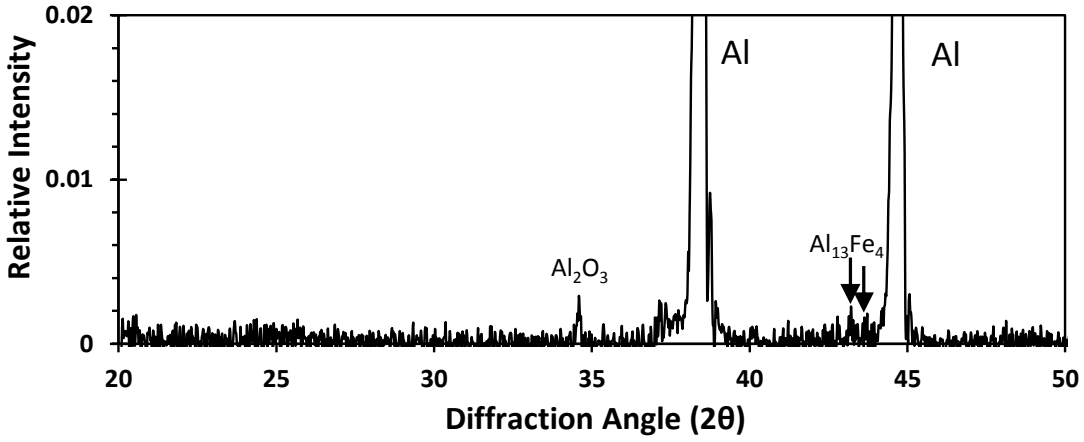

(a)

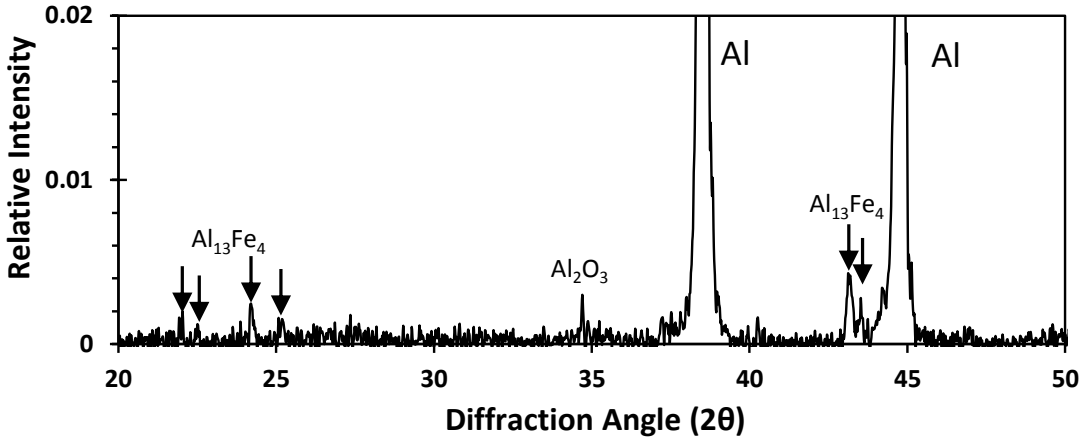

(b)

Figure 37 - XRD traces acquired from Al-Fe powder (a) before and (b) after SPS processing at 550°C.

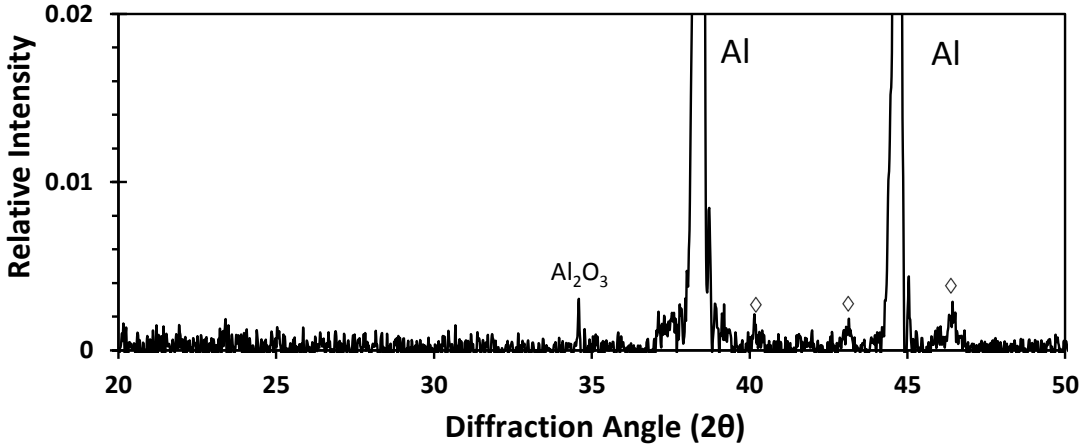

(a)

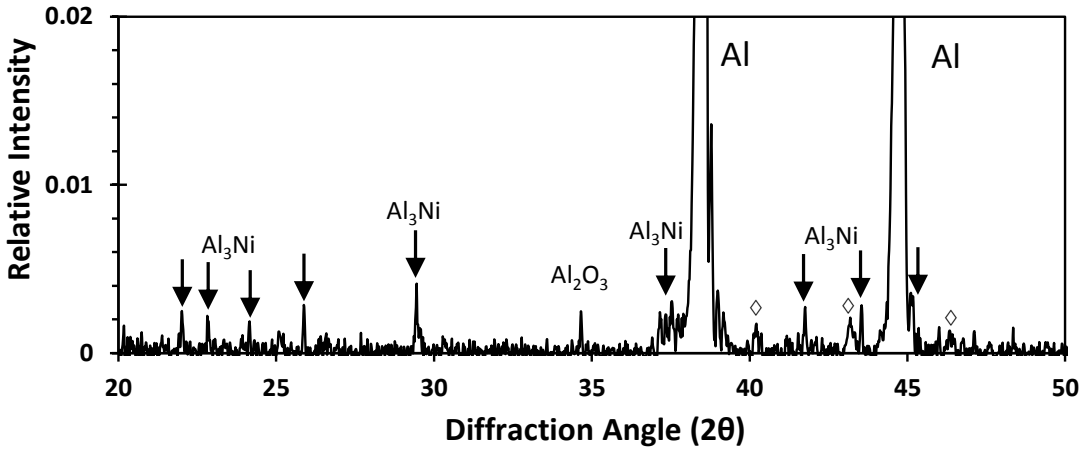

(b)

Figure 38 - XRD traces acquired from Al-Ni powder (a) before and (b) after SPS processing at 550°C. The diffracting species responsible for peaks annotated with the ◊ symbol could not be identified.

4.4.2 Multiple transition metal additions

To complement data from binary powders, the SPS response of a ternary (Al-Fe-Ni) formulation was also assessed. Figure 39 shows the transitions in the relative density and hardness of this alloy for the full range of SPS temperatures considered. The former attribute showed large gains over the temperature range studied. A linear dependence could be traced from 97.7% of full theoretical at 400°C to 100.0% at 550°C. Hence, unlike binary systems, a satisfactory density was not achieved at any temperatures below the peak value considered as density did not taper off in a gradual manner.

The bulk hardness values of Al-Fe-Ni specimens were superior to those of Al and both of the binary powders at all SPS temperatures assessed. For instance, a comparison of the data among SPS samples processed at 550°C revealed that Al-Fe-Ni maintained hardness advantages of 8, 15, and 26 HRH over Al-Fe, Al-Ni and Al materials respectively. Similar to the binary systems, the hardness of Al-Fe-Ni was also expected to be underpinned by the volume fraction of intermetallics present. A comparison of the micrographs in binary (Figure 35) and ternary (Figure 40) formulations confirmed that secondary phases were present in greater abundance in the Al-Fe-Ni product, consistent with the higher bulk concentration of transition metals added. It is postulated that this would have imparted a higher resistance to plastic yielding during SPS processing and thereby invoked the noted difference in densification behaviour. SEM images of Al-Fe-Ni also confirmed full densification in the 550°C specimen and the occurrence of morphological changes in the secondary phases as the SPS temperature increased. Such transitions were consistent with the density data in Figure 39(a), and confirmed that microstructural coarsening had again transpired.

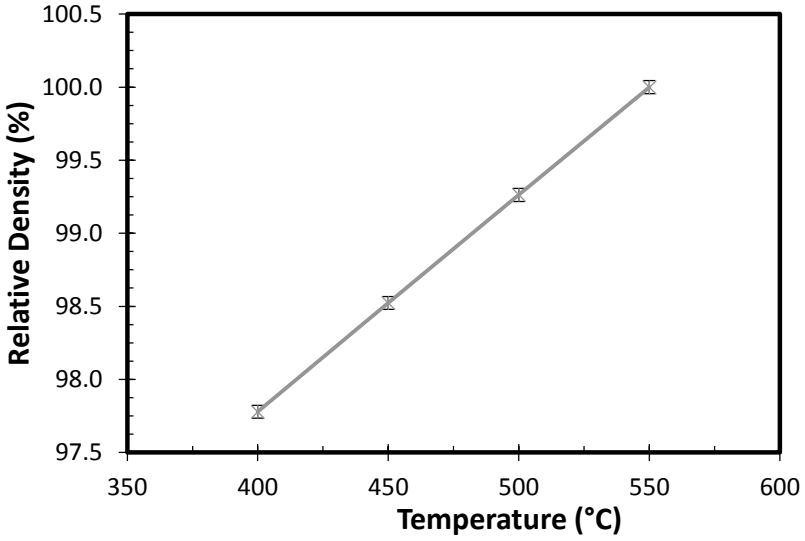

(a)

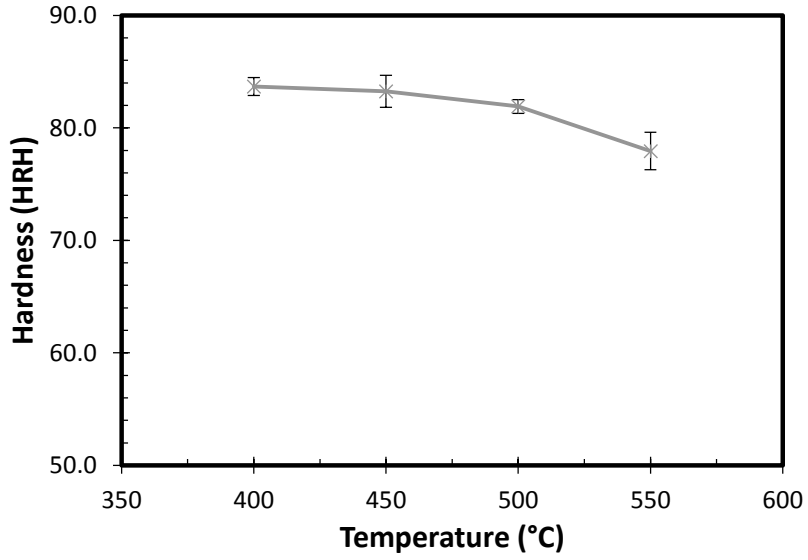

(b)

Figure 39 - Data describing the variation in (a) density and (b) hardness as functions of peak SPS temperature for Al-Fe-Ni.

In an attempt to identify the secondary phase(s) present in Al-Fe-Ni XRD techniques were again employed. The resultant traces of the raw powder and the specimen sintered at 550°C are shown in Figure 41. Many of the secondary peaks present in the spectra from the raw powder coincided with the phase Al_9FeNi. However, all such peaks were relatively small and broad, consistent with diffracting particles that were of an exceptionally small size. The same peaks for Al_9FeNi prevailed after SPS processing but were now narrower and of a higher relative intensity. This indicated that the crystallite size and the concentration thereof had increased, consistent with Figure 40. For a number of peaks, a plausible source of the diffracting species was not identifiable. This was common to both traces and indicated that crystallographic variants of Al_9FeNi and/or completely distinct auxiliary phases existed within the microstructures. The majority of these peaks were common to both traces and transitioned from short/broad to tall/narrow as a result of SPS. As such, it can be inferred that these species had also coarsened akin to the behaviour noted for Al_9FeNi.

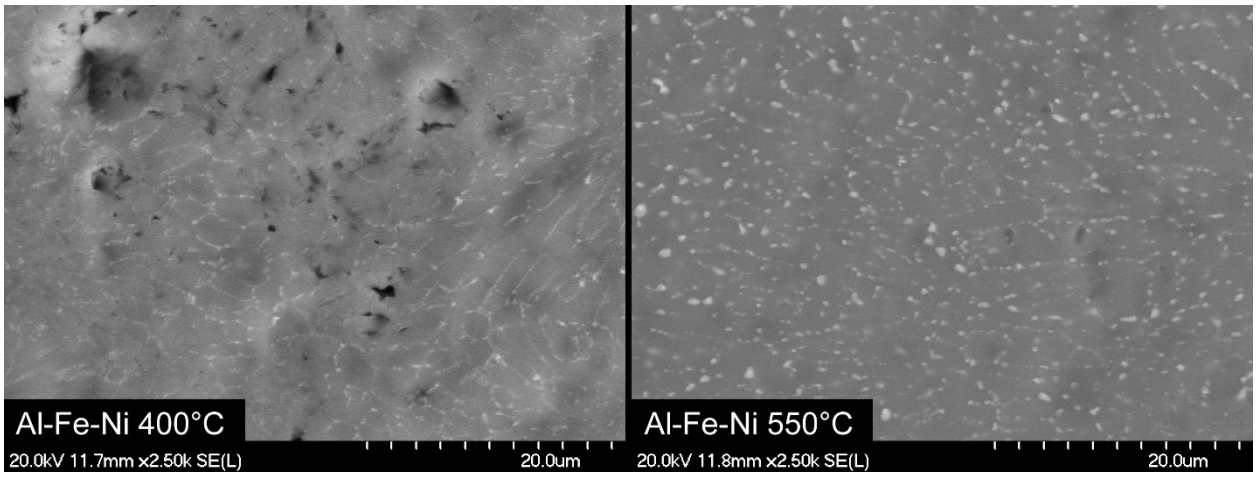

Figure 40 - SEM micrographs of Al-Fe-Ni and sintered at peak SPS temperatures of 400°C and 550°C.

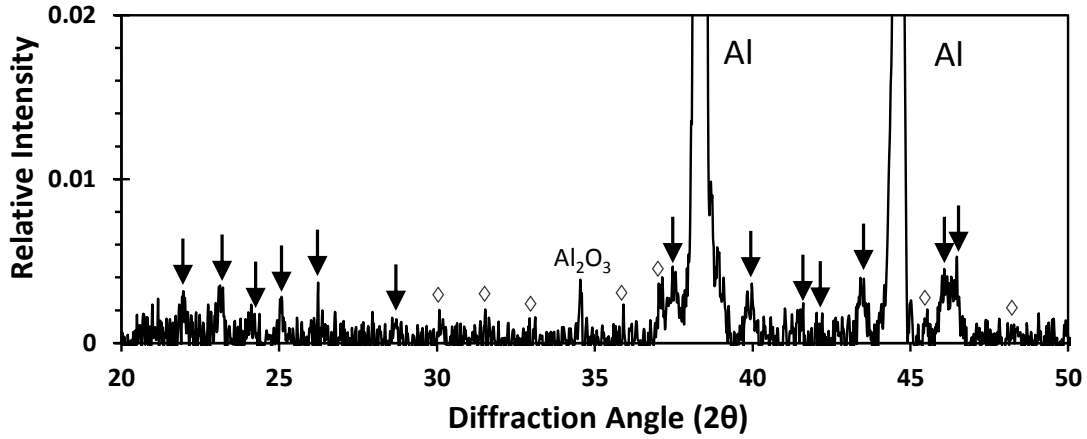

(a)

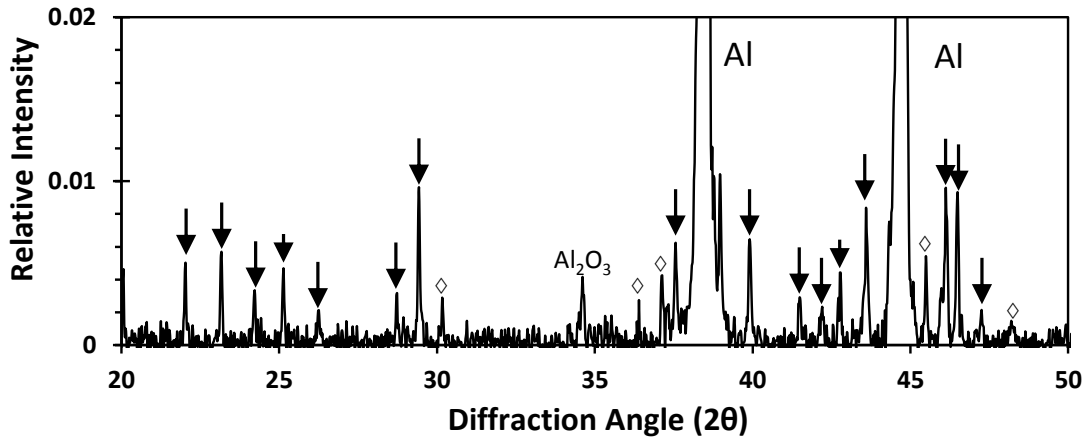

(b)

Figure 41 - XRD trace acquired from a specimen of Al-Fe-Ni SPSed at 550°C. Arrowed peaks coincide with the phase Al_9FeNi. The diffracting species responsible for peaks annotated with the ◊ symbol could not be identified.

4.5 Conclusions

Al, Al-Ni, Al-Fe and Al-Fe-Ni powders were processed through SPS under a variety of temperatures. Characterisation of the consolidated products allowed the following conclusions to be reached:

1. Full densification was achieved in all powder systems provided that an appropriate SPS temperature was employed.
2. The presence of transition metals had minimal effect on the densification behaviour of binary chemistries. However, the increased concentrations of these features in Al-Fe-Ni were found to influence this attribute.
3. SPS processing invoked microstructural coarsening in binary and ternary systems alike. At the highest temperature considered the phases present were largely reflective of an equilibrium condition but remained as a homogenous distribution of fine (typically sub-micron) particles.
4. The principal intermetallics present in Al-Fe, Al-Ni, and Al-Fe-Ni after SPS processing were $Al_{13}Fe_4$, Al_3Ni, and Al_9FeNi. Other phases were present in select instances and these were thought to result from the rapid solidification conditions inherent to gas atomization.
5. Al-Fe-Ni achieved the highest hardness of all the alloys assessed in this study. In a fully dense condition, the final hardness of this material was 78 HRH; 26 points higher than the Al counterpart.

4.6 Acknowledgements

The authors would like to acknowledge the Auto21 Networks of Centres of Excellence and the Natural Sciences and Engineering Research Council of Canada, (NSERC) for financial support via grant C502-CPM. Dr. Bernd Mais (Ecka Granules) is acknowledged for the provision of the powders employed, as are Mr. Rene Kirchner (FCT Systeme GmbH), Dr. Jason Milligan (McGill University) and Mr. David Walker (McGill University) for their assistance with SPS trials.

CHAPTER 5. SUMMARY

This research focused primarily on exploring the fundamental variables in SPS processing, with insight into developing a knowledge base for more complicated alloy systems. This was done by performing a battery of tests on 5 different air atomized aluminum powders, and by varying 5 SPS parameters. The performances of these samples were then quantified by measurements of density, hardness, tensile properties, and residual gas content as well as metallographic inspection. Select samples were replicated using a conventional APM 'press and sinter' approach. These were performed to compare the requirement of specific sinter-aids for the two processes, as well as any benefits either may have with respect to the elimination of residual impurities.

5.1 Processing Parameter Effects

Selected from literature review and APM experience, the objective was to determine what parameters have the greatest impact and what combination of these would be suitable for future alloy development. The following process parameters were selected from the plethora of options available in SPS processing.

5.1.1 Pressure

Uniaxial pressure was applied prior to heating, and held until the cooling regimen of the cycle was complete. The effects of these tests indicated that a sharp increase in both density and hardness were present. Similar to compaction curves in conventional PM, there was a decreasing gain in properties at the higher pressures studied. For safety considerations, the maximum pressure of the graphite die was limited to 50 MPa. Without more exotic die configurations able to endure higher pressures, 50 MPa was deemed sufficient for these alloy systems as full density was essentially realized in all powders assessed.

5.1.2 Heating Rate

SPS benefits from the very high heating rates available. Although higher heating rates were possible, research emphasized those in the range of 50 to 500 K min^{-1}. A literature review indicated that high heating rates would engage a different densification mechanism that

would ultimately improve densification. Realistically, these gains were minimal in comparison to other process parameters. Furthermore, increasing heating rates also contributed to temperature control issues, which was anticipated to be partially responsible for any performance gains. Accordingly, the most appropriate heating rate was found to be 50 k min^{-1}.

5.1.3 Hold Time

One of the claimed benefits of SPS is that of a reduced processing time in comparison to conventional APM. Experiments in this study were performed with an isothermal hold at the sintering temperature from 30 to 300 s. Density gains with extended sintering time were apparent, although minimal. Simultaneously a softening effect occurred, due to the coarsening of the microstructure. To reduce these effects, while also promoting densification, a sintering time of 120 s was deemed to be a sufficient; a time that was appreciably lower than that required in conventional APM (~18000 s).

5.1.4 Hold Temperature

The peak processing temperature in SPS has proven to be one of the key driving factors for property development. Temperatures from 400°C to 600°C were employed for most powders although an upper limit of 550°C was imposed for alloyed systems to avoid melting and the concomitant degradation of the graphite tooling. Sharp increases in density were observed with increasing temperature over the ranges considered. The increased thermal energy softened the base powder, presumably allowing for plastic yielding, climb-controlled creep and grain boundary diffusion. Concurrently, a softening of the final material was recorded with these ameliorated densities. This mechanism was predicted in Figure 10, whereby higher sintering temperature motivated grain coarsening, weakening the material.

Tensile tests were perform on select samples, albeit manufactured from larger 80 mm pucks. These tests showed that the development of tensile properties is heavily reliant on the sintering temperature. At lower temperatures (400°C, 450°C) samples exhibited poor

ductility, similar to APM materials. However, higher temperatures (500°C, 550°C) promoted ductility values on par with wrought materials; the yield strength remained essentially unchanged, while UTS benefited from higher ductility due to work hardening. It was presumed that the higher sintering temperatures allowed for enhanced rupture/removal of the oxide layer and in turn, increased amounts of metallic bonding.

5.1.5 Specimen size

The effects of specimen are of obvious interest. While 20mm samples are easier to produce, they are of little commercial relevance. 80 mm samples were manufactured to observe any inconsistencies with specimen size. For the given process parameters, 20 mm samples showed full density at 550°C, with less than a 1% drop at the lowest temperature. The 80mm sample exhibited a much more temperature sensitive response. Full density was essentially achieved at 550°C, while at 400°C, the density was less than 97% TD. Temperature inhomogeneity due to tooling geometry were a likely cause, leading to regions of the sample being sintered at a temperature lower than the desired set point.

5.2 Chemical Effects

A commercially pure aluminum powder was used as a baseline material for comparison sake. However, for successful alloy development, the individual effects of magnesium, iron and nickel have been studied to observe their response to SPS. Magnesium was of primary concern, as it is a common APM additive used in disrupting the resilient aluminum oxide layer. Contrary to the sinter-aiding properties of magnesium, iron and nickel additions were explored for their ability to increase mechanical properties.

5.2.1 Magnesium

Magnesium additions instilled significant improvements in both physical and mechanical properties in comparison to the commercially pure powder. Densification was improved in tests concerning hold time and sintering temperature. Sintering time was shortened, and the ultimate temperature to achieve full density was lowered. Systems without magnesium rely primarily on temperature to soften the powder, and ultimately fracture the oxide layer.

Magnesium additions in the prealloyed powder should have allowed for reduction of this oxide layer, promoting increased levels of metallic bonds. As an additional benefit, the solid solution strengthening effect of magnesium increased hardness.

5.2.2 Iron and Nickel

The three transition element bearing powders, Al-Fe, Al-Ni and Al-Fe-Ni were SPSed using parameters similar to those use for pure aluminum. Densification was not inhibited with the prealloyed addition of these elements. Hardness was substantially improved over the baseline material. For equivalent amounts, iron proved to be a slightly more potent strengthener. This is an effect of the intermetallic phase present in iron-bearing materials ($Al_{13}Fe_4$) being inherently stronger than that in the nickel-bearing material (Al_3Ni).

5.3 Residual Gas Content

The amounts of residual hydrogen and oxygen after sintering were measured to determine if any 'cleansing' effect had transpired; a phenomena that SPS has reportedly been able to achieve. For pure aluminum and magnesium-bearing powders, this impurity elimination effect was in fact observed. Hydrogen values in samples SPSed at 400°C were lower than that of the initial powder, while at 600°C they had been reduced to a level largely comparable to wrought materials. Residual oxygen concentration at 400°C was also lower than that of the starting raw powder, with further reductions occurring at higher sintering temperatures. Contrary to hydrogen results, considerable oxygen remained in samples processed at the highest temperatures although the values were reduced substantially relative to APM counterparts.

The elimination of these gasses was theorized to be a product of several different reactions occurring throughout the heating cycle. At low temperatures, physiosorbed water was volatilized, removing it from the sample. Upon further heating, aluminum hydroxide and hydrated aluminum oxide were decomposed, liberating either gaseous water and/or hydrogen.

CHAPTER 6. DISCUSSION OF FUTURE WORK

The subjects listed in this section are recommendations for future work.

- Investigation of the ductility of samples as functions of parameters other than temperature. The ultimate sinter quality is reflected in the ability of an alloy to endure plastic deformation. This would provide more substantial information than judging sinter quality by density measurements, as consolidation and metallic bonding appear to be unrelated in SPS. Specifically, determining the minimum time at peak sintering temperature required to develop satisfactory mechanical properties.
- Investigate sintering response of fundamental powders (Pure Al and Al-0.4Mg) using closer ultimate temperature profile (10 K rather than the 50 K used throughout this work)
- Perform an investigation on the tensile behaviour of iron and nickel-bearing materials to quantify their strengthening benefits. Further elaborate on the type and amount of transition element additions added to further investigate potential strengthening mechanisms of multiphase systems.
- Investigate the effects of heat-treatments and elevated temperature exposure on the mechanical properties of transition-element bearing materials
- Investigate the effects of other typical APM alloy additions (Sn, Si, Zn, etc…) and combinations thereof. Quantify elements based on their ability to modify densification ability as well as their modification of mechanical properties.
- Investigate APM and wrought aluminum alloy systems to determine the efficacy of SPS in their processing. For example, investigate relevant aerospace aluminum grades (7075, 6061) and perform comparisons to wrought counterparts.

REFERENCES

[1] W. D. Callister, Materials Science and Engineering: An Introduction, New York: John Wiley & Sons, 2007.

[2] R. M. German, Powder Metallurgy & Particulate Materials Processing, Princeton, New Jersey: Metal Powder Industries Federation, 2005.

[3] M. P. Mosher, "Effects of Cr Addition on the Metallurgy and P/M Processing Response of Alumix 431D," Unpublished masters thesis, Halifax, 2009.

[4] "Production Sintering Practices," in *ASM Metals Handbook Volume 7: Powder Metal Technologies and Applications*, Materials Park, ASM, 1998.

[5] J. E. Garay, "Current-activated, pressure-assisted densification of materials," *Annual Review of Materials Research,* pp. 445-468, 2010.

[6] G. B. Schaffer, T. B. Sercombe and R. N. Lumley, "Liquid phase sintering of aluminum alloys," *Materials Chemistry and Physics,* no. 67, pp. 85-91, 2001.

[7] R. W. Cooke, R. L. Hexemer, I. W. Donaldson and D. P. Bishop, "Dispersoid strengthening of Al-Cu-Mg P/M alloy utilising transition metal additions," *Powder Metallurgy,* pp. 191-199, July 2012.

[8] G. N. Grayson, G. B. Schaffer and J. R. Griffiths, "On the fatigue of sintered aluminium alloys," *Materials Forum,* pp. 981-985, 2004.

[9] D. Kent, G. B. Schaffer and J. Drennan, "Age hardening of a sintered Al-Cu-Mg-Si-(Sn) alloy," *Materials Science and Engineering,* pp. 65-73, 2005.

[10] K. Kondoh, A. Kimura and R. Watanabe, "Behavior of sintering aluminum alloy powder by using deoxidizing resolution of Al2O3 surface film by magnesium," *Quarterly Journal of the Japan Welding Society,* pp. 377-389, 2001.

[11] H. I. Sanderow, "Powder Metallurgy Methods and Design," in *ASM Handbook Volume 7: Powder Metal Technologies and Applications*, Materials Park, ASM, 1998, pp. 23-26.

[12] A. Dudhmande, T. Schubert, M. Balasubramanian and B. Kieback, "Sintering Properties of new P/M aluminium alloys and composites," *Metal Matrix Composites,* pp. 301-306, 2005.

[13] G. B. Schaffer and S. H. Huo, "Distortion in a sintered 7000 series aluminum alloy," *Powder Metallurgy,* vol. 43, no. 2, 2000.

[14] M. Azadbeh and Z. A. Razzaghi, "Properties evolution during transient liquid phase sintering of PM Alumix 431," *Advances in Materials Science and Engineering,* 2009.

[15] T. Schubert, T. Weibgarber, B. Kieback, H. Balzer and H.-C. Neubing, "PM aluminium structural parts for automotive application," *PM applications,* 2004.

[16] L. Meluch, "Warm compaction of alumiunum alloy Alumix 123," unpublished, Birmingham.

[17] R. Orru, R. Licheri, A. M. Locci, A. Cincotti and G. Cao, "Consolodation/synthesis of materials by electric current activated/assisted sintering," *Materials Science and Engineering R,* pp. 127-287, 2009.

[18] D. M. Hulbert, A. Anders, D. V. Dudina, J. Andersson, D. Jiang, C. Unuvar, U. Anselmi-Tamburini, E. J. Lavernia and A. K. Mukherjee, "The absence of plasma in "spark plasma sintering," *Journal of Applied Physics,* 2008.

[19] S. Nouari, "Spark Plasma Sintering of Al6061 and AL2124 Alloys," *Advanced Materials Research,* Vols. 284-286, pp. 1656-1660, 2011.

[20] G. Xie , O. Ohashi and N. Yamaguchi, "Reduction of surface oxide films on Al-Mg alloy powders by pulsed electric current sintering," *Journal of Materials Research,* vol. 19, no. 3, pp. 815-819, 2004.

[21] G. Xie, O. Ohashi , T. Sato, N. Yamaguchi, M. Song, K. Mitsuishi and K. Furuya, "Effect of Mg on the sintering of Al-Mg alloy powders by pluse electric-current process," *Materials Transactions,* vol. 45, no. 3, pp. 904-909, 2004.

[22] G. Xie, O. Ohashi , T. Yoshioka, M. Song, K. Mitsuishi, H. Yasuda, K. Furuya and T. Noda, "Effect of interface behavior between particles on properties of pure Al powder compacts by spark plasma sintering," *Materials Transactions,* vol. 42, no. 9, pp. 1846-1849, 2001.

[23] G. Xie, O. Ohashi, K. Chiba, N. Yamaguchi, M. Song, K. Furuya and T. Noda, "Frequency effect on pulse electric current sintering process of pure aluminum powder," *Materials Science and Engineering A,* vol. 359, no. 1-2, pp. 384-390, 2003.

[24] G. Xie, O. Ohashi, M. Song, K. Furuya and T. Noda, "Behavior of oxide film at the interface between particles in sintered al powders by pulsed electric-current sintering," *Metallurgical and Materials Transactions A,* vol. 34A, pp. 699-703, 2003.

[25] G. Xie, O. Ohashi, M. Song, K. Mitsuishi, H. Yasuda, K. Furuya and T. Noda, "Electron microscopic observation of interfaces of aluminum powder compacts prepared by spark plasma sintering," *Journal of Electron Microscopy,* vol. 51, no. Supplement, pp. S149-S153, 2002.

[26] G. Xie, O. Ohashi, M. Song, K. Mitsuishi and K. Furuya, "Reduction mechanism of surface oxide films and characterization of formations on pulse electric-current sintered Al-Mg powders," *Applied Surface Science,* vol. 241, pp. 102-106, 2005.

[27] G. Xie, O. Ohashi, N. Yamaguchi, M. Song, K. Mitsuishi, K. Furuya and T. Noda, "Behavior of oxide film at interface between particles of Al-Mg alloy powder

compacts prepared by pulsed electric-current sintering," *Japan Journal of Applied Physics,* vol. 42, no. 7B, pp. 4725-4728, 2003.

[28] M. Zadra, F. Casari, L. Girardini and A. Molinari, "Spark plasma sintering of pure aluminum powder: mechanical properties and fracture analysis.," *Powder Metallurgy,* vol. 50, no. 1, pp. 40-45, 2007.

[29] H. Kwon, D. H. Park, Y. Park, J. F. Silvain, A. Kawasaki and Y. Park, "Spark plasma sintering behavior of pure aluminum depending on various sintering temperatures," *Metals and Materials International,* vol. 16, no. 1, pp. 71-75, 2010.

[30] D. Liu, Y. Xiong, T. Topping, Y. Zhou, C. Haines, J. Paras, D. Martin, D. Kapoor, J. Schoenung and E. Lavernia, "Spark Plasma Sintering of Cryomilled Nanocrystalline Al Alloy - Part IIL Influence of Processing Conditions on Densification and properties," *Metallurgical and Materials Transactions A,* vol. 34A, pp. 340-350, 2012.

[31] J. Ye, L. Ajdelsztajn and J. Schoenung, "Bulk nanocrystalline aluminum 5083 alloy fabricated by a novel technique: cryomilling and spark plasma sintering," *Metallurgical and Materials Transactions A,* vol. 37A, pp. 25569-5679, 2006.

[32] M. Kubota and P. B. Wynne, "Electron Backscattering diffraction analysis of mechanically milled and spark plasma sintered pure aluminum," *Scripta Materialia,* vol. 57, pp. 719-722, 2007.

[33] Z. A. Munir, U. Anselmi-Tamburini and M. Oyanagi, "The effect of electric field and pressure on the synthesis and consolidation of materials: A review of the spark plasma sintering method," *Journal of Materials Science,* pp. 763-777, 2006.

[34] E. A. Olevsky, S. Kandurkuri and L. Froyen, "Consolidation enhancement in spark-plasma sintering: Impact of high heating rates," *Journal of Applied Physics,* 2007.

[35] W. Chen, U. Anselmi-Tamburini, J. E. Garay, J. R. Groza and Z. A. Munir, "Fundamental investigations on the spark plasma sintering/synthesis process I. Effect of dc pulsing on reactivity," *Materials Science and Engineering,* pp. 132-138, 2005.

[36] S.-X. Song, Z. Wang and G.-P. Shi, "Heating mechanism of spark plasma sintering," *Ceramics International,* 2012.

[37] W. Li, E. A. Olevsky, J. McKittrick, A. L. Maximenko and R. M. German, "Densification mechanisms of spark plasma sintering: multi-step pressure dilatometry," *Journal of Materials Science,* pp. 7036-7046, 2012.

[38] E. A. Olevsky and L. Froyen, "Impact of thermal diffusion on densification during SPS," *Journal of the American Ceramic Society,* pp. 122-132, 2008.

[39] X. Song, X. Liu and J. Zhang, "Neck formation and self-adjusting mechanism of neck growth of conducting powders in spark plasma sintering," *Journal of the American Ceramic Society ,* pp. 494-500, 2006.

[40] U. Anselmi-Tamburini, J. E. Garay and Z. A. Munir, "Fundamental investigations of the spark plasma sintering/synthesis process III. Current effect on reactivity," *Materials Science and Engineering,* pp. 24-30, 2005.

[41] P. A. Beck, J. C. Kremer and L. Demer, "Grain growth in high purity aluminum," *Physics Review,* p. 555, 1947.

[42] G. Dirras, J. Gubicza, D. Tingaud and S. Billard, "Microstructure of Al-Al2O3 nanocomposite formed by in situ phase transformation during Al nanopowder consolidation," *Materials Chemistry and Physics,* vol. 129, pp. 846-852, 2011.

[43] M. A. Trunov, M. Schoenitz, X. Zhu and E. L. Dreizin, "Effect of Polymorphic phase transformations in Al2O3 film on oxidation kinetics of aluminum powders," *Combustion and Flame,* vol. 140, pp. 310-318, 2005.

[44] X. Phung, J. Groza, E. A. Stach, L. N. William and S. B. Ritchey, "Surface characterization of metal nanoparticles," *Materials and Engineering A,* vol. 359, pp. 261-268, 2003.

[45] B. Rufino, F. Boulc'h, M. V. Coulet, G. Lacroix and R. Denoyel, "Influences of particle size on thermal properties of aluminum powder," *Acta Materialia,* vol. 55, pp. 2815-2827, 2007.

[46] E. A. Bloch, "Dispersion-strengthened aluminum alloys," *Metallurgical Reviews,* vol. 6, no. 48, pp. 193-240, 1961.

[47] M. Balog, C. Poletti, F. Simancik, M. Walcher and W. Rajner, "The effect of native Al2O3 skin distruption on properties of fine Al powder compacts," *Journal of Alloys and Compounds,* vol. 509S, pp. S235-S238, 2011.

[48] D. Kent, J. Drennan and G. B. Schaffer, "A morphological study of nitride formed on Al at low temperature in the presence of Mg," *Acta Materialia,* no. 59, pp. 2469-2480, 2011.

[49] M. Halmann, A. Frei and A. Steinfeld, "Carbothermal reduction of alumina: Thermochemical equilibrium calculations and experimental investigation," *Energy,* vol. 32, no. 12, pp. 2420-2427, 2007.

[50] M. Tokita, "Mechanisms of spark plasma sintering," in *Proceedings of the International Symposium on Microwave, Plasma and Thermochemical Processing of Advanced Materials*, Osaka Universities, Japan, 1997.

[51] G. M. Le, A. Godfrey and N. Hansen, "Structure and strength of aluminum with sub-micrometer/micrometer grain size prepared by spark plasma sintering," *Materials and Design,* vol. 49, pp. 360-367, 2013.

[52] R. M. German, Powder Metallurgy & Particulate Materials Technology, Princeton: MPIF, 2005.

[53] D. M. Hulbert, A. Anders, D. V. Dudina, J. Andersson, D. Jiang, C. Unuvar, U. Anselmi-Tamburini, E. J. Lavernia and A. K. Mukherjee, "The absense of plasma in "spark plasma sintering"," *Journal of Applied Physics,* vol. 104, no. 3, 2008.

[54] S.-X. Song, Z. Wang and G.-P. Shi, "Heating mechanism of spark plasma sintering," *Ceramics International,* 2012.

[55] D. A. Molinari, "Densification mechanisms in spark plasma sintering: Effect of particle size and pressure," *Powder Technology,* vol. 221, pp. 220-227, 2012.

[56] C. L. Mendis, H. P. Jhawar, T. T. Sasaki, K. Oh-ishi, K. Sivaprasad, E. Fleury and K. Hono, "Mechanical properties and microstructures of Al-1Fe-(0-1)Zr bulk nano-crystalline alloy processed by mechanical alloying and spark plasma sintering," *Materials Science and Engineering A,* vol. A, no. 541, pp. 152-158, 2012.

[57] N. Tsuji, Y. Ito, Y. Saito and Y. Minamino, "Strength and ductility of ultrafine grained aluminum and iron produced by ARB and annealing," *Scripta Materialia,* no. 47, pp. 893-899, 2002.

[58] G. Xie , O. Ohashi and N. Yamaguchi, "Reduction of surface oxide films on Al-Mg alloy powders by pulsed electric current sintering," *Journal of Materials Research,* vol. 19, no. 3, pp. 815-819, 2004.

[59] The Aluminum Association, 1998.

[60] *Standard test methods for tension testing of metallic materials,* West Conshohocken, PA: ASTM International, 2012.

[61] J. Milligan, R. Gauvin and M. Brochu, "Consolidation of cryomilled Al-Si using spark plasma sintering," *Philosophical Magazine,* vol. 93, no. 19, pp. 2445-2464, 2013.

[62] I. A. MacAskill, R. L. Hexemer Jr, I. W. Donaldson and D. P. Bishop, "Effects of magnesium, tin and nitrogen on the sintering response of aluminum powder," *Journal of Materials Processing Technology,* vol. 210, pp. 2252-2260, 2010.

[63] Y.-W. Kim, W. M. Griffith and F. H. Froes, "Surface oxides in P/M aluminum oxides," *Journal of Metals,* vol. 37, no. 8, pp. 27-33, 1985.

[64] M. Yamasaki and Y. Kawamura, "Effect of vacuum degassing on surface characteristics of rapidly solidified Al-based alloy powders," *Materials Transactions,* vol. 45, no. 4, pp. 1335-1338, 2004.

[65] M. Yamasaki and Y. Kawamura, "Changes in the surface characteristics of gas-atomized pure aluminum powder during vacuum degassing," *Materials Transactions,* vol. 47, no. 8, pp. 1902-1905, 2006.

[66] Z. Zhang, S. Dallek, R. Vogt, Y. Li, T. D. Topping, Y. Zhou, J. M. Schoenung and E. J. Lavernia, "Degassing behavior of nanostructures Al and its composites," *Metallurgical and Materials Transactions A,* vol. 41A, pp. 532-541, 2010.

[67] A. Nylund and I. Olefjord, "Surface analysis of air exposed rapidly solidified aluminum powder," *Powder Metallurgy,* vol. 36, no. 3, pp. 193-197, 1993.

[68] R. Watanabe, D. S. Choi and A. Kawasaki, "Gas chromatographic analysis of degassing of aluminum and aluminum alloy powders," *Materials Science Forum,* Vols. 534-536, pp. 809-812, 2007.

[69] S. D. Kirchoff, J. Y. Adkins, W. M. Griffith and I. A. Martorell, "Effective method for degassing evaluation of aluminum PM alloys," in *Rapidly Solidified Powder Aluminum Alloys*, M. E. Fine and E. A. Starke, Eds., Philadelphia, American Society for Testing and Materials, 1986, pp. 354-366.

[70] P. J. Meschter, R. J. Lederich, J. E. ONeal and P. S. Pao, "Study on effects of powder and flake chemistry and morphology on the properties of Al-Cu-Mg-X-X-X powder metallurgy advanced aluminum alloys," NASA Langley Research Center, Hampton, 1985.

[71] T. Voisin, L. Durand, N. Karnatak, S. La Gallet, M. Thomas, Y. Le Berre, J.-F. Castagné and A. Couret, "Temperature control during spark plasma sintering and application to up-scaling and complex shaping," *Journal of Materials Processing Technology,* vol. 213, pp. 269-278, 2013.

[72] R. W. Cooke, R. L. Hexemer, I. W. Donaldson and D. P. Bishop, "PM processing of an Al-Cu-Mg alloy with a low Cu:Mg ratio," *Powder Metallurgy,* vol. 55, no. 1, pp. 29-35, 2012.

[73] C. D. Boland, R. L. Hexemer, I. W. Donaldson and D. P. Bishop, "Industrial processing of a novel Al-Cu-Mg PM alloy," *Materials Science and Engineering A,* vol. 559, pp. 902-908, 2012.

[74] D. P. Bishop, B. Hofmann and K. R. Couchman, "Properties and attributes of commercially available AC2014-type aluminum P/M alloys," in *Advances in Powder Metallurgy and Particulate Materials*, 2000.

[75] D. W. Heard, I. W. Donaldson and D. P. Bishop, "Metallurgical assessment of a hypereutectic aluminum-silicon PM alloy," *Journal of Materials Processing and Technology,* vol. 209, pp. 5902-5911, 2009.

[76] A. D. P. LaDelpha, H. C. Neubing and D. P. Bishop, "Metallurgical assessment of a 7xxx series PM alloy," *Materials Science and Engineering A,* vol. A520, pp. 105-113, 2009.

[77] G. B. Schaffer and S. H. Huo, Powder Metallurgy, 3 ed., 1999, pp. 219-226.

[78] K. Kondoh, A. Kimura and R. Watanabe, *Powder Metallurgy,* vol. 44, no. 2, pp. 161-164, 2001.

[79] "Properties of Wrought Aluminum and Aluminum Alloys," in *ASM Metals HandBook Volume 2 - Properties and Selection: Nonferrous Alloys and Special-Purpose Materials*, ASM, 1990, pp. 222-481.

[80] K. Kondoh, A. Kimura and R. Watanabe, *Japan Welding Society ,* vol. 19, no. 1, pp. 167-169, 2001.

[81] T. T. Sasaki, T. Ohkubo and K. Hono, "Microstructure and mechanicle properties of bulk nanocrystalline Al-Fe alloy processed by mechanical alloying and spark plasma sintering," *Acta Materialia,* vol. 57, pp. 3529-3538, 2009.

[82] A. Zuniga, L. Ajdelsztajn and E. J. Lavernia, "Spark plasma sintering of a nanocrystalline Al-Cu-Mg-Fe-Ni-Sc Alloy," *Metallurgical and Materials Transactions A,* vol. 37A, pp. 1343-13-52, 2006.

[83] G. A. Sweet, M. Brochu, R. L. Hexemer, I. W. Donaldson and D. P. Bishop, "Microstructure and mechanical properties of air atomized aluminum powder consolidated via spark plasma sintering," *Materials Science & Engineering A,* vol. 608, pp. 273-282, 2014.

[84] N. A. Belov, A. A. Askenov and D. G. Eskin, Iron in Aluminum Alloys: Impurity and Alloying Element, CRC Press, 2002.

[85] M. Ceylan, S. N. Ylavac, M. Gunduz and T. Karaaslan, "Investigation into the effects of rapid quenching on the solidification of Al-Cu and Al-Mg alloys," *Journal of Materials Processing Technology,* vol. 41, no. 4, pp. 447-459, 1994.

[86] M. Warmuzek, "Metallographic techniques for aluminum and its alloys," in *ASM Handbook, Metallography and Microstructures*, vol. 9, ASM International, 2004, pp. 711-751.

[87] Z. Zhongtao, L. Yinyan, Z. Qihan, L. Zhengxin and M. Ruzhang, "Mossbauer study of precipitates in rapidly solidifed Al-Fe-Ni alloys," *Z. Metallkd,* vol. 87, no. 1, pp. 40-44, 1996.

[88] H. Tsubakino, U. Ishihara and A. Yamamoto, "Precipitation sequence in high purity Al-Ni dilute alloys by resistivity measurements," *Journal of Japan Institute of Light Metals,* vol. 51, no. 7, pp. 356-360, 2001.

APPENDIX A: COPYRIGHT RELEASE

6.1 Elsevier Release

ELSEVIER LICENSE
TERMS AND CONDITIONS
Jun 16, 2014

This is a License Agreement between Greg Sweet ("You") and Elsevier ("Elsevier") provided by Copyright Clearance Center ("CCC"). The license consists of your order details, the terms and conditions provided by Elsevier, and the payment terms and conditions.

All payments must be made in full to CCC. For payment instructions, please see information listed at the bottom of this form.

Supplier	Elsevier Limited The Boulevard,Langford Lane Kidlington,Oxford,OX5 1GB,UK
Registered Company Number	1982084
Customer name	Greg Sweet
Customer address	1360 Barrington Street Halifax, NS B3H4R2
License number	3410881037153
License date	Jun 16, 2014
Licensed content publisher	Elsevier
Licensed content publication	Materials Science and Engineering: A
Licensed content title	Microstructure and mechanical properties of air atomized aluminum powder consolidated via spark plasma sintering
Licensed content author	G.A. Sweet,M. Brochu,R.L. Hexemer,I.W. Donaldson,D.P. Bishop
Licensed content date	1 July 2014
Licensed content volume number	608
Licensed content issue number	None
Number of pages	10
Start Page	273
End Page	282
Type of Use	reuse in a thesis/dissertation
Portion	full article
Format	electronic

Are you the author of this Elsevier article?	Yes
Will you be translating?	No
Title of your thesis/dissertation	Advanced Sintering Techniques of Aluminum: Spark Plasma Sintering
Expected completion date	Aug 2014
Estimated size (number of pages)	110
Elsevier VAT number	GB 494 6272 12
Permissions price	0.00 USD
VAT/Local Sales Tax	0.00 USD / 0.00 GBP
Total	0.00 USD

Terms and Conditions

INTRODUCTION

1. The publisher for this copyrighted material is Elsevier. By clicking "accept" in connection with completing this licensing transaction, you agree that the following terms and conditions apply to this transaction (along with the Billing and Payment terms and conditions established by Copyright Clearance Center, Inc. ("CCC"), at the time that you opened your Rightslink account and that are available at any time at http://myaccount.copyright.com).

GENERAL TERMS

2. Elsevier hereby grants you permission to reproduce the aforementioned material subject to the terms and conditions indicated.

3. Acknowledgement: If any part of the material to be used (for example, figures) has appeared in our publication with credit or acknowledgement to another source, permission must also be sought from that source. If such permission is not obtained then that material may not be included in your publication/copies. Suitable acknowledgement to the source must be made, either as a footnote or in a reference list at the end of your publication, as follows:

"Reprinted from Publication title, Vol /edition number, Author(s), Title of article / title of chapter, Pages No., Copyright (Year), with permission from Elsevier [OR APPLICABLE SOCIETY COPYRIGHT OWNER]." Also Lancet special credit - "Reprinted from The Lancet, Vol. number, Author(s), Title of article, Pages No., Copyright (Year), with permission from Elsevier."

4. Reproduction of this material is confined to the purpose and/or media for which permission is hereby given.

5. Altering/Modifying Material: Not Permitted. However figures and illustrations may be altered/adapted minimally to serve your work. Any other abbreviations, additions, deletions

and/or any other alterations shall be made only with prior written authorization of Elsevier Ltd. (Please contact Elsevier at permissions@elsevier.com)

6. If the permission fee for the requested use of our material is waived in this instance, please be advised that your future requests for Elsevier materials may attract a fee.

7. Reservation of Rights: Publisher reserves all rights not specifically granted in the combination of (i) the license details provided by you and accepted in the course of this licensing transaction, (ii) these terms and conditions and (iii) CCC's Billing and Payment terms and conditions.

8. License Contingent Upon Payment: While you may exercise the rights licensed immediately upon issuance of the license at the end of the licensing process for the transaction, provided that you have disclosed complete and accurate details of your proposed use, no license is finally effective unless and until full payment is received from you (either by publisher or by CCC) as provided in CCC's Billing and Payment terms and conditions. If full payment is not received on a timely basis, then any license preliminarily granted shall be deemed automatically revoked and shall be void as if never granted. Further, in the event that you breach any of these terms and conditions or any of CCC's Billing and Payment terms and conditions, the license is automatically revoked and shall be void as if never granted. Use of materials as described in a revoked license, as well as any use of the materials beyond the scope of an unrevoked license, may constitute copyright infringement and publisher reserves the right to take any and all action to protect its copyright in the materials.

9. Warranties: Publisher makes no representations or warranties with respect to the licensed material.

10. Indemnity: You hereby indemnify and agree to hold harmless publisher and CCC, and their respective officers, directors, employees and agents, from and against any and all claims arising out of your use of the licensed material other than as specifically authorized pursuant to this license.

11. No Transfer of License: This license is personal to you and may not be sublicensed, assigned, or transferred by you to any other person without publisher's written permission.

12. No Amendment Except in Writing: This license may not be amended except in a writing signed by both parties (or, in the case of publisher, by CCC on publisher's behalf).

13. Objection to Contrary Terms: Publisher hereby objects to any terms contained in any purchase order, acknowledgment, check endorsement or other writing prepared by you, which terms are inconsistent with these terms and conditions or CCC's Billing and Payment terms and conditions. These terms and conditions, together with CCC's Billing and Payment terms and conditions (which are incorporated herein), comprise the entire agreement between you and publisher (and CCC) concerning this licensing transaction. In the event of any conflict between your obligations established by these terms and conditions and those

established by CCC's Billing and Payment terms and conditions, these terms and conditions shall control.

14. Revocation: Elsevier or Copyright Clearance Center may deny the permissions described in this License at their sole discretion, for any reason or no reason, with a full refund payable to you. Notice of such denial will be made using the contact information provided by you. Failure to receive such notice will not alter or invalidate the denial. In no event will Elsevier or Copyright Clearance Center be responsible or liable for any costs, expenses or damage incurred by you as a result of a denial of your permission request, other than a refund of the amount(s) paid by you to Elsevier and/or Copyright Clearance Center for denied permissions.

LIMITED LICENSE

The following terms and conditions apply only to specific license types:

15. **Translation**: This permission is granted for non-exclusive world **English** rights only unless your license was granted for translation rights. If you licensed translation rights you may only translate this content into the languages you requested. A professional translator must perform all translations and reproduce the content word for word preserving the integrity of the article. If this license is to re-use 1 or 2 figures then permission is granted for non-exclusive world rights in all languages.

16. **Posting licensed content on any Website**: The following terms and conditions apply as follows: Licensing material from an Elsevier journal: All content posted to the web site must maintain the copyright information line on the bottom of each image; A hyper-text must be included to the Homepage of the journal from which you are licensing at http://www.sciencedirect.com/science/journal/xxxxx or the Elsevier homepage for books at http://www.elsevier.com; Central Storage: This license does not include permission for a scanned version of the material to be stored in a central repository such as that provided by Heron/XanEdu.

Licensing material from an Elsevier book: A hyper-text link must be included to the Elsevier homepage at http://www.elsevier.com . All content posted to the web site must maintain the copyright information line on the bottom of each image.

Posting licensed content on Electronic reserve: In addition to the above the following clauses are applicable: The web site must be password-protected and made available only to bona fide students registered on a relevant course. This permission is granted for 1 year only. You may obtain a new license for future website posting.

For journal authors: the following clauses are applicable in addition to the above: Permission granted is limited to the author accepted manuscript version* of your paper.

***Accepted Author Manuscript (AAM) Definition:** An accepted author manuscript (AAM) is the author's version of the manuscript of an article that has been accepted for publication and which may include any author-incorporated changes suggested through the processes of submission processing, peer review, and editor-author communications. AAMs do not include other publisher value-added contributions such as copy-editing, formatting, technical enhancements and (if relevant) pagination.

You are not allowed to download and post the published journal article (whether PDF or HTML, proof or final version), nor may you scan the printed edition to create an electronic version. A hyper-text must be included to the Homepage of the journal from which you are licensing at http://www.sciencedirect.com/science/journal/xxxxx. As part of our normal production process, you will receive an e-mail notice when your article appears on Elsevier's online service ScienceDirect (www.sciencedirect.com). That e-mail will include the article's Digital Object Identifier (DOI). This number provides the electronic link to the published article and should be included in the posting of your personal version. We ask that you wait until you receive this e-mail and have the DOI to do any posting.

Posting to a repository: Authors may post their AAM immediately to their employer's institutional repository for internal use only and may make their manuscript publically available after the journal-specific embargo period has ended.

Please also refer to Elsevier's Article Posting Policy for further information.

18. **For book authors** the following clauses are applicable in addition to the above: Authors are permitted to place a brief summary of their work online only.. You are not allowed to download and post the published electronic version of your chapter, nor may you scan the printed edition to create an electronic version. **Posting to a repository:** Authors are permitted to post a summary of their chapter only in their institution's repository.

20. **Thesis/Dissertation**: If your license is for use in a thesis/dissertation your thesis may be submitted to your institution in either print or electronic form. Should your thesis be published commercially, please reapply for permission. These requirements include permission for the Library and Archives of Canada to supply single copies, on demand, of the complete thesis and include permission for UMI to supply single copies, on demand, of the complete thesis. Should your thesis be published commercially, please reapply for permission.

Elsevier Open Access Terms and Conditions

Elsevier publishes Open Access articles in both its Open Access journals and via its Open Access articles option in subscription journals.

Authors publishing in an Open Access journal or who choose to make their article Open Access in an Elsevier subscription journal select one of the following Creative Commons

Please refer to Elsevier's Open Access Policy for further information.

21. **Other Conditions**:

v1.7

If you would like to pay for this license now, please remit this license along with your payment made payable to "COPYRIGHT CLEARANCE CENTER" otherwise you will be invoiced within 48 hours of the license date. Payment should be in the form of a check or money order referencing your account number and this invoice number 501329377.
Once you receive your invoice for this order, you may pay your invoice by credit card. Please follow instructions provided at that time.

Make	**Payment**	**To:**
Copyright	**Clearance**	**Center**
Dept		**001**
P.O.	**Box**	**843006**
Boston,	**MA**	**02284-3006**

For suggestions or comments regarding this order, contact RightsLink Customer Support: customercare@copyright.com or +1-877-622-5543 (toll free in the US) or +1-978-646-2777.

Gratis licenses (referencing $0 in the Total field) are free. Please retain this printable license for your reference. No payment is required.

6.2 MPIF Release

June 17, 2014

PM2014 Wold Congress Proceedings
Metal Powder Industries federation
105 College Road East
Princeton, NJ 08540-6692

I am preparing my MASc thesis for submission to the Faculty of Graduate Studies at Dalhousie University, Halifax, Nova Scotia, Canada. I am seeking your permission to include a manuscript version of the following paper(s) as a chapter in the thesis:

EFFECTS OF TRANSITION METAL ADDITIONS ON THE SPARK PLASMA SINTERING RESPONSE OF ALUMINUM POWDERS, G.A. Sweet, D.P. Bishop, M. Brochu, R.L. Hexemer Jr. and I.W. Donaldson

Canadian graduate theses are reproduced by the Library and Archives of Canada (formerly National Library of Canada) through a non-exclusive, world-wide license to reproduce, loan, distribute, or sell theses. I am also seeking your permission for the material described above to be reproduced and distributed by the LAC(NLC). Further details about the LAC(NLC) thesis program are available on the LAC(NLC) website (www.nlc-bnc.ca).

Full publication details and a copy of this permission letter will be included in the thesis.

Yours sincerely,

Greg Sweet

Permission is granted for:

a) the inclusion of the material described above in your thesis.

b) for the material described above to be included in the copy of your thesis that is sent to the Library and Archives of Canada (formerly National Library of Canada) for reproduction and distribution.

Name: James P. Adams Title: Vice President, Technical Services

Signature: [redacted] Date: June 17, 2014